Quartz Crystal Microbalance with Dissipation Monitoring: Sensing Beyond Cell-Substrate Adhesion

A Thesis

Submitted to the Faculty

of

Drexel University

by

Jennifer Ying Chen

in partial fulfillment of the

requirements for the degree

of

Doctor of Philosophy

September 2017

DREXEL UNIVERSITY
Graduate College

DISSERTATION/THESIS APPROVAL FORM

This form is for use by all doctoral and master's students with a dissertation/thesis requirement. Please print clearly as the library will bind a copy of this form with each copy of the dissertation/thesis. All doctoral dissertations must conform to university format requirements, which is the responsibility of the student and supervising professor. Students should obtain a copy of the Thesis Manual located on the Graduate College or library website.

Dissertation/Thesis Title: Quartz Crystal Microbalance with Dissipation Monitoring: Sensing Beyond Cell-Substrate Adhesion

Author: Jennifer Ying Chen

This dissertation/thesis is hereby accepted and approved.

Signatures:

Examining Committee

Chair

Members

Academic Advisor

Department Head

Graduate College 3141 Chestnut Street Main 301 Philadelphia, PA 19104
Tel: 215.895.0366 Fax: 215.895.0495 Email: graduatecollege@drexel.edu Web: www.drexel.edu/graduatecollege

(Last Updated 3/1/2016)

Dedications

For my parents, Li Ying Lin and Zhuo Fang Chen, who worked endlessly to make sure I have the opportunity to pursue my hopes and dreams. Thank you for your infinite love, care, and support.

To my grandfather, Tso Chin, who made sacrifices to travel across the world to settle in a foreign land to provide a better life and better opportunities for his family.

Acknowledgements

I would first like to thank my advisor and mentor, Dr. Jun Xi, for supporting me and pushing me to be the best researcher I could be. I've learned tremendously under your advisement. Thank you for all the advice you have given me, for always having my best interest at heart, and for having the belief in me to achieve.

I would like to thank Dr. Reinhard Schweitzer-Stenner, for being an excellent advisor. Thank you for the guidance and support that was offered along the way. Thank you again for the time and energy that you've dedicated to my work.

I thank Dr. Lynn S. Penn for being a very supportive dissertation committee chair. Thank you for your guidance and all the advice you have given me.

I want to thank all the members of my thesis committee from the Department of Chemistry, Dr. Joe P. Foley, Dr. Haifeng Ji, and Dr. Daniel King for their support and assistance. I want to thank Dr. Nianli Sang from the Department of Biology and Dr. Zhihong Wang from University of the Sciences for their participation in my dissertation committee.

I would like to thank the members of the Jun Xi group both past and present. I would like to thank Dr. Minghong Li for showing me the way in the lab. I also want to thank Marcela Garcia, Wenjian Du, and Ahmed Bulhassan for all their support, advice and friendship. Finally, I would like to thank my undergraduate students, Ammar Shahid, Stephanie Shore, Evira Soultogianni, Tucker Collins, and Yue Pan for assisting me on my projects.

I also want to thank Tina Lewinsky, Sue Tang, Genell Sodano, Edward Doherty, Virginia Nesmith, Daniel Gray, Tim Wade, Jon Soffer, and Kyle Hess for all their help.

I want to thank Ms. Mona Bradwell and Mr. Kilfe Gebremedhin for encouraging me to pursue a career in science. Without your encouragement this accomplishment would not have been possible.

I would also like to thank Keith R. Hagigal for your endless love, for being my #1 supporter, and for always having confidence in me. Thank you for being that one person who I can talk to about all my stress and worries.

Lastly I would like to thank all my family and friends for their support and all the encouraging words. Without all of you I would not be the person I am today.

Table of Content

List of Tables

List of Figures

Abstract

Quartz Crystal Microbalance with Dissipation Monitoring:
Sensing Beyond Cell-Substrate Adhesion
Jennifer Ying Chen
Prof. Reinhard Schweitzer-Stenner
Prof. Jun Xi

The quartz crystal microbalance with dissipation monitoring (QCM-D) is an ultrasensitive mechanical sensing device that is capable of providing real-time, non-invasive measurements of changes in resonance frequency and energy dissipation responses of cells immobilized onto the sensor surface. The majority of its applications in cell research have been limited to the study of the adhesive interaction between cells and the substrate surface and the evaluation of the effect of an external stimulant on the adhered cells. The overall objective of this thesis work was to further exploit the capabilities of the QCM-D in cell research by addressing important problems that are relevant to fundamental biology and medicine.

In the project presented in Chapter 4, we examined the EGF-induced cell de-adhesion, a critical step in normal embryonic development, wound repair, inflammatory response, and tumor cell metastasis. We were able to successfully establish the change in the energy dissipation factor (ΔD-response) as a specific and quantitative measure of cell adhesion. With this novel measure of cell adhesion, we characterized this complex de-adhesion process, which appeared to exhibit an initial rapid cell de-adhesion, a transition, and a slow re-adhesion. We also shed light on the dynamic coordination of the three downstream pathways of epidermal growth factor receptor (EGFR) signaling in mediation of the epidermal growth factor (EGF)-induced de-adhesion process. In chapter 5, continuing with the theme of applying this novel measure to the characterization of cell

adhesion, we examined the adhesion process of human epidermal keratinocytes on the implant type of surface. We identified three distinct stages of this adhesion process and developed several new strategies for strengthening the adhesion between soft tissue/skin/bone and implants. In chapter 6, we extended this novel measure of cell adhesion to the investigation of GPCR signaling by capitalizing the regulatory role of G protein-coupled receptor (GPCR) signaling in mediation of cell adhesion. We were able to dissect the multiplicity of the ligand-induced GPCR signaling and obtain mechanistic insights into the promiscuous coupling of $G_{\alpha q}$, $G_{\alpha s,}$ and $G_{\alpha i}$ pathways as well as their dynamic coordination.

In chapters 7 and 8, we explored the potential of cell-based QCM-D assay in detection of biomarkers. In chapter 7, we were able to relate the ΔD-response with the cellular response mediated by the high-affinity EGFR, the subclass of EGFR that is more relevant to cancer development. Lastly in chapter 8, we demonstrated that this cell-based QCM-D assay has the sensitivity and specificity to detect some of the potential biomarkers of ovarian cancer.

In conclusion, this thesis work has demonstrated that the QCM-D is a highly sensitive, label-free technique that has the capabilities to probe some of the most important cellular processes, such as cell adhesion and cell signaling and to serve as a sensing platform for biomarker detection.

(page intentionally left blank)

Chapter 1: Introduction to Cell Adhesion

1.1 Cell Adhesion

Cell adhesion is defined as the ability for a cell to attach to another cell as cell-cell adhesion or to the extracellular matrix (ECM) as cell-substrate (or cell-ECM, cell-matrix) adhesion. Change in cell adhesion is a signature event in a wide range of disorders including, cancers[1, 2], arthritis[3, 4], atherosclerosis[5, 6], and osteoporosis[7, 8]. For example, the progression of many cancers involves migration of the cells in a tumor from their primary location to different locations upon losing their adhesiveness at the primary location[1, 2]. At the new locations, these migrated tumors cells re-adhere, divide, and multiply allowing the cancer to continue to develop. A comprehensive understanding of the cell adhesion process can potentially provide further insight into the development of cancers and other cell adhesion related disorders.

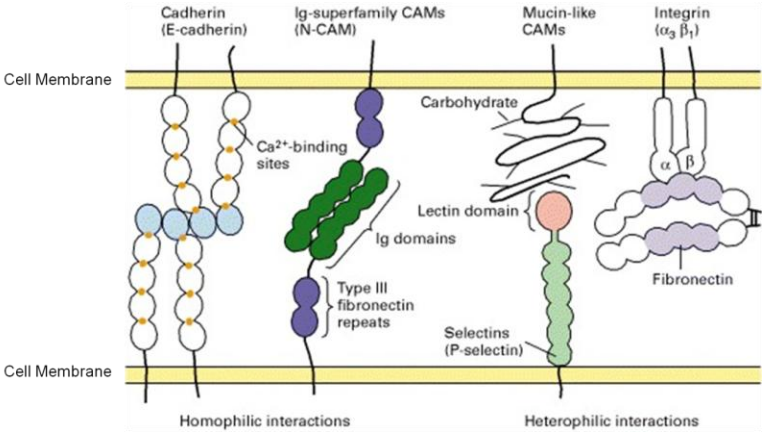

Figure 1.1. The four main classes of cell adhesion molecules (CAMs). (Adapted from reference 9)

Both cell-cell and cell-substrate adhesion are mediated by cell adhesion molecules (CAMs) that reside along the plasma membrane of cells. CAMs can bind extracellularly to the outer membrane of neighboring cells and/or the surface of the substrate[10], while connected intracellularly to the cytoskeleton[9]. There are four main classes of CAMs: cadherins, selectins, integrins, and the immunoglobulin (Ig) superfamily [9, 11] (Figure 1.1). Integrins are the main mediator of cell-substrate adhesion where all other CAMs are responsible for cell-cell adhesion.

1.1.1 Cell-Cell Adhesion

Cell-cell adhesion is known to play an essential role in cell morphogenesis, cell growth, and cell communication[12]. The primary class of CAMs that mediate cell-cell adhesion is cadherins, which are transmembrane proteins that contain a common extracellular domain of about 100 amino acids known as the cadherin-specific module[13]. Cadherins are the key constituents of the cell-cell junction complexes – adheren junction and desmosomes[14]. Cadherins are also connected to bundles of actin filaments and keratin filaments, respectively, by means of catenin adapter proteins[14].

Another class of CAMs that mediate cell-cell adhesion is the Ig CAM superfamily. Members of this class contain one or more copies of the Ig fold, a structure with two anti-parallel beta sheets, a single transmembrane helical segment, and a cytoplasmic tail[15]. The Ig CAM superfamily functions in many biological processes that occur in a wide range of cell types. The most important function of the Ig CAM superfamily is its involvement in the establishment and maintenance of neural connections in the nervous system[16].

Selectins are another class of CAMs that mediate cell-cell adhesion. They are a small group of lectin-like adhesion receptors[17]. Selectin structure consists of a lectin-like domain, an epidermal growth factor domain, two to nine complement regulatory protein (CRP) repeats, a single transmembrane helical segment and a cytoplasmic tail[17]. The major physiological role of selectin is to bind leukocyte and facilitate its adherence to the surface of endothelial cells and platelets during inflammatory processes[18].

1.1.2 Cell-Substrate Adhesion

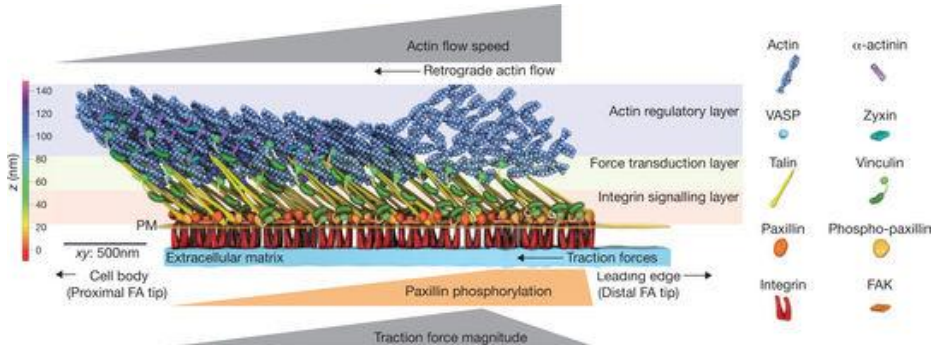

Figure 1.2. 3D structure of focal adhesions (FAs). (Adapted from reference 19)

Cell-substrate adhesion plays an important role in organizing cells into tissue. In response to environmental cues, cell-substrate adhesion also regulates cellular behaviors, such as cell migration, proliferation, gene expression, and activation of signal transduction pathways that mediate cell growth[11]. The primary class of CAMs that mediate cell-matrix adhesion is integrin, which consists of heterodimers of subunits α and β that are non-covalently associated. Non-covalent associations, include hydrogen bonding, van der Waals forces, and electrostatic interactions. Both subunits of the

integrin are single type-I transmembrane proteins with an extracellular domain that can bind to extracellular matrix proteins and a cytoplasmic tail that can link intracellularly to the cytoskeleton[20]. This linkage allows for bi-directional force transmission across the plasma membrane and therefore relays information between the inside and outside of the cell. In mammals, there are at least 24 known integrin heterodimers, composed of 18 different types of α subunits and 8 different types of β subunits[20]. The extracellular domain is composed of parts of both α and β subunits. The combination of the binding domain of the two subunits provides a diverse population of integrins with each integrin recognizing a distinct ECM ligand[21]. The binding of the integrin to the matrix makes possible the transmission of chemical signals into the cell. The chemical signal provides information on the location, environment, and adhesive state of the cell and dictates the corresponding cellular response, such as migration, differentiation, and motility[22, 23].

Focal adhesions (FAs) and hemidesmosomes are the two common forms of integrin-dependent cell-matrix junctions[24]. Focal adhesion complexes are formed by clustering of integrins on the cell surface. Clusters of integrins become the central locations for recruiting adaptor proteins, scaffold proteins, and signaling proteins to the inner surface of the plasma membrane[25] (Figure 1.2). A mature focal adhesion that varies in size between 1 to 5 μm contains various actin-binding proteins, kinases and membrane-binding proteins, such as vinculin, talin, paxillin, tensin, p130Cas, and α-actinin. The actin-binding proteins facilitate the linkage between the actin cytoskeleton and the ECM[25]. The linkage allows for the generation of tension needed to modify cell morphology and control the traction force for cell migration. There are also multiple

signaling proteins (e.g., focal adhesion kinase) that transmit cell signals to regulate cell proliferation, survival, and migration[22].

Unlike focal adhesions, hemidesmosomes (HD) connect the extracellular matrix to the intermediate filaments (IF) of the cytoskeleton. One important function of hemidesmosomes is to aid the adhesion of epithelial cells to the underlying membrane in stratified epithelia of skin, and in parts of the gastrointestinal and respiratory tracts[26, 27]. Hemidesmosome complexes contain $\alpha_6\beta_4$ integrin, HD1/plectin, and the bullous pemphigoid (BP) antigens BP180 and BP230[26]. Alteration of the expression of hemidesmosomal constituents may result in several types of blistering disorders of the skin and are found to be involved in the development and progression of certain cancers[28, 29].

1.1.3 Cell Adhesion Process

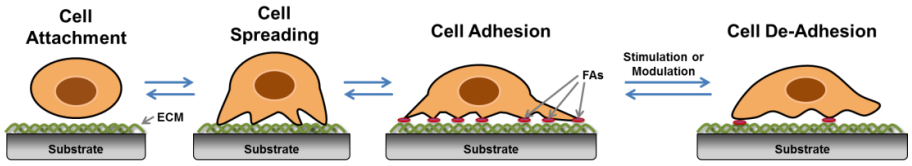

Figure 1.3. The cell adhesion process. First, a cell comes in contact with the substrate and loosely attaches onto the substrate surface. Second, the cell begins to flatten, spread its membrane and simultaneously form focal contact over the substrate surface. Lastly, the cell form focal adhesion complexes (FAs) that connect the extracellular matrix (ECM) with intracellular actin filaments, which securely anchor the cell to the substrate surface. With exogenous stimulation and modulation the cell can de-adhere from the ECM[30].

In general, the cell adhesion process begins with an initial stage, where a cell settles onto a substrate to form a very loose physical attachment to the surface. In the following stage, the cell flattens and begins to spread its membrane over the substrate

surface (Figure 1.3). During and after the cell spreading step, the transmembrane receptors (integrins) along with other intracellular proteins (e.g., actin, vinculin, etc.) form adhesion complexes with the ECM that adheres to the surface of the substrate [31]. As mentioned before, the clustering of these adhesion complexes leads to the establishment of focal adhesions, which anchor the cell securely to the surface of the substrate. Conversely, disassembly of focal adhesions will reduce the level of cell adhesion and lead to de-adhesion of the cell[32-34].

1.2 Mediating Cell Adhesion by Cell Signaling

Cell adhesion molecules have been long researched as molecules involved in the generation of tissue structures. However, cell adhesion complexes not only play an important role in providing the architectural structure for tissues, but are also critically involved in multiple signal transduction processes[35]. The cell adhesion complex serves as a bi-directional path that transmits regulatory signals in and out of cells. Cells rely on cell signaling to coordinate various downstream effectors, various small chemical species (e.g., ions, enzymes) that bind to specific proteins, to regulate essential cellular functions, including adhesion, migration, proliferation, and differentiation[36]. The two signaling pathways involved in the regulation of cell-substrate adhesion that will be focused on in this thesis are the epidermal growth factor receptor (EGFR) pathway and the G protein coupled receptor (GPCR) pathways.

1.2.1 Epidermal Growth Factor Receptor (EGFR)

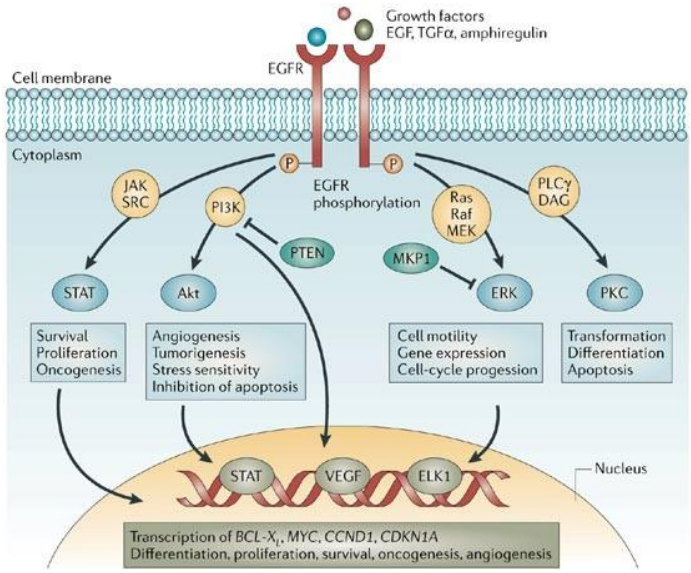

Figure 1.4. Epidermal growth factor receptor (EGFR) signaling pathway (Adapted from reference 37)

The epidermal growth factor receptor (EGFR) belongs to the type 1 growth factor receptor tyrosine kinase (RTK) family, also known as erbB or human epidermal growth factor receptor (HER) family[38]. ErbB receptors are made up of an extracellular ligand-binding region, a single transmembrane-spanning region, and a cytoplasmic tyrosine kinase domain. Ligands that bind specifically to EGFR are epidermal growth factor (EGF), transforming growth factor-α (TGF-α), herpin-binding EGF, and amphiregulin[39]. Although EGFR has affinity for diverse ligands, EGF is considered to be one of the most important ligands for EGFR[40]. When EGFR is activated, it is involved in signal transduction for the regulation of many normal physiological functions, such as cell growth, cell proliferation, cell motility, and cell differentiation[39]. Abnormal expression and signaling of EGFR have been associated with the development of epithelial

malignancies in humans[41]. EGFR was the first receptor identified as a proto-oncogene[42]. Many studies have shown that the up-regulation of EGFR is correlated with tumor progression in numerous human cancers[43].

Upon the ligand engagement, EGFR undergoes a conformational change, which leads to first receptor homo- and/or heterodimerization at the cell surface and then autophosphorylation of multiple tyrosine residues in the cytoplasmic domains[39]. The autophosphorylation activates EGFRs and initiates many downstream signaling cascades, including the mitogen-activated protein kinase/ extracellular signal-regulated kinase (MAPK/ERK) pathway, the phosphatidylinositol 3-kinase (PI3K), and the phospholipase C-γ (PLCγ) signaling pathway, and the signal transducer and activator of transcription (STAT) pathway[11] (Figure 1.4). The ERK/MAPK, PI3K, and PLCγ pathways have been well studied because of their importance in regulation of cell motility, cell migration, and cell invasion[44, 45].

The ERK/MAPK pathway is one of the principal signaling cascades that cells use for responding to extracellular and intracellular cues. The MAPK pathway is responsible for the growth factor-induced cell motility and invasion, and the ERK pathway mediates in cell motility and cell proliferation. Abnormal activation of ERK/MAPK pathway is a common occurrence in many human cancers[46]. Upon activation, the ERK1/2 signaling activates one of its downstream effectors calpain. As an intracellular protease, calpain is responsible for de-adhesion of the trailing portion of the cell during cell migration[47-49], evidenced by the fact that inhibition of calpain significantly decreases the invasiveness of prostate tumor cells[50]. ERK1/2 signaling can also stimulate myosin light chain (MLC)

kinase, which subsequently phosphorylates the myosin light chain protein, allowing it to interact with actin filament to generate contraction forces[51].

The PI3K signaling pathway is responsible for the regulation of cellular survival, proliferation, and growth. Activated by either receptor tyrosine kinases (RTKs) or G protein coupled receptors (GPCRs), the PI3K pathway induces the production of phospholipids to further activate a serine/threonine kinase Akt and other downstream effectors proteins to promote cell survival and proliferation[11]. The tumor suppressor PTEN is the most important regulator of the PI3K signaling pathway. Loss of PTEN had been linked to the uncontrolled signaling of the PI3K pathway and the development of cancer[49]. Another downstream effector of the PI3K pathway is GTPase RhoA, which is responsible for mediating cell de-adhesion[52].

The PLCγ pathway when activated by EGF is a major regulator of cell motility. Activation of PLCγ leads to the hydrolysis of membrane associated phospholipids, which then leads to the activation of protein kinase C and mobilization of actin binding proteins like gelsolin and cofilin that assist in cytoskeletal reorganization for cell migration[11]. Inhibition and gene altering studies of the PLCγ signaling pathway have shown decreased cell migration and invasion of fibroblasts, keratinocytes, and carcinoma cells[53, 54].

1.2.2 G protein Coupled Receptor (GPCR)

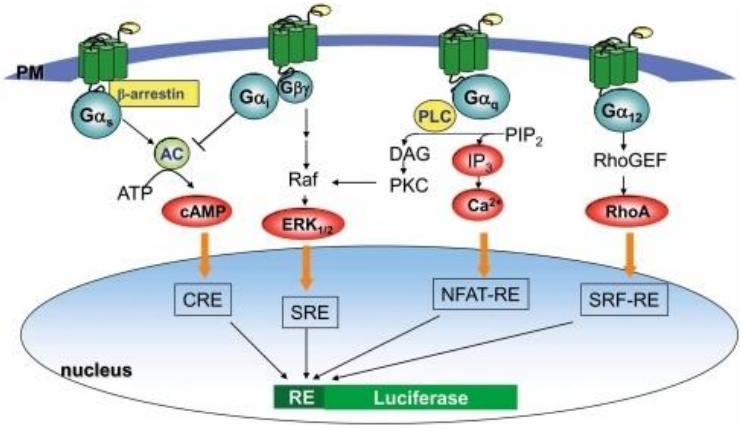

Figure 1.5. G protein coupled receptor (GPCR) signaling pathway (Adapted from reference 55)

G protein coupled receptor (GPCR) is one of the largest families of mammalian proteins[56]. It is involved primarily in mediating and controlling the signal transduction that regulates normal physiological functions, such as secretion, neurotransmission, growth, cellular differentiation, and immune response[57]. It also participates in pathological progression of a wide variety of diseases[58]. GPCRs are known as seven transmembrane domain receptors (7TM) due to their common central domain consisting of seven transmembrane helices connected by the intracellular loops and three extracellular loops[59]. GPCRs can sense a wide variety of extracellular stimuli, such as ions, biogenic amines, purines, lipids, peptides, and proteins[57].

The GPCR signaling system contains three major parts: the receptor, the heterotrimeric αβγ G protein, and the effector[56]. Binding of a ligand to the receptor activates the exchange of the guanidine diphosphate (GDP) in the G_α subunit of the heterotrimeric G protein to a guanidine triphosphate (GTP), which subsequently induces

the dissociation of the heterotrimeric G protein into G_α subunit and $G_{\beta\gamma}$ dimer[60]. The dissociated G_α subunit, depending on its major subtype (G_s, $G_{i/o}$, $G_{q/11}$, and $G_{12/13}$), then couples with a specific effector protein to influence a diverse set of downstream signaling cascades that regulate biological behaviors, including apoptosis, transcription, cell migration, cell adhesion, and cell proliferation[61-63] (Figure 1.5).

The effector of the subtype G_q mediated pathway (or $G_{\alpha q/11}$ pathway, or $G_{\alpha q}$ pathway) is phospholipase C-β (PLCβ), which cleaves phospholipid phosphatidylinositol 4,5-bisphosphate (PIP_2) into diacylglycerol (DAG) and inositol-1,4,5-trisphosphate (IP_3) [64]. IP_3 then binds and opens the IP_3 calcium channel, which then releases calcium ions into the cytoplasm[64]. The G_s and G_i mediated pathways (or $G_{\alpha s}$ pathway and $G_{\alpha i}$ pathway, respectively) share the same type of effector, adenylyl cyclase, which is usually stimulated by $G_{\alpha s}$ but inhibited by $G_{\alpha i}$[65]. Adenylyl cyclase catalyzes adenosine triphosphate (ATP) to 3',5'-cyclic adenosine monophosphate (cAMP). cAMP, as a second messenger then activates a secondary effector protein kinase A (PKA) and other downstream effectors[61]. PKA, the well-studied effector, phosphorylates numerous metabolic enzymes, including glycogen synthase, phosphorylase kinase, acetyl CoA carboxylase, and others. The activation of these enzymes promotes glycogen synthesis and breakdown, and inhibits lipid synthesis[66]. The $G_{\alpha 12/13}$ subtype is responsible for the activation of RhoGEF, which then activates the small G protein RhoA[66], which regulates multiple downstream effectors. Many of these effector proteins are cytoskeletal proteins. A lot of research has been done on RhoA-mediated activation of Rho kinases (ROCK1/2), which is responsible for regulation of the formation of actin stress fibers[67].

There has been research that shows overexpression or mutation of some GPCR subtypes in numerous cell types contributes to dysregulated growth and tumor development[68]. In the G_s subtype, the *gsp* oncogene is a mutation identified in $G_{\alpha s}$ of pituitary and thyroid tumors and is capable of activating adenylyl cyclase (AC) to promote cell growth[69]. In the G_i subtype, the *gip2* oncogene has been identified and it promotes tumor growth through the activation of the MAPK pathways[70].

There has been an increasing interest in determining the mechanism of GPCR mediated cell adhesion, cell migration, and cell proliferation because it may give further insight into tumor invasion[71-74]. G_s-coupled receptors have been shown to play a role in promoting the activation of PKA and in controlling MAPK pathways that regulate remodeling of actin cytoskeleton and cell migration[75]. Studies have shown G_i-coupled receptors can activate Rho and Rac to regulate actin remodeling[76]. G_q-coupled receptors have been reported to enhance cell motility by activating PLC/PKC/calmodulin signaling and stimulating GTPase Rho[77]. $G_{12/13}$-coupled receptors are known regulators of Rho and Cdc42 activation which control formation of stress fibers and filopodia, which is the membrane protrusion in migrating cells.

1.3 Current Methods of Studying Cell Adhesion

For decades, the study of cell adhesion has been a great interest of many interdisciplinary fields, including materials science, pharmacology, biophysics, etc.[78] Such a great interest has led to the development of various methods for studying and characterizing cell adhesion.

1.3.1 Mechanical Methods of Studying Cell Adhesion

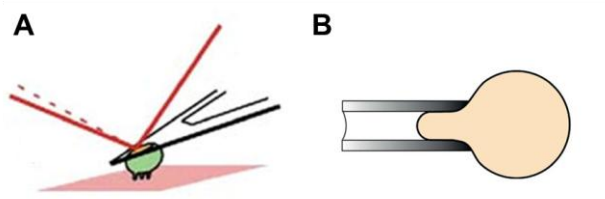

Figure 1.6. Schematic of whole cell detachment techniques. (A) Cytodetachment technique. (Adapted from reference 79) (B) Micropipette aspiration. (Adapted from reference 80)

Mechanical methods that study cell detachment events involve application of an external force to the adhered cells in order to free the cell from the substrate surface. The amount of applied force that detaches the cells is defined as the cell adhesion strength. Cell detachment studies can be separated into two main categories: whole cell detachment and cell population detachment. Whole cell detachment techniques focus on the removal of the entire single cell from its substrate, and the measured force represents the adhesion strength of a single cell. Several commonly used techniques for whole cell detachment are the cytodetachment and micropipette aspiration[81]. Cytodetachment technique uses an atomic force microscopy (AFM) probe to physically pull individual cells that are immobilized on a functionalized substrate away from the surface of the substrate[82]. The elastic deflection of the AFM probe is measured to quantify the force needed to detach the individual cell from the substrate surface (Figure 1.6A). The force per cell area gives the average shear stress of each cell[82]. The micropipette aspiration technique uses a micropipette to apply a suction force to aspirate the adhered cell from the matrix (Figure 1.6B). The minimal suction force needed to detach a cell from the surface provides information on the mechanical properties of the cell, such as the

adhesion strength of cells on different substrates materials, viscoelasticity of living cells, and cortical tension of cells[83].

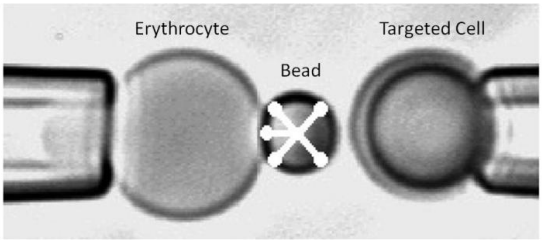

Figure 1.7. Set-up of a biomembrane force probe (BFP). (Adapted from reference 84)

Cell bond detachment techniques focus on the amount of force needed to break the adhesive bond between the cell and the substrate. The technique used to study cell bond detachment is single cell force spectroscopy (SCFS), which uses a nano/micromanipulator or micropipette to apply force to detach the cell. A microscope is used to observe the cell while it's being manipulated. SCFS offers two modes: an imaging mode and a force mode. The imaging mode is utilized to study the structures and mechanics of isolated biomolecules, cytoskeletal structures, and components of the cell nucleus. The force mode is used to examine the mechanical properties of the cell, such as the adhesion strength[85]. The most commonly used SCFS techniques for single cell detachment are AFM probe, biomembrane force probe (BFP), and optical tweezers. For the AFM probe technique, cells that are immobilized on an AFM cantilever exert their adhesion force onto the cantilever. The deflection of the cantilever is translated into the stiffness and adhesion strength of individual cells[86]. BFP is a versatile tool that has the ability to quantify single molecular bonds in a wide range of forces (0.1 pN to 1 nN). The probe used in BFP is a biotinylated erythrocyte with a streptavidin-coated glass bead

attached (Figure 1.7). The probe is then brought in close contact with the targeted cell, and adhesion will form between the probe and the cell. Once the adhesion is formed, the detachment force can be measured while the cell is being pulled away from the probe by a piezoelectric actuator[87]. Another SCFS method is optical tweezers, which uses a highly focused laser beam as the probe to capture and manipulate microscopic small dielectric particles. The dielectric particles can be precoated with different proteins. The coated dielectric particle is then brought into adhesive contact with a cell attached to a surface (Figure 1.8). Then the particle is pulled away from the cell by increasing the laser power until the trapping force is strong enough to detach the particle from the cell. The technique is able to measure forces less than pN[88].

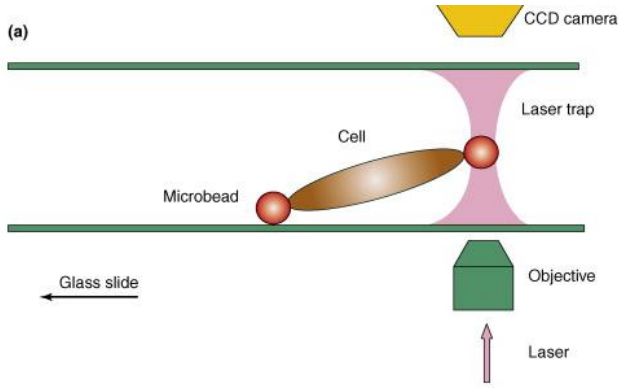

Figure 1.8. Schematic diagram showing an example of an optical tweezers setup. (Adapted from reference 89)

Cell population detachment techniques focus on the measurement of the force needed to remove 50 % of the cell population. Some cell population techniques use centrifugation, spinning disk, and flow chamber. Centrifugation assay is a commonly used method to measure cell adhesion strength because of the simplicity of the

measurement and accessibility of the equipment in laboratories. The assay begins with the immobilization of cells in a multi-well plate. Then the plate is spun in a certain centrifugal force to detach the cells[90]. Spinning disk uses a rotating disk device to produce a shear stress. To apply cells on the rotating disk, cells are seeded onto a round glass cover slip and the cover slip is mounted onto the rotating device. Then the disk will rotate between 500 – 3000 rpm. The cells are counted to determine the fraction of cell still adhered before and after spinning[91]. Flow chamber utilizes a fluid flow to induce a shear stress on the cells for the measurement of adhesion strength. There are two types of flow chambers, the radial flow chamber and parallel chamber, and these types differ by the directionality of the flow of fluid within the chamber. The cells are immobilized on a substrate within the flow chamber and fluid is pumped in and out through the inlet and outlet of the chamber, respectively. The constant flow of fluid produces a shear stress to detach the cells from the surface. The shear stress can be controlled by flow rate of the fluid[92].

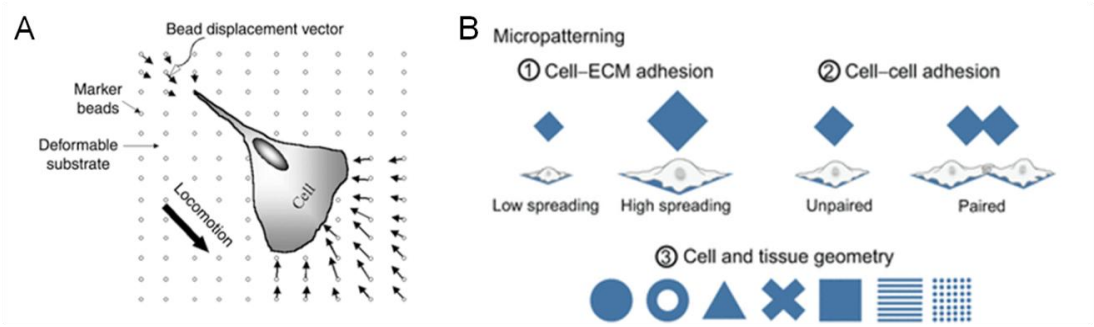

Figure 1.9. Schematic of techniques studying cell adhesion patterns. (A) Polyacrylamide gel-based traction force microscopy (PA-TFM). (Adapted from reference 93) (B) Cell micropatterning. (Adapted from reference 94)

The study of cell attachment focuses on examination of the formation of adhesion bonds between the cell's surface receptors and/or the substrate surface as well as examination of cellular behavior, such as changes of morphology during the cell attachment[78]. Examination of individual cells by assessing the interaction forces between a single cell and its substrate is particularly effective to provide information on the cell's migration patterns and traction forces. Methods, such as polyacrylamide (PA) gel-based traction force microscopy (PA-TFM) and micropatterning technique, are commonly used for such study. PA-TFM probes the force exerted by individual cells through contact to the substrate surface also known as traction force. When cells attach onto the surface of a polyacrylamide gel embedded with fluorescent beads, the cells will produce traction force that will move the fluorescent beads. The displacement of the fluorescent beads can be tracked and used to quantify the cell adhesion and movement (Figure 1.9A)[95]. Cell micropatterning involves fabricating a cell substrate with microscopic features that imposes their effects on the cell's attachment, shape and spreading (Figure 1.9B). This method has been found effective in investigating the response and sensitivity of a cell to specific environmental cues[96].

The adhesion behavior of a group of cells is often examined by either wash assay or microfluidic techniques. Both of these techniques can provide information on cell adhesion based on the balance between adhesive forces of the cells and the dispersive hydrodynamic forces due to the fluid flow[97]. For the wash assay, cells are cultured in multi-well plates under static flow conditions. After the removal of all the non-adhered cells with washing, the adhered cells can be analyzed with the use of cell counting, DNA content analysis, antibody binding, specific protein quantification, etc.[78] In microfluidic

techniques, the cells cultured inside a channel are examined under dynamic flow conditions. Such conditions could be used to mimic the blood flow in the human body and allow for the examination of cell spreading and migration under the influence of a fluid flow.

1.3.2 Imaging Methods to Study Cell Adhesion

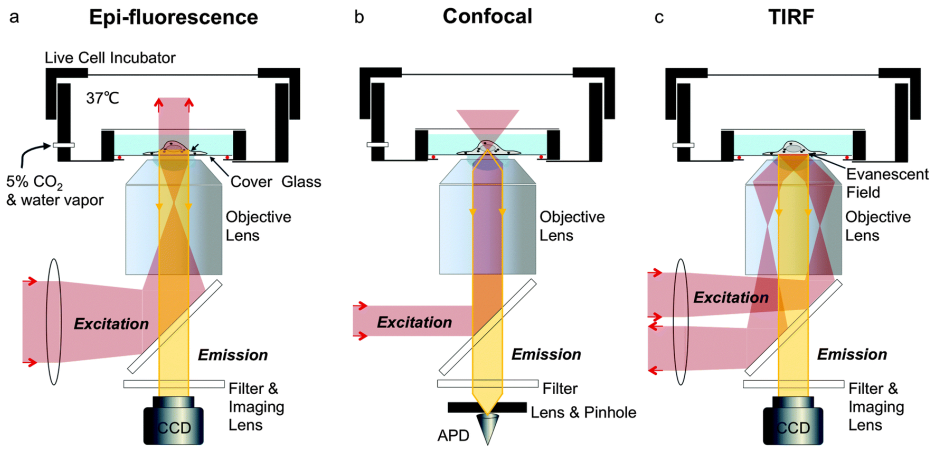

Figure 1.10. Schematic of microscopy techniques. (a) Wide field microscopy also known as epi-fluorescence microscopy. (b) Confocal microscopy. (c) TIRF (total internal reflection fluorescence) microscopy. (Adapted from reference 98)

Imaging methods focus on the visualization and tracking of the cell and its adhesion-associated structures, such as actin filaments and specific proteins in the focal adhesion complexes. Advancements in instrumentation have allowed imaging methods to study molecular interactions and dynamics within living cells with high resolution. Most of imaging methods use fluorescent tags (protein or dye) to visualize, track, and quantify adhesion-associated structures. The main stream imaging methods include wide field microscopy, point-scanning confocal microscopy, and total internal reflection

fluorescence microscopy. The most widely used method to image fluorescently labeled protein is wide field microscopy. In wide field microscopy, light passes through a filter set and then through a dichromatic mirror. Next, the shorter wavelength of light is reflected onto the sample through an objective. Finally, the longer wavelength emitted light from the florescent tags in the sample travels back through the objective and passes through the dichromatic mirror to be collected by a camera (Figure 1.10a). This technique provides a direct visualization of the entire cell and allows the location of the target molecules to be readily defined[99]. A more advanced microscopy technique is point-scanning confocal microscopy. In this technique samples are illuminated by a laser of a specific wavelength instead of a light source used in wide field microscopy (Figure 1.10b). The use of a laser to illuminate specific regions of the sample instead of the entire sample minimizes out-of-focus background fluorescence and offers higher sensitivity and resolution compared to the wide field microscopy[100]. Total internal reflection fluorescence (TIRF) microscopy is the ideal method to image cell–matrix interactions. In TIRF, cells attached on a transparent surface (e.g., glass slide) are illuminated with a laser beam through the transparent surface. The laser beam is positioned to go through the solid/liquid interface at an angle that is equal or greater than the critical angle of total internal reflection to produce evanescent wave. The evanescent wave penetrates and illuminates the sample in a very short depth of approximately 100 nm (Figure 1.10c). This small illumination region leads to a high signal-to-noise ratio and highly sensitive detection of adhesion structures[101].

1.3.3 Use of Label-Free Whole Cell Assay to Study Cell Adhesion

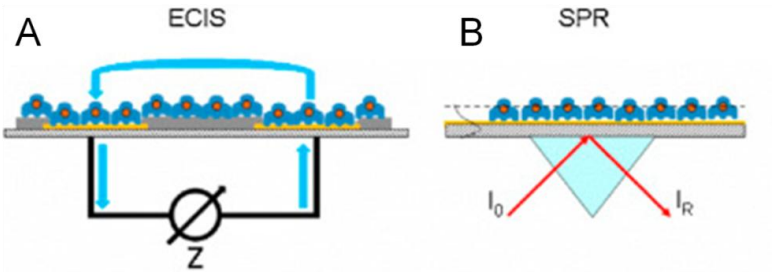

Figure 1.11. Schematic of label-free whole cell assay. (A) Electric cell-substrate impedance sensing (ECIS). (B) Surface plasmon resonance (SPR). (Adapted from reference 102)

Label-free whole cell assays measure the integrated cellular response that reflects the overall cellular response to the external stimulation[61]. In addition, label-free whole cell assays do not need labels that may potentially alter the physiological cellular environment for the targets of interest. Current label-free whole cell assays are primarily based on impedance, optical, or acoustic sensor technologies, which can detect changes in cellular features, such as cell adhesion, cell morphology, cell proliferation, and cell death[62-64]. Label-free whole cell assays have the ability to measure responses in real time and provide time-dependent profiles of cellular responses. These profiles are able to provide information on the kinetics of cellular response. Impedance and optical sensor technology will be briefly discussed here and acoustic sensor technology (e.g., quartz crystal microbalance) will be discussed in Chapter 2.

Impedance-based cell monitoring technology was invented by Drs. Ivar Giaever and Charles R. Keese in 1984 and is currently known as electric cell-substrate impedance sensing (ECIS) (Figure 1.11A)[103]. The core components of the impedance sensor are two electrodes, one small working electrode and one large counter electrode. Live cells in

medium are grown between the two electrodes and a sinusoidal voltage is applied to the sensor to generate electric field between the electrodes[104]. The presence of cells impedes on the electric field because the cell membrane can act as an insulating agent. This then forces the current to flow between or beneath the cells, which leads to changes in impedance. The impedance is a measurement of the changes in the electrical conductivity or permeability of the cell layer[105]. Impedance-based measurements have been applied to study a wide range of cellular events, including cell adhesion and spreading[106], cell micromotion[107], cell morphological changes[106], cell death[108], and cell signaling[109].

Optical sensor technology has been widely used for diverse biological applications[60, 104], including receptor biology[110], ligand pharmacology[111], and cell adhesion[112, 113]. The one that is most widely used for cell study is surface plasmon resonance (SPR). In SPR, a polarized light strikes an electrically conducting surface between two media at a specific angle known as the resonance angle (Figure 1.11B). This then generates an electron charge density wave also known as plasmon. At the resonance angle, the minimal light is reflected back to the detector[62]. When a material binds to the sensor surface, this causes the resonance angle to shift, and the shift is in proportion to the mass of the material attached to the sensor surface.

Chapter 2: Introduction of Quartz Crystal Microbalance (QCM) Technology

2.1 Basic Principles of QCM Technology

The QCM is an acoustic sensing device that is capable of probing the surface interaction based on changes in mass and mechanical properties of the material coupled to the sensor surface. The QCM has been utilized in chemical[67], physical[71], biological[72, 73], and biomedical research[74]. In recent years, the QCM has begun to show its effectiveness in cell biology studies with a special focus on cell-surface interactions[114-120]. This is because the QCM is not only highly sensitive and easy to use, but more importantly label-free and non-invasive, two of the most important factors to the success of cell studies.

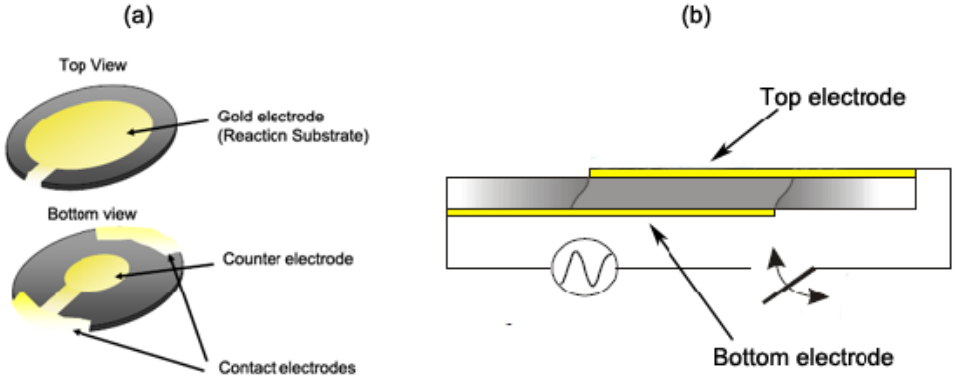

Figure 2.1. Schematic diagram of a quartz crystal sensor. (a) Top and bottow views of the sensor. (b) Cross-sectional view of the sensor. (Adapted from QSense®, (http://www.biolinscientific.com/q-sense/))

The key component of the QCM sensor system is a thin AT-cut quartz disk of 14 mm in diameter and less than 0.5 mm in thickness. Two metal electrodes are positioned on the top and bottom sides of the quartz disk (Figure 2.1). Quartz crystals are found in two main types of cuts, X-cut and AT-cut, and different cut types will produce different

piezoelectric responses[121]. The X-cut crystal is cut normal to the x-axis. The main problem with this type of crystal is there are large frequency drifts with temperature[122]. In 1934, Lack *et al.* were the first to introduce AT-cut crystals[123]. The "T" specifies that the quartz is a temperature-compensated cut, and the "A" stands for the first of such cuts to be discovered. AT-cut crystals are obtained by cutting the quartz crystal at an angle of 35^{o} from the z-axis[122] (Figure 2.2). This AT-cut type is used widely in the industry because it delivers good performance over a wide temperature range.

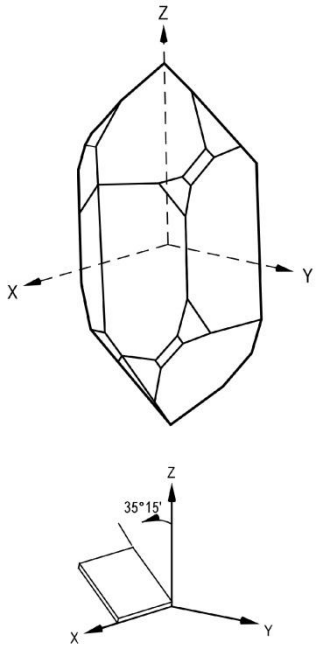

Figure 2.2. Illustration of AT-cut quartz crystal. (Adapted from reference 122)

When an oscillating current is applied, the quartz crystal, which is a piezoelectric material, undergoes an in-plane shear-mode oscillation[124]. Such oscillation is sensitive to the change in mass coupled to the sensor surface, which shifts the resonance frequency of the oscillating crystal. In 1959, Sauerbrey showed that the change in resonance frequency

is linearly proportional to the change in mass coupled to the surface of the quartz crystal[125],

$$\Delta m = -\frac{C}{n}\Delta f_n \qquad (1)$$

where Δf_n is the change in resonance frequency of the oscillating crystal vibrating at the nth mode, Δm is the mass deposited per unit area of crystal surface, and C is the mass sensitivity constant of the instrument. For a 5-MHz crystal, C is 17.7 ng/Hz·cm^2. The Sauerbrey equation is valid when the material coupled to the sensor surface is much lighter than the mass of the quartz crystal, and the adhered material is rigid and elastic and evenly distributed over the sensor surface. When the above criteria are met, the resonance frequency of the oscillating crystal is sensitive to the nanogram-scale change of mass. Across the disk-shaped sensor crystal, the mass sensitivity follows a Gaussian like distribution: the center of the disk has the maximum mass sensitivity and the sensitivity decreases exponentially towards the edge of the disk.

In the early years of the QCM, most studies that were focused on chemical and surface modification research were conducted *in vacuo* and/or gas phase[126]. Later on the QCM was adapted to applications in liquid medium, such as biotechnology and biosensing. One major drawback encountered in such applications was that the shift of resonance frequency no longer obeys the Sauerbrey relationship due to the viscous damping of the oscillating crystal by the liquid medium. To assess the damping effect, the QCM instrument was reconfigured as quartz crystal microbalance with dissipation monitoring (QCM-D) to measure not only the change in frequency Δf, but also the change in energy dissipation factor ΔD of the oscillating sensor crystal[124, 127]. The energy dissipation factor D is a dimensionless quantity that is defined as,

$$D = \frac{E_{dissipated}}{2\pi E_{stored}} \quad (2)$$

where $E_{dissipated}$ is the energy dissipated during one cycle of oscillation and E_{stored} is the total energy stored in the oscillating system. ΔD is typically used to quantify the change of energy dissipation and can be determined in the QCM-D based on the time-dependent decay of the freely oscillating crystal after the rapid excitation[124, 127]. Some other QCM instruments measure the change in energy dissipation in motion resistance (ΔR), which is equivalent to ΔD measured by the QCM-D[128, 129].

The QCM technique is considered non-invasive to mammalian cells, because the lateral displacement of the surface of the sensor crystal during oscillation rarely exceeds 1 nm[130]. Secondly, the sensing region is limited to a narrow region between the bottom of the cell layer and the sensor surface. This sensing region can be determined based on the penetration depth (δ) of the shear wave generated by the oscillating sensor crystal through the following:

$$\delta = \sqrt{\frac{\eta}{\pi \rho f_n}} \quad (3)$$

where η is the viscosity of the liquid, ρ is the density of the liquid, and f_n is the frequency of the n^{th} mode of vibration[124]. An estimate of δ can be made by assuming cells have similar properties as water. For mode n = 3, the shear wave has a penetration depth of approximately 100 to 150 nm from the surface of a 5-MHz sensor disk[131]. This depth coincides with the distance between the bottom of the cell layer and the surface of the substrate[132]. Therefore the QCM is highly sensitive to the change of cell adhesion while much less sensitive to any change above the basal region of the cell[133].

Taking into account that the cell membrane is an organized system, the viscosity of cells compared with water could vary. Bicknese *et al.* examined the cytoplasmic viscosity near the cell plasma membrane and determined the viscosity of the cell plasma membrane is 1.1 ± 0.2 cP at 37^{o}C compared with 0.70 cP for water at 37^{o}C[134]. Use of these viscosities in equation 3 to determine the penetration depth gives values that differ only by a factor of 1.25. Either way, the sensing region is still within the basal region of the cell.

2.2 Detection of Cell-Substrate Adhesion

Some of the earliest cell studies were focused on the adhesion of various cell types[133, 135-139]. In those studies, the entire cell adhesion process on the QCM sensor surface was examined in real time. These experiments demonstrated a correlation between the surface coverage with cells and the changes in resonance frequency Δf of the sensor crystal[135, 136, 140]. Such correlation is more qualitative and does not obey the Sauerbery equation. This is consistent with the fact that cells behave more like a viscoelastic material, not like a rigid mass[133, 137-139].

The process of cell attachment also shifts energy dissipation response ΔD or motion resistance response ΔR[133, 139, 141-145]. The ΔD-response has been primarily used as a qualitative measurement of mechanical properties of cell adhesion. The exact components or mechanical processes that cause the change in energy dissipation still remain controversial. Rodahl *et al.* attributed the energy dissipation to the damping by the liquid medium trapped between the cell and the substrate surface, in the cell membrane, and in the interior of each cell[141]. Wegner *et al.* suggested several possible dissipative

processes, such as the deposition of ECM, the change in structure and mechanical properties of cellular components, including actin cortex and cell membrane[133]. Marx *et al.* proposed that the dissipation is due to the remodeling of actin filaments that are intrinsically connected to cell adhesion molecules[143]. Our recent modeling study suggests that the rupture of cell-ECM bonds is primarily responsible for the observed energy dissipation, whereas either viscous damping by the trapped liquid or viscous slip of the stress fibers can also be a major contributor depending on the stage of cell adhesion. A comprehensive understanding of the energy dissipation response is essential for the development of a theoretical framework needed for QCM-D based cell study.

To evaluate the cell adhesion, Fredriksson *et al.* used the ratio of $\Delta D/\Delta f$ to quantify the energy loss per unit of attached cell mass and compare the effects of cell types and surface coatings on cell adhesion[142]. This ratio, when plotted against time, provides information on the kinetics of the cell adhesion process as well as the time-dependent change in mechanical property of the adhered cell layer.

2.3 Application of the QCM Detection in Other Areas of Cell Study

2.3.1 Examination of Material Biocompatibility

Understanding the mechanisms of cell-substrate interactions has provided the motivation for the development of biomaterials in medical implants and tissue engineering. The most important property of biomaterial is its biocompatibility, which is typically evaluated based on how well target cells adhere and grow on the material surface. In recent years, the QCM has been used for such evaluation because of its ability to monitor the cell adhesion process in a non-invasive and real-time manner[146-149].

Tantalum (Ta) and chromium (Cr) are two medically relevant surfaces found in biomedical implants. The QCM was used to compare the adhesion of pre-osteoblastic cells on these two surfaces[139]. The results showed larger frequency and energy dissipation shifts when cells adhered to the tantalum-coated surface, suggesting that tantalum is more biocompatible than chromium. Hydroxyapatite, a surface coating that has been widely used for implants, has also been examined with the use of the QCM for its effectiveness in cell attachment[146-148]. The ability of evaluating real-time cell-substrate interactions with high sensitivity makes the QCM a useful bio-analytical tool to assess the material biocompatibility.

2.3.2 Detection of Biomarkers

Dysregulation of cellular processes are responsible for the development of many diseases. A detailed understanding of these cellular processes and quick determination of the abnormality in the processes can provide the information needed for the early diagnosis and successful treatment of many human diseases. The QCM sensor system has shown the sensitivity and time resolution required for measurement of the signature responses of the cell during the cellular processes including growth[150], apoptosis[34], morphological change[151, 152], cell cycles[153], signaling transduction[154, 155], migration[156], etc. The signature responses in the form of Δf and/or ΔD reveal changes in cell morphology, cell mechanics, cell adhesion, etc. and can be utilized for identification of the dysregulated cellular processes and serve as potential biomarkers for medical diagnosis.

The mechanical properties of cells have been closely linked to the physiological state of the cells[157]. For example, malignant cancer cells often appear to be softer than

normal cells[158, 159]. Zhou *et al.* used the QCM to evaluated viscoelastic properties of two different cell lines, HMEC (normal breast cells) and MCF-7 (malignant breast cells), based on the cell viscoelastic index (CVI=$\Delta R/\Delta f$), during the adhesion and spreading processes[152]. They determined MCF-7 cells were softer than HMEC cells during cell adhesion because MCF-7 cells exhibited a CVI that was 2.5-fold lower than HMEC cells. Zhang *et al.* also used the $\Delta D/\Delta f$ ratio to determine that diabetic red blood cells (RBCs) appeared stiffer than normal RBCs when adhering to endothelial cells[160]. Abnormal RBC cells have been associated with vascular complications in diseases, such as diabetes, sickle cell anemia, and malaria[160].

Expression levels of specific receptors have a prominent influence on the physiological state of the cell and can be used as biomarkers of human diseases [43, 70, 161]. Garcia *et al.* studied the effect of EGFR expression on cell adhesion[162]. The abnormality in expression of EGFR can interfere with the regulation of EGFR signaling pathways[163] and may lead to the development of epithelial malignancies in humans[164]. Furthermore, overexpression of EGFR, which has previously been linked to enhanced cell motility, plays a crucial role in tumor invasion and metastasis[163, 165]. The study by Garcia and coworkers showed that cells that overexpress EGFR were able to disassemble the focal adhesions more rapidly and remain in a low adherent state for a longer period of time than cells that express normal levels of EGFR. Their results suggest that EGFR-overexpressing cells may be in a more favorable state for the initiation and maintenance of cell migration.

The adhesion pattern/strength is also a characteristic of the physiological state of the cell. Chronaki *et al.* used the QCM to examine the difference in adhesion pattern

between normal and cancer human thyroid cells on different surfaces, including titanium, gold, and fibrinogen-coated gold cancer[166]. Their results indicate that the two types of cells demonstrate different adhesion patterns and can be potentially used as a diagnostic tool for thyroid cancer. In recent years, the detection of whole cells has shown significant importance in clinical diagnosis of cancer and cancer therapy. One of the major challenges of such an approach in detection of cancer cells is to find cancer-selective probes that are highly specific towards the binding of the targeted cancer cells[167]. Shan *et al.* developed an aptamer-based QCM biosensor[168] for detection of leukemia cells. The aptamer-based QCM sensors were modified with the immobilized aptamer that specifically recognizes the leukemia cells. Zhang *et al.* successfully developed a chitosan–folic acid conjugated QCM sensor to detect and capture MCF-7 breast cancer cells through the specific binding of folic acid to folate receptors that are overexpressed on the MCF-7 cancer cell membrane[169]. Atay and coworkers constructed a QCM sensor to detect highly metastatic breast cancer cells with the immobilized transferrin molecules on QCM sensor surface[170]. Highly metastatic breast cancer cells are known to express a higher level of transferrin receptors compared to less metastatic breast cancer cells[171, 172]. The capability of QCM in differentiating metastatic stages of cancers cells can potentially be useful for the screening of patient serum or biopsy samples for metastatic breast cancer cells.

In summary, the QCM is a non-invasive measuring device that can track changes of specific cellular functions and/or properties in a real-time manner. Such capability of the QCM can be utilized to detect biomarkers for diagnosis and prognosis of human diseases. The QCM-based biomarker detection has the advantages over many of the

conventional methods, which are expensive and time-consuming, and require high expression of protein markers or antibodies present in the test samples[173].

2.3.3 Evaluation of Cell-Drug Interactions

The cell-based QCM sensor system has shown the capability in evaluation of the cell-drug interactions. Garcia *et al.* evaluated the effects of selected inhibitors of downstream signaling pathways of the EGFR on the EGF-induced de-adhesion of engineered MCF-10A cells[174]. The potencies of these inhibitors were determined and are correlated well with the values reported in the literature. Elmlund *et al.* used the QCM to examine the effects of trastuzumab, a humanized anti-HER2 monoclonal antibody, on the overexpressed human epidermal growth factor receptor 2 (HER2) of SKOV-3 epithelial cancer cells[175]. It has been reported that HER2 receptors are overexpressed in many aggressive forms of breast cancers.

The QCM has also been used to evaluate the response of tumor cells to chemotherapeutics. Braunhut *et al.* used the QCM to examine responses of human mammary epithelial tumor cells to taxanes[143]. They observed the characteristic shifts of frequency and motion resistances during the apoptosis of tumor cells. These distinct shift patterns can potentially provide an indicator for predicting therapeutic outcome prior to treating a patient. Similar cytotoxcity studies have been conducted with gold nanoparticles and paclitaxel on HepG2 cells[176], adriamycin and selenium nanoparticles on Bel7402 cells[177], selenium ferroferric oxide nanoparticles on osteoblast-like MG-63 cells[178], derivate of vitamin E α-tocopherol amidomalate on WB F344 and B16F10 cells[179], gallic acid and anthocyanins on HT1080. The designing and implementing fast,

cost-effective and informative evaluation of cell-drug interactions is a critical step in the early stage of the drug discovery process. It is a critical step because it allows for effective identification of novel leads in large compound libraries. Since the QCM technique is a highly sensitive method for the evaluation of cell-drug interactions, QCM may become a forthcoming approach for the drug screening process.

Chapter 3: Materials and Methods

3.1 Materials

Table 3.1. Cell lines

Cell Line Number	Source of Cell Line	Manufacturer
A431 (CRL-1555)	Human epidermoid carcinoma	ATCC (Manassas, VA)
MCF-10A (CRL-10317)	Human mammary epithelial	ATCC (Manassas, VA)
SK-OV-3(HTB-77)	Human ovarian adenocarcinoma	ATCC (Manassas, VA)
HEK 001 (CRL-2404)	Human epidermal keratinocyte	ATCC (Manassas, VA)

Table 3.2. Cell culture reagents

Reagent	Manufacturer
Cholera toxin	Sigma-Aldrich (St. Louis, MO)
Dulbecco's modified Eagle's medium	Invitrogen (Carlsbad, CA)
Dulbecco's modified Eagle's medium: nutrient mix F12	Invitrogen (Carlsbad, CA)
Fetal bovine serum	Invitrogen (Carlsbad, CA)
Horse serum	Invitrogen (Carlsbad, CA)
Hydrocortisone	Sigma-Aldrich (St. Louis, MO)
Insulin	Sigma-Aldrich (St. Louis, MO)
Keratinocyte-SFM	Invitrogen (Carlsbad, CA)
RPMI 1640 medium	Corning (Manassas, VA)
20X Phosphate buffered saline (20X PBS)	Teknova (Hollister, CA)
Penicillin/Streptomycin	Invitrogen (Carlsbad, CA)
Trypsin-EDTA	Invitrogen (Carlsbad, CA)

Table 3.3. QCM-D assay reagents

Reagent	Manufacturer
Hanks' balanced salt solution (HBSS)	Invitrogen (Carlsbad, CA)
4-(2-hydroxyethyl)-1-piperazineethanesulfonic acid (HEPES)	Invitrogen (Carlsbad, CA)
Dimethyl sulfoxide (DMSO)	BDH (London, England)
Sodium dodecyl sulfate (SDS)	J.T Baker (Philipsburg, NJ)

Table 3.4. Ligands and modulators

Ligand/Modulator	Manufacturer
Adenosine triphosphate (ATP)	Applichem (Darmstadt, Germany)
Bradykinin (BK)	American Peptide (Sunnyvale, CA)
Chloera toxin (CTX)	Sigma (St. Louis, MO)
Cytochalasin D (CD)	Enzo Life Sciences (Farmingdale,NY)
Edelfosine	Fischer Chemicals (Fair Lawn, NJ)
Epidermal growth factor (EGF)	Peprotech (Rockhill, NJ)
Epinephirne (Epi)	MP Biomedical LLC (Santa Ana, CA)
Fibronectin (FN)	BD Biosciences (San Jose, CA)
Histamine dihydrochloride (Hist)	Alfa Aesar (Ward Hill, MA)
Isoproterenol hydrochloride (ISO)	EMD Bioscience (Darmstadt, Germany)
L-779450 (Raf kinase inhibitor IV)	EMD Bioscience (Darmstadt, Germany)
LY294002	Cayman Chemical (Ann Arbor, MI)
Lysophosphatidic acid (LPA)	Caymen Chemical (AnnArbor, MI)
5'-N-Ethylcarboxamidoadenosine (NECA)	Tocris Biosciences (Bristol, UK)
Nicotinic acid (NA)	Alfa Aesar (Ward Hill, MA)
PD158780	EMD Bioscience (Darmstadt, Germany)
PD98059	Enzo Life Sciences (Farmingdale,NY)
Pertussis toxin (PTX)	EMD Bioscience (Darmstadt, Germany)
Thrombin (Thr)	Fischer Chemicals (Fair Lawn, NJ)
U0126-EtOH	Selleckchem (Houston, TX)
U73122 1	Cayman Chemical (AnnArbor, MI)
Wortmannin	Enzo Life Sciences (Farmingdale,NY)
ZSTK474	Selleckchem (Houston, TX)

Table 3.5. Antibodies

Antibody	Source of Antibody	Manufacturer
Alexafluor 546	Goat	Invitrogen (Carlsbad, CA)
EGFR monoclonal antibody mAb 2E9	Human	Santa CruzBiotechnology, Inc. (Santa Cruz, CA)
Monoclonal mouse anti-vinculin	Mouse	Invitrogen (Carlsbad, CA)

Table 3.6. Cell staining reagents

Reagents	Manufacturer
Ammonium chloride	Amersco (Solon, OH)
Bovine serum albumin (BSA)	EMD Bioscience (Darmstadt, Germany)
Ethylene glycol tetraacetic acid (EGTA)	EMD Bioscience (Darmstadt, Germany)
4-(2-hydroxyethyl)-1-piperazineethanesulfonic acid (HEPES)	J.T Baker (Philipsburg, NJ)
Magnesium chloride	BDH (London, England)
Paraformaldehyde (PFA)	Electron microscopy sciences, (Hatfield, PA)
Piperazine-N,N′-bis (PIPES)	J.T Baker (Philipsburg, NJ)
Triton X	Amersco (Solon, OH)
Vectashield	Vector Laboratories (Burlingame, CA)

Table 3.7. Instrumentation

Instrumentation	Manufacturer
Nanoscope IIIA multimode atomic force microscope	Digital Instruments, Inc. (Tonawanda, New York)
Q-Sense Analyzer (QCM-D E4)	Biolin Scientific Q-Sense (Stockholm, Sweden)
Q-Sense open module (QOM 401)	Biolin Scientific Q-Sense (Stockholm, Sweden)
Zeiss Axioplan 2 microscope system	Scientific Imaging Company (Campbell, CA)

Table 3.8. Software

Software	Description	Manufacturer
ImageJ software	Used to process fluorescence images	National Institutes of Health (Bethesda, MD)
Origin software	Used to graph and analyze QCM-D data	Origin (Northampton, MA)
Qsoft 401 2.0.0.275 software	Used to monitor and record the ΔD and Δf	Biolin Scientific Q-Sense (Stockholm, Sweden)
Qtools software (Qsoft 3.0.1.178)	Used to convert Qsoft data files to excel data files	Biolin Scientific Q-Sense (Stockholm, Sweden)
Slidebook 5.0 software	Used to take and process fluorescence images	Intelligent Imaging Innovations (Denver, CO)

3.2 Solution and Sample Preparation

3.2.1 Cell Culture Medium

DMEM growth medium contains the following additives to the DMEM medium: 10 % FBS, 100 U/mL penicillin, and 100 μg/mL streptomycin. (U/mL is a unit used for enzyme activity; 1 U/mL is the amount of enzyme that catalyzes conversion 1 micromole of substrate/min.) DMEM/F12 growth medium contains the following additives to the DMEM/F12 medium: 5% horse serum, 20 ng/mL EGF, 0.5 μg/mL hydrocortisone, 50 ng/mL cholera toxin, 10 μg/mL insulin, 100 U/mL penicillin, and 100 μg/mL streptomycin. RPMI 1640 growth medium includes the following additives to the RPMI 1640 medium: 10 % FBS, 100 U/mL penicillin, and 100 μg/mL streptomycin. Keratinocyte-SFM growth medium contains: 20 ng/mL EGF, 2 mM L-glutamine, 100 U/mL penicillin, and 100 μg/mL streptomycin. DMEM, DMEM/F12, RMPI 1640 serum free growth medium were prepared with the addition of 100 U/mL penicillin and 100 μg/mL streptomycin to the corresponding media. Keratinocyte-SFM serum free medium were prepared with the addition of 2 mM L-glutamine, 100 U/mL penicillin, and 100 μg/mL streptomycin to the Keratinocyte-SFM medium.

3.2.2 Assay Buffer and Sample Preparation

1X PBS rinsing buffer was prepared from the dilution of 20X PBS stock in distilled water and autoclaved at 121^{o}C and 2 x 10^{5} Pa for 20 min. The QCM-D assay buffer (20 mM HEPES, pH 7.2) was prepared from the dilution of 100 mM HEPES buffer in HBSS buffer. No pH adjustment is needed.

3.2.3 Cell Staining Solutions

1X PHEM buffer was used in cell staining procedures. 1X PHEM buffer contains 60 mM PIPES, 25 mM HEPES, 10 mM EGTA, 2 mM $MgCl_2$. Concentrated NaOH was added to adjust the pH of 1X PHEM buffer to 6.9. Cell fixation solution contains 3 % PFA and 0.1 % Triton X100 in 1X PHEM buffer. Quenching solution contains 0.25 % ammonium chloride in 1X PBS solution. Blocking solution contains 2 % BSA and 0.1 % Triton X100 in 1X PBS solution.

3.3 Cell Culture Methods

Cell culturing was performed under sterile conditions in a bio-safety cabinet. All cell lines were seeded in T75 Corning culture flasks and maintained under a humidified atmosphere at 37°C and 5 % CO_2. Change of the medium took place three times a week and subculturing of cells took place once a week. The cells were usually harvested at 90-95 % confluency. A431 cells were cultured in DMEM medium containing 10 % FBS, 100 U/mL penicillin, and 100 μg/mL streptomycin. Wild-type MCF-10A cells were cultured in DMEM/F12 medium containing 5 % horse serum, 20 ng/mL EGF, 0.5 μg/mL hydrocortisone, 50 ng/mL cholera toxin, 10 μg/mL, 100 U/mL penicillin, and 100 μg/mL streptomycin. SKOV-3 cell were cultured in in RPMI1640 medium containing 10 % FBS, 100 U/mL penicillin, and 100 μg/mL streptomycin. HEK001 cells were cultured in Keratinocyte-Serum Free medium containing 5 ng/mL EGF, additional 2 mM L-glutamine, 100 U/mL penicillin, and 100 μg/mL streptomycin.

3.4 Sensor Preparation

QCM-D sensors were prepared by washing the sensors with ethanol and water. Then the sensors were exposed to UV/ozone for 20 min and UV light in a tissue culture hood for another 30 min. Next each sensor with gold surface facing upward was placed in a 12-well tissue culture plate. The sensor coated with cells was prepared as follows: when cells reached 90-95 % confluency, the growth medium was removed and the adhered cells were rinsed with PBS buffer twice to remove the residual medium. Next 0.25 % trypsin–EDTA was added and the cells were allowed to be incubated in the 37°C/5 % CO_2 incubator for 10 min. Once the cells were detached from the bottom of the flask, the growth medium was added to quench the trypsin digestion. The detached cells were then transferred to a 15-mL centrifuge tube and spun at 1,200 rpm for 4 min. The supernatant was aspirated off and replaced with fresh growth medium. The pellet of cells was broken up by gently pipetting the cells up and down. The cell density (cell/mL) was determined by application of an optical grid to 10 μL of cell suspension on a glass slide, and the number of cells in each grid space was counted under the microscope. The volume of suspension placed onto freshly prepared QCM-D sensors in a 12-well plate was controlled so that the same number of cells was seeded onto each sensor. Once the cells were settled down onto each sensor, the 12-well plate was placed in a humidified atmosphere at 37°C and 5 % CO_2 to allow the cells to adhere to the sensors and grow. Upon reaching 90–95 % confluency, the cells were washed with PBS buffer and starved in the corresponding serum-free medium for 18 h prior to QCM-D measurements.

3.5 QCM-D Measurements

A Q-sense analyzer (QCM-D E4, Biolin Scientific) was used to record changes in the energy dissipation factor (ΔD) and the resonance frequency ($\Delta f_n/n$) as a function of time at third mode of vibration (n=3). For simplicity, Δf is used to represent $\Delta f_3/3$. Typically at least 10 replicates were done of each experiment described in subsequent chapters, and the figures present representative QCM profiles.

3.5.1 Ligand and Pharmacological Modulators Studies

All measurements were performed on 14-mm diameter gold-deposited, AT-cut sensor crystals with a fundamental frequency of 5 MHz (QSX 301). On the day of the QCM-D measurement, the cells grown on the sensors were carefully rinsed with assay buffer (20 mM HEPES in HBSS buffer, pH 7.2). The bottom surface of each sensor where the electrical circuitry is located was dabbed dried with a Kimwipe to remove residual buffer. Each sensor was mounted in an open module (Q-sense) and surfaces were covered with 400 μL of the assay buffer. The modules were then mounted onto the QCM-D platform and incubated at 37°C until stable baselines were achieved. Then the assay buffer was removed from each module, and a pre-warmed solution containing a ligand compound in 400 μL of the assay buffer was added. Δf and ΔD were monitored and recorded simultaneously at 37^{o}C for 2 h upon the addition of the ligand compound. For experiments involving pre-treatments with pharmacological modulators, the cells were incubated with the pretreatment solutions containing the modulators at 37°C for a minimum of 40 min prior to the addition of the ligand compound.

**The results reported in this thesis were from experiments done on gold-surfaced

crystals, but identical experiments done on silica-surfaced crystals yielded essentially identical results (Figure 3.1).

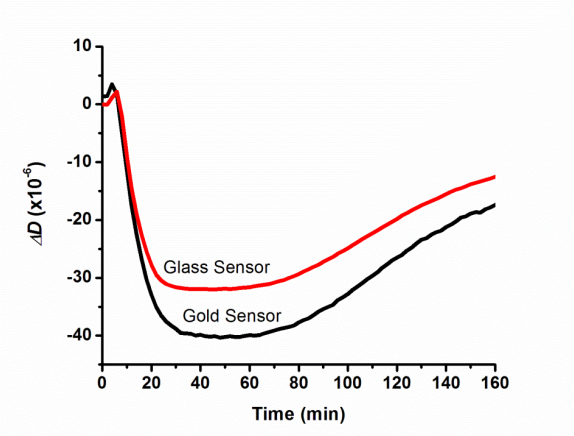

Figure 3.1. Comparison of real-time QCM-D measurements (at the third mode of vibration) of the EGF-induced Δ*D*-responses of MCF10A using gold coated quartz crystal sensors and glass coated quartz crystal sensors[155].

3.5.2 Cell Attachment/Cell Adhesion Studies

The QCM-D sensors were prepared from AT-cut quartz crystals in the form of 14-mm discs with a top surface-coating of a 120-nm thick layer of deposited titanium (QSX 310 Ti, Biolin Scientific). The QCM-D sensors were cleaned with water and ethanol and exposed to UV-ozone for 20 minutes. They were then transferred to a tissue culture hood, where they were exposed to UV light. Each sensor was then mounted into an open module (Biolin Scientific). To each of the four modules was added 600 μL of keratinocyte-serum free cell culture media with 20mM HEPES. The modules were maintained at 37°C for 50 minutes to achieve stable baselines. Samples of approximately 75,000 cells in 600 μL of keratinocyte-serum free cell culture media with 20 mM HEPES were prepared. Then the keratinocyte-serum free cell culture media in each module was

replaced with the prepared cell sample. Δf and ΔD responses were recorded simultaneously at 37^{o}C for 18-20 h upon the addition of cell samples. Ligands or modulators were added at the same time along with the cell samples when needed.

3.5.3 QCM-D Data Analysis

The dose-response curve was generated by fitting the average amplitudes (± 1 std. dev.) of ΔD-responses as a function of specific ligand concentrations with the following equation,

$$\Delta D = \frac{ax}{EC_{50} + x}$$

where x is the concentration of the ligand. a corresponds to the maximum ΔD-response, which can be determined through curve fitting. Amplitude is defined as the difference between the experimental value and the control value, each taken at its maximum or minimum ΔD-response and varies for each ligand examined. EC_{50} values were determined from the curve fitting with the aid of Origin software (Origin, Northampton, MA, USA). The use of the log functional plot or sigmoid plot for this analysis would not significantly alter the resulting EC_{50} values.

3.6 Immunofluorescence Imaging and Quantitation of Focal Adhesion

3.6.1 Immunofluorescence Sample Preparation

For immunofluorescence studies, cells were first seeded on coverslips in a 12-well tissue culture plate and then allowed to attach and grow in growth medium overnight in a humidified atmosphere at 37°C and 5 % CO_2. Next day, the cells were starved in serum-free growth medium for 18 h. The following day, the starved cells were pre-incubated in

assay buffer (20 mM HEPES in HBSS buffer, pH 7.2) at 37°C for 1 h. After pre-incubation, the assay buffer was replaced with 1 mL of pre-warmed ligand solution in assay buffer. The cells were incubated at 37°C with the ligand solution for various lengths of exposure time. Next the cells were fixed and permeabilized using a solution containing 0.1 % Triton X-100 and 3 % paraformaldehyde in PHEM buffer (60 mM PIPES, 25 mM HEPES, 10 mM EGTA, 2 mM $MgCl_2$, pH 6.9). After the fixation/ permeabilization step, vinculin, a cell adhesion complex protein, was immunostained with a combination of a primary monoclonal mouse anti-vinculin antibody (Invitrogen) at a concentration of 1:200 in blocking buffer (PBS with 2 % BSA) and a secondary Alexafluor 546 goat anti-mouse (Invitrogen) antibody at a concentration of 1:200 in staining buffer (PBS with 2 % BSA). After each step, the cells were rinsed thoroughly with blocking buffer. Lastly, the coverslip with cells were mounted onto glass slides using Vectashield medium with DAPI (Vector Laboratories, Inc., Burlingame, CA).

3.6.2 Fluorescence Imaging

The cells were examined and imaged with a wide field inverted fluorescence microscope Zeiss Axioplan 2 (Carl Zeiss, Thornwood, NY) equipped with a Plan-Apo 63x/1.40 NA objective, a deep cooled CCD camera (ORCA-AG; Hamamatsu Photonics). Images were taken in the TRITC channel at 50 ms exposures and processed with the use of Slidebook 5.0 software.

3.6.3 Fluorescence Quantitation

For quantitation of focal adhesion, ImageJ software (http://rsb.infor.nih.gov/ij/) was used. For each image a background area, an area of the image with no cells, was first selected and then ten randomly selected cells were selected and measured for fluorescence intensities. The fluorescence intensity of focal adhesions was determined by subtracting the background intensity from the immunostained vinculin fluorescence intensity of each selected cell. To determine statistical significance, p-values were determined (student's t-test) by comparing the fluorescence intensity between time points. A value of $p < 0.05$ was considered statistically significant.

3.7 Fibronectin-Coated Sensors

3.7.1 Coating Procedure

Prior to QCM-D experiments, the sensor crystals were cleaned with water and ethanol and exposed to UV-ozone for 20 minutes. They were transferred to a tissue culture hood, where they were exposed to UV light for a period of time. The sensors were then transferred into a 12-well plate and incubated in a solution of 30 μg/mL fibronectin in PBS at 37^{o}C for 1 h. Then they were rinsed with PBS twice, dried and mounted onto the open modules for QCM-D experiments.

3.7.2 Sensor Surface Characterization.

An AFM (Veeco NanoScope 3D multimode atomic force microscope) was used to examine the roughness of surface. 10 μm regions of the sensor surface were scanned at a rate of either 1.61 Hz or 4.07 Hz.

Chapter 4: Assessing EGF-Induced Cell De-Adhesion Using the Quartz Crystal Microbalance with Dissipation Monitoring **

4.1 Introduction

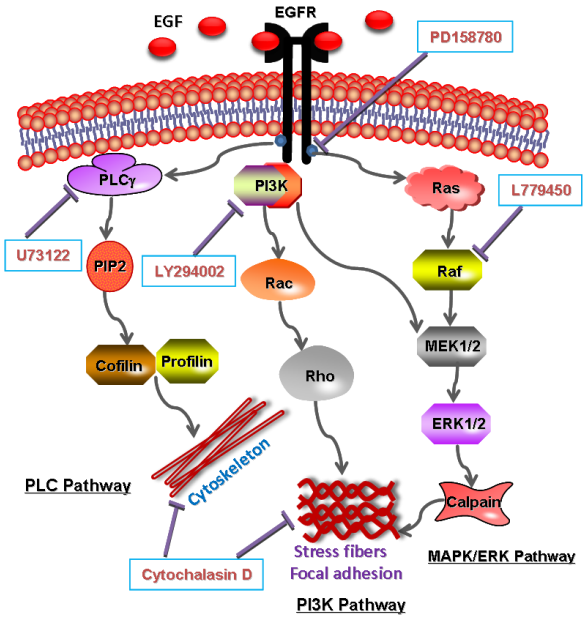

Figure 4.1. The three main downstream pathways of EGFR signaling that are potentially involved in regulation of cell de-adhesion of MCF10A cells. The possible targeted sites of pharmacological intervention are indicated with the name of each inhibitor. This map was created based on the original pathway map from SABiosciences (Valencia, CA)[155].

Adhesion to the extracellular matrix (ECM) and to adjacent cells is an essential biological process for cell survival, differentiation, and migration during embryonic development, adult homeostasis, wound healing, and tumorigenesis[180]. The primary class of membrane receptors mediating cell adhesion is integrins. Integrins can simultaneously

** Parts of this chapter are adapted from:
Chen, J.Y., Shahid, A., Garcia, M.P., Penn, L.S. & Xi, J. Dissipation monitoring for assessing EGF-induced changes of cell adhesion. *Biosens Bioelectron* **38**, 375-381 (2012).

bind ECM fibrils on the outside of cells and actin filaments (stress fibers) in the inside of cells[181]. The clustered integrins form adhesion complexes located across the bottom surface of cells known as focal adhesion, which are primarily responsible for cell attachment to ECM and substratum. These cell adhesion complexes are mediated by multiple signaling pathways including epidermal growth factor receptor (EGFR) mediated signaling pathways[182].

EGFR is a transmembrane receptor. When activated with the binding of epidermal growth factor (EGF), EGFR regulates cell growth, proliferation, motility and differentiation through its downstream signaling pathways [183, 184] (Figure 4.1), such as the mitogen-activated protein kinase/extracellular signal-regulated kinase (MAPK/ERK) pathway[185], the phosphoinositide 3-kinase (PI3K) pathway[49], and the phospholipase C (PLC) pathway[53]. Overexpression and/or mutation of EGFR may lead to dysregulation of these downstream signaling pathways and the development of epithelial malignancies such as cancers[163, 164]. It is known that EGF stimulation induces cell de-adhesion that often results from disassembly of focal adhesions[54, 186]. Cell de-adhesion is the reverse of cell adhesion, which leads to a weaker adhesion of adherent cells to the underlying substrate[187] and in part facilitates cell migration by allowing cells to break attachment at the rear while they form new attachments at the front[188]. The EGF-induced de-adhesion, which is mediated by the downstream signaling pathways of EGFR, is thought to be a critical step in normal embryonic development, wound repair, inflammatory response, and tumor cell metastasis[189].

In this chapter, we used the QCM-D technique to study cell de-adhesion mediated by EGFR signaling. Here we monitored the ΔD-response to EGF stimulation of human

breast epithelial cells (MCF10A). The observed time-dependent Δ*D*-response revealed a complex process that includes an initial fast cell de-adhesion, a transition, and finally, a slow re-adhesion. These aspects of the process were then compared both qualitatively and quantitatively with the results of fluorescence imaging. We also examined the role of three downstream pathways of EGFR signaling in the mediation of the de-adhesion process by assessing the effect of pathway-specific pharmacological intervention on the Δ*D*-responses. All three pathways, the phosphoinositide 3-kinase (PI3K) pathway, the mitogen-activated protein kinase/ extracellular signal-regulated kinase (MAPK/ ERK) pathway, and the phospholipase C (PLC) pathway, have previously been linked to the mediation of cell adhesion and de-adhesion in other cell lines[44, 45].

4.2 Results

4.2.1 Establishing the Δ*D*-Response Induced by EGF

To assess the EGF-induced cell de-adhesion process, first we used a QCM-D to track the short-term, EGF-induced response of confluent monolayers of human epithelial breast cells (MCF10A). Figure 4.2A shows the results of a typical QCM-D experiment in which both Δ*f*- and Δ*D*-responses at the third mode of vibration were recorded simultaneously for a confluent monolayer of MCF-10A cells to which 10 nM EGF had been added at 37°C. This mode of vibration specifically probes the basal area of the cell layer, which corresponds to an approximate depth of 100 nm from the surface of the sensor[131]. Once the EGF ligand was added to the cells, the Δ*D*-response curve exhibited a sharp upward spike and the Δ*f*-response curve exhibited a sharp downward spike. Both spikes were artifacts of the manual pipetting due to the addition of EGF to the cell layer.

After the initial spike, the Δ*D*-response curve shows a rapid decline that continues until ~40 min. This period is assigned as phase I of the Δ*D*-response. At ~40 min, the rate of the Δ*D*-response decline begins to decrease until a valley is reached at ~60 min. Then the curve displays a slow rise from the valley for the next 15 to 20 min. The transition of decreasing Δ*D* to increasing Δ*D* is defined as phase II of the Δ*D*-response. After the transition, the Δ*D*-response curve begins a steady increase for the next 80 min, which is assigned as phase III.

Next we examined the Δ*D*-response induced by EGF is dose dependent. Figure 4.2B shows the Δ*D*-responses at various concentrations of EGF. It is apparent that the higher the concentration of EGF, the greater the magnitude of the Δ*D*-response. The dose-dependency was further assessed by fitting the amplitude of the Δ*D*-response at 60 min as a function of the EGF concentration (Figure 4.2C). An EC_{50} value of 1.2 nM if used as an approximate measure of binding affinity [190] agrees well with K_d-values of EGFR obtained by others[191]. As an aside, it should be noted curve in figure 4.2C is not sigmoidal, nor is it semi-logarithmic when the values of the Δ*D*-response are converted to the corresponding natural logarithms. Absence of either of these features may surprise pharmacokineticists, but the absence is explained by the facts that the concentration range used in our experiments was too small to show such features, if they do indeed exist.

To further confirm the Δ*D*-response induced the EGF stimulation is mediated through the EGFR pathway, a potent inhibitor of EGFR tyrosine kinase, PD158780[192] was used to inhibit the EGFR signaling pathway. Figure 4.2D shows that the Δ*D*-response was substantially reduced when the cells were pre-treated with a 100 nM solution of PD158780 prior to the exposure to 10 nM EGF. All of these results indicate

that the Δ*D*-response is a highly sensitive and specific measure of EGF-induced cellular response mediated by EGFR signaling.

The QCM-D can monitor changes in energy dissipation and changes in resonance frequency. Unlike the Δ*D*-response, the Δ*f*-response showed no dose-dependence (Figure 4.2E). All of the Δ*f*-response curves exhibited similar changes as a function of time after recovering from the initial downward spikes. These curves show slight variation from each other and are close to the negative control (0 nM of EGF). Considering that the Δ*f*-response measures primarily the change in mass, the results in Figure 4.2E indicate that the basal area of the cell layer exhibits a minimal mass change as a result of EGFR signaling. Overall, the Δ*f*-response is not as sensitive and specific a measure of EGF-induced cellular response as its counterpart in Δ*D*-response, and so further attention will be focused only on the Δ*D*-response.

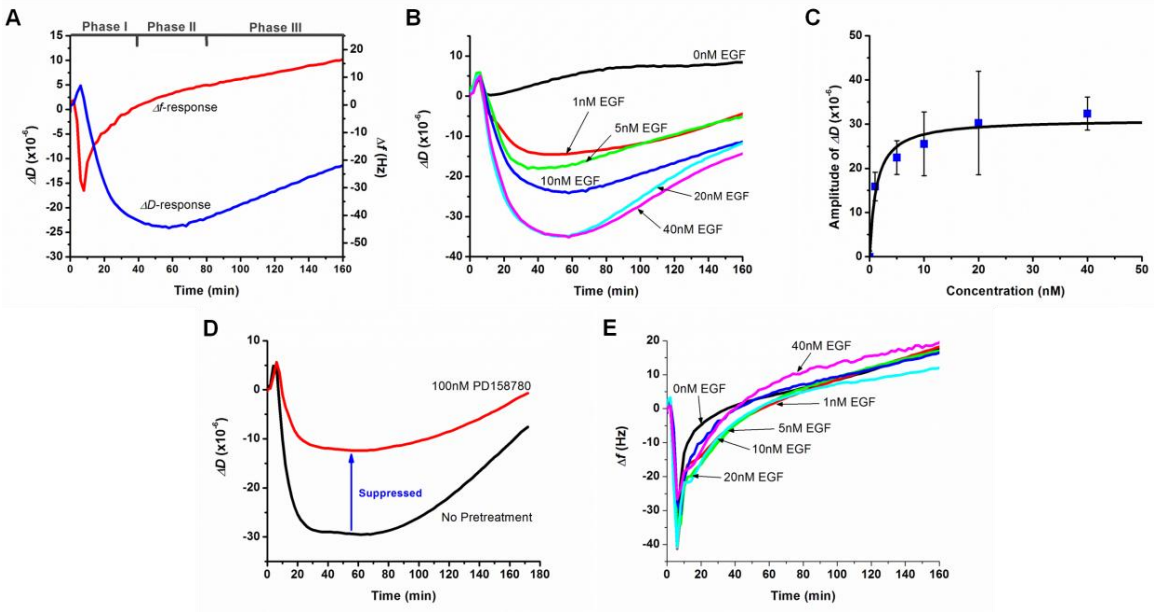

Figure 4.2. Real-time QCM-D measurements (at the third mode of vibration) of the responses of MCF-10A cells to EGF at 37°C. (A) The simultaneously recorded Δ*D*- and Δ*f*- responses as a function of time in the presence of 10 nM EGF. Triphasic pattern of the Δ*D*-response: I, 0 to 40 min; II, 40 to 80 min; III, 80 to 160 min. (B) The Δ*D*-responses at the following concentrations: 0, 1, 5, 10, 20, and 40 nM. (C) The amplitudes of Δ*D*-responses at 60 min as a function of EGF concentrations. The data were fit with the dose-response function. EC_{50} = 1.2 nM. (D) The Δ*D*-response of the cells induced by 10 nM EGF was suppressed by 100 nM PD158780, a known inhibitor of EGFR tyrosine kinase. The inhibition is shown by the difference in Δ*D*-response of the cells with and without the pretreatment of PD158780. (E) The Δ*f*-responses at the following concentrations: 0, 1, 5, 10, 20, and 40 nM[155]. (At least ten replicates were done of each experiment.)

4.2.2 Correlating the EGF-Induced Δ*D*-Response with Cell De-Adhesion

To further verify the link between the Δ*D*-response and cell adhesion, we visually examined EGF-induced changes in number and size of focal adhesions as a function of time with the aid of immunostained vinculin within the focal adhesion complex. As shown in Figure 4.3A, prior to exposure to EGF, a large number of prominent focal adhesions are seen as short bright streaks of vinculin in both the central portions and peripheries of the cells. This is a clear indication of strong cell adhesion. When the cells were exposed to 10 nM EGF for 30 min, the stained vinculin became fewer in number,

smaller in size, and less intense in brightness (Figure 4.3B). These changes are characteristic of reduced level of cell adhesion, attributed to EGF-induced disassembly of the focal adhesion complexes[54, 186, 193]. A 60-min exposure to EGF further diminished the focal adhesions in size and number, as shown in Figure 4.3C. However, a longer exposure to EGF of 100 min and 150 min did not cause any further reduction of focal adhesions. They showed a slight increase in size and number, suggesting cell re-adhesion occurs during the later stages of the EGF exposure (Figure 4.3D). After a 150-min exposure to EGF, focal adhesions (Figure 4.3E) became even more noticeable compared with that of 100-min treatment, and this is correlated to a continuing re-adhesion. The observations made between 60 and 100 min can be interpreted as a period of transition from de-adhesion to re-adhesion. To summarize, when exposed to EGF, a monolayer of cells exhibits a complex pattern of adhesion that consists of a sequence of de-adhesion (0 to 60 min), transition (around 60 min), and re-adhesion (60 to 150 min).

To have a quantitative assessment of the relationship between the Δ*D*-response and the level of cell adhesion, the changes in level of the focal adhesions were determined according to the areal density of immunofluorescently stained vinculin at each time point. The results of the quantification are summarized in bar graph form in Figure 4.3F. The reduction, transition, and restoration of the focal adhesions imply a time-dependent change in level of cell adhesion, which matches very well with the pattern of the Δ*D*-response shown in Figure 4.2A. When the quantified immunofluorescence data and the Δ*D*-response are superimposed (Figure 4.3G), there is a strong correlation between the two. This quantitative correlation indicates a linear relationship between the magnitude of the Δ*D*-response and the level of cell adhesion.

This suggests that the Δ*D*-response is a specific and quantitative measure of the level of cell adhesion. This correlation is further supported by the experimental evidence that the EGF-induced Δ*D*-response was substantially suppressed when cells were pretreated with cytochalasin D (Figure 4.3H), an actin-disrupting drug that is known to abolish the cell de-adhesion[194].

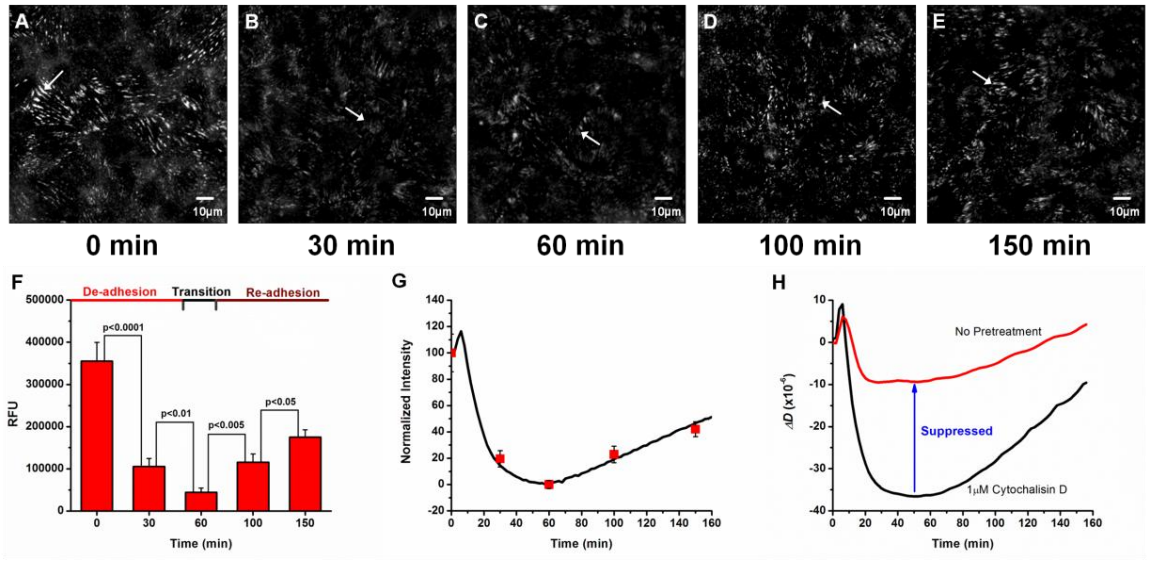

Figure 4.3. The correlation between the Δ*D*-response and the cell adhesion. (A) to (E) show the fluorescence images of focal adhesion in a monolayer of cells after various lengths of time of exposure to 10 nM EGF: (A) 0 min, (B) 30 min, (C) 60 min, (D) 100 min, and (E) 150 min. The focal adhesion was indicated by the immunostained vinculin. An example of focal adhesion given in each of the figures was pointed by an arrow. (F) Quantitation of the density of focal adhesion in relative fluorescence unit (RFU) as a measure of cell adhesion strength (mean ± SEM; N = 10). (G) A linear proportion is shown between the normalized intensity of the Δ*D*-response and the normalized RFU of focal adhesion. The trend is highly significant ($p < 0.0001$) compared to random data. (H) The Δ*D*-response of the cells induced by 10 nM EGF was suppressed by 1 μM Cytochalasin D, a known inhibitor of actin filament. The inhibition is shown by the difference in Δ*D*-response of the cells with and without the pretreatment of Cytochalasin D[155].

4.2.3 Assessing the Effect of Signaling Pathways on the Δ*D*-Response

The PI3K, MAPK/ERK, and PLC pathways are the three known EGFR pathways that have been linked to the mediation of cell adhesion and de-adhesion [44, 45, 50]. To obtain insight into how each of these pathways mediates the EGF-induced change in cell

adhesion of a monolayer of MCF10A cells, we perturbed each pathway pharmacologically by inhibiting the activity of a selected signaling protein in the pathway. We then assessed the effect of the pharmacological intervention on the Δ*D*-response.

To probe the MAPK/ERK pathway (Figure 4.1), we treated cells with 1 and 10 μM of L779450[46], a potent cell-permeable inhibitor of Raf kinase, for 30 min prior to EGF stimulation. The magnitude of the Δ*D*-response diminished as the concentration of the inhibitor was increased, indicating a dose-dependent suppression of the EGF-induced cell de-adhesion (Figure 4.4A). This suggests that the MAPK/ERK pathway is responsible for activating the EGF-induced de-adhesion in MCF10A cells. It has been previously shown by others the MAPK/ERK signaling pathway is responsible for the EGF-induced de-adhesion in fibroblasts through the disassembly of focal adhesion[54], a process involving the cleavage of focal adhesion with the ERK-activated cellular protease, calpain[45].

To probe the PI3K pathway, we treated cells with LY294002 (Figure 4.1), a potent inhibitor of PI3K[195]. The inhibition of the P13K pathway resulted in a dose-dependent reduction in the magnitude of the Δ*D*-response of the cells (Figure 4.4B). This suggests that the PI3K pathway, like the MAPK/ERK pathway, is responsible for activating EGF-induced cell de-adhesion, most likely through its downstream effectors, including small GTPase Rho A, and/or through crosstalk with the MAPK/ERK pathway[44].

To probe the PLC pathway we treated cells with U73122 (Figure 4.1) a potent inhibitor of PLCγ (an isotype of phospholipase)[196]. The inhibition of the PLC pathway

did not reduce, but rather enhanced the Δ*D*-response in a dose dependent manner (Figure 4.4C). The inhibition of the PLC pathway suppresses re-adhesion that occurs in phase III of the EGF-induced response. The implication is that the EGF-activated PLC pathway is the one responsible for increasing cell adhesion, and this implication is consistent with a previous report that PLCγ promotes cytoskeleton remodeling important to cell adhesion and motility[165]. Overall, all three EGFR pathways contribute collectively to the mediation of the EGF-induced cell adhesion.

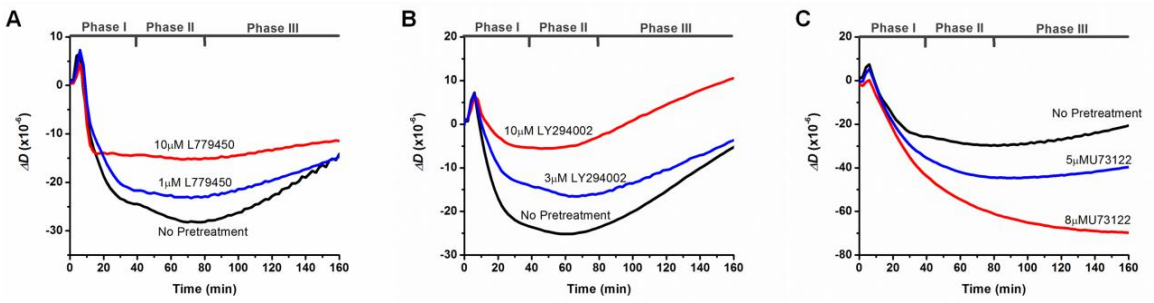

Figure 4.4. The assessment of the signaling pathways responsible for regulation of the Δ*D*-response of the cells. (A) The Δ*D*-response of the cells induced by 10 nM EGF was suppressed by 1 and 10 μM L779450, a known inhibitor of Raf kinase. (B) The Δ*D*-response of the cells induced by 10 nM EGF was suppressed by 3 and 10 μM LY294002, a known PI3K inhibitor. (C) The Δ*D*-response of the cells induced by 10 nM EGF was further enhanced by 5 and 8 μM U73122, a known PLC inhibitor[155]. (At least ten replicates were done of each experiment.)

4.3 Discussion/Conclusions

In this study, the real-time Δ*D*-response was demonstrated to be a sensitive, specific, and quantitative measure of the change in level of focal adhesions of MCF10A cells induced by EGF. Thus, the Δ*D*-response serves as a reliable indicator of cell adhesion. The link between the change in energy dissipation and the change in cell adhesion has previously been suggested based on the study of the dynamic, localized

mechanical behavior of A431 cells and also the studies of the attachment and detachment of several other cell lines[133, 139, 142-144]. All these previous studies had reached the same conclusion that an increase in cell attachment results in an increase in energy dissipation and a decrease in cell attachment (detachment) causes a decrease in dissipation. Here we have characterized the EGF-induced change of cell adhesion at the molecular level by assessing the time-dependent changes in local density of vinculin, a sensitive molecular marker for cell adhesion. The result of this characterization reveals a complex adhesion pattern that begins with rapid de-adhesion, then goes through a transition, and ends with slow re-adhesion. Both the timing and the level of adhesion matched well with that of the pattern exhibited by the Δ*D*-response (Figure 4.3G). This led to our finding of the dynamic, quantitative correlation between the Δ*D*-response and the level of cell adhesion.

In this study, we also demonstrated that the Δ*D*-response is a far more sensitive measure of EGF-induced cell de-adhesion than the Δ*f*-response. The Δ*D*-response can be used to analyze the overall cellular response of cells amplified from the local change of cell adhesion through multiple associated dissipative processes. On the other hand, the Δ*f*-response measures only the changes of the protein composition of the cell adhesion complex and is restricted to the mass change in a small and localized area, which results in low detection sensitivity.

With this highly sensitive approach, we examined the regulation of the EGF-induced changes in cell adhesion mediated by the PI3K, MAPK/ERK, and PLC pathways. We have confirmed that all three pathways are responsible for regulation of cell adhesion. The distinct inhibitory profiles are indication that each of these pathways has a distinct role at different stages of EGF-induced changes in cell adhesion. When the

MAPK/ERK pathway and PI3K pathway were inhibited, phase I (de-adhesion) of the Δ*D*-responses was suppressed, which suggests these two pathways are responsible for the cell de-adhesion process in the EGFR signaling (Figures 4.4A and 4.4B). However, the re-adhesion (increase in Δ*D*-response in phase III) was present in both inhibition profiles of the MAPK/ERK and the PI3K pathway (Figures 4.4A and 4.4B), which suggest that they are not responsible for re-adhesion. Moreover, when the PLC pathway was inhibited, phase III did not exhibit an increase in the Δ*D*-response, indicating the PLC pathway is responsible for re-adhesion (Figure 4.4C). Collectively these pathways along with others regulate this biological process in a temporally sophisticated manner. Systematically dissecting these unique profiles of the Δ*D*-response will provide insight into the coordination of the dynamic network of EGFR signaling.

In this study, we have demonstrated that the QCM-D technique is capable of providing real-time monitoring of changes in dissipation of a layer of EGF-treated cells, and is an indicator of changes in cell adhesion. We determined that changes in cell adhesion induced by EGF exhibit a complex temporal pattern regulated by several downstream pathways of EGFR signaling. Because of its non-invasiveness to mammalian cells,[130] the QCM-D technique is preferable for assessing cell adhesion to techniques that requiring invasive forces or non-native dyes or particles. Because cell adhesion is an essential connection between other cellular functions, the QCM-D can potentially be exploited for fundamental study of cellular processes, such as cell signaling, trafficking, and mechanotransduction, as well as for biomedical research on drug and biomarker screening.

Chapter 5: Using the Dissipation Monitoring Function of the QCM-D for the *In Vitro* Assessment of the Cell-Implant Interaction

5.1 Introduction

Most amputees currently utilize a stump-socket interface to connect their prosthetic limb[197]. Socket prostheses are designed to be securely fastened around the residual limb through the use of belts, cuffs or suctions[197, 198]. Even though advancements in socket prostheses have greatly improved the mobility and the wearability of prostheses for amputees over the years, there are still many limitations, such as the potential of causing irritation of the adjacent soft tissues, difficulty in mounting due to weight fluctuations and muscular atrophy, and difficulty in fitting individuals with short residual limbs[199].

Transcutaneous prosthetic implants have been developed to overcome some of these limitations. In the 1960s, Branemark was among the first group of researchers who established the use of transcutaneous prostheses in dental and auricular implantology[200]. A transcutaneous prosthetic implant is an abutment that penetrates through the soft tissue and skin and is directly anchored to the bone. Clinical studies have shown patients with transcutaneous prosthetic implant exhibited improvements in mobility and osseoperception[201]. Although transcutaneous prosthetic implants show promising benefits for amputees, they have a very high failure rate. Besides that they become loosened over time, failures of most transcutaneous prosthetic implants are due to marsupilisation, avulsion, and infection[199, 200, 202]. The primary reason for these complications could be attributed to an insufficient seal between the implant and the soft tissue/skin due to their poor attachment to the implant[203]. The success rate of transcutaneous prosthetic implants

can be greatly increased by enhancing the adhesion between soft tissue/skin and implant to promote wound healing and reduce infection[204].

Cell adhesion is involved in many essential biological processes, including wound healing, cell migration, embryonic development, and tumorigenesis[181]. Biochemical techniques, such as colorimetric and fluorometric biochemical assays, are able to characterize the cell adhesion process through specific cellular events, such as gene expression, generation of secondary messengers and/or translocation of labeled targets[66, 205]. Many of these techniques require labeling agents, which can affect cellular behavior and therefore lead to compromised physiological response of cells. In addition, many of these techniques require cell lysis and/or fixation steps that lead to cell death. Therefore, they are limited to the endpoint detection of cellular processes. Furthermore, biochemical techniques do not provide information about mechanical properties of cells induced by a cellular process. Mechanical techniques, such as atomic force microscopy[86], optical tweezers[88] and centrifugation techniques[90], can provide the mechanical properties of cell adhesion; however, these approaches, by applying strong external forces to the cells, can affect the behavior and response of the cells. Therefore, the result from these methods may be often misleading. In recent years, innovative label-free systems, including piezoelectric[130], optical[206], electrochemical[140], impedimetric, thermometric, and magnetic sensor systems[207], have been developed for detection of cellular response[78]. Some of the cellular responses that have been used for detection are based on changes in morphology, adhesion, proliferation, and cellular movements[207].

In recent years, the quartz crystal microbalance (QCM) has become an effective tool to study cell-surface interactions in a non-invasive and real-time manner with the

focus on cell-substrate interactions[114-120]. Cell-substrate interaction primarily involves the surface receptor integrin, which is responsible for conveying a chemical signal into the cell that provides information about the cell's location, environment, and adhesive state. Integrin also connects the cytoskeleton of a cell to a surface substrate, which allows the cell to modify its morphology in response to environmental stimuli. The QCM technique has also been used to study the effects of various ECM proteins, such as fibronectin, vitronectin, and laminin, and other coatings, such as gold, tantalum, chromium, polystyrene, silicon dioxide, and hydroxyapatite, on the adhesion and spreading of various cell types [146-149]. Furthermore, the QCM has been utilized to monitor the effect of the chemical and the morphological properties of the substrate surface on the attachment and spreading of cells[142, 179, 208 209].

In this study, we used the QCM-D to investigate the cell adhesion process of human epidermal keratinocytes (HEK001) to the surface coated with titanium, a material commonly used for medical implants (e.g., transcutaneous prosthetics). Human epidermal keratinocytes were chosen because keratinocyte is the predominant cell type in the epidermis, the outermost layer of the skin, and plays an essential role in sealing the soft tissue–implant interface[210, 211]. In this work, we explored the ability of the QCM-D to probe the adhesion process of human epidermal keratinocytes and detect the effects of the substrate coating and pharmacological treatment on cell adhesion. Our further understanding of the adhesion of human epidermal keratinocytes on the implant type of surface will provide leads on future development of therapies for enhancing osseointegration and minimizing infection caused by the medical implants.

5.2 Results/Discussion

5.2.1 Real-Time Monitoring of Cell Attachment and Spreading

In this study, our primary aim is to develop a method with the use of the QCM-D to probe the cell adhesion process. We hope to find ways to modulate the adhesiveness of cells to the substrate surface coated with titanium, a material commonly used for transcutaneous prosthetics. The QCM-D experiments conducted in this study utilized the open module setup instead of the typical flow module setup used by others[148, 151]. The typical flow module setup procedure for cell adhesion experiments begins with rinsing of the sensor with fetal bovine serum (FBS)-containing cell medium to saturate the surface with FBS and other proteins. Then cells are introduced slowly over the sensor for a period of time until they settle down onto the sensor surface. This is followed by a constant flow of complete cell medium throughout the rest of the experiment. Westas *et al.* showed that there is a large variation of cell coverage due to the microfluidics of the QCM-D[148]. The open module setup procedure also begins incubating the sensor with complete cell medium. Next, the cell medium is removed and cells are seeded on the top surface of the sensor. The cells are then allowed to settle and attach for the duration of the experiment and the entire adhesion process is monitored with the use of the QCM-D. In this study the attachment and spreading behaviors of cells were monitored for periods of 10-20 h to determine long term adhesion behaviors. With the open module setup, both Δf and ΔD-responses of the cell adhesion process exhibited sigmoidal profiles similar to what others have obtained with the flow modules set-up [133, 135-139, 151] (Figure 5.1).

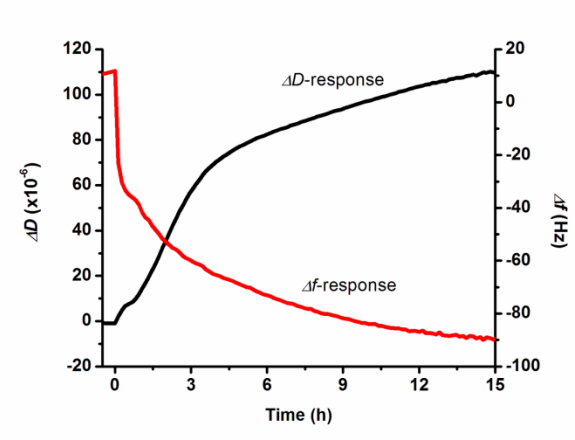

Figure 5.1. Simultaneous, real-time recording of Δ*D*- and Δ*f*- responses (at the third mode of vibration) upon the addition of HEK001 cells onto a titanium-coated QCM-D sensor.

5.2.2 Comparison of Δ*f*- and Δ*D*-Responses in Examining Cell Adhesion and Coverage

The QCM-D measures the change in mass of cells and the change in viscoelastic properties of cells in the form of shifts in resonance frequency (Δ*f*) and energy dissipation (Δ*D*), respectively. The amount of cells seeded onto the QCM-D sensor surface dictates the corresponding Δ*f*- and Δ*D*- responses. This phenomenon has previously been shown by others[135, 136, 140]. Figures 5.2C-F show images of the adhered cells on the QCM-D sensors with starting cell counts of 100k, 75k, 50k, and 25k, respectively. When more cells were added, a higher surface coverage by the adhered cells was observed (Table 5.1). Figure 5.2A shows the Δ*D*-response of each cell adhesion process with a specific starting cell count and the higher the starting cell count, the stronger the Δ*D*-response. The steepest change in each of the Δ*D*-response profile occurs between 1.5 to 5 h. Such increases are likely due to the increase in the number and strength of adhered cells. It has been previously demonstrated the Δ*D*-response has a strong correlation with the level of focal adhesions[155, 174]. According to the Sauerbrey equation, the Δ*f*-response of the cell

adhesion was expected to be correlated with the mass change of the adhered cells. However, the Δ*f*-responses do not exhibit a clear mass-dependency. In fact, some of the Δ*f*-responses were almost indistinguishable even though their starting cell counts were vastly different (Figure 5.2B). The lack of mass-dependency can be attributed to the fact that the cells behave more like viscoelastic material than a rigid mass[133, 137-139]. The results of this study indicate that the Δ*D*-response is a far more sensitive and specific measure of cell-substrate adhesion than the Δ*f*-response[155]. For the remaining experiments of this study, the Δ*D*-response has been used to evaluate the adhesion process of HEK001 cells and a cell density of 75k cells used to avoid over-crowding of cells on the titanium-coated sensor.

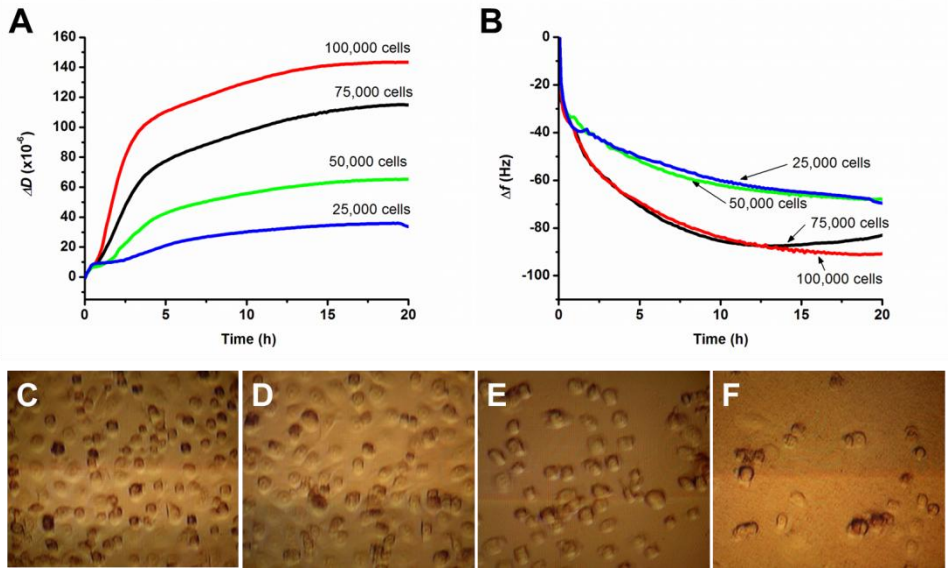

Figure 5.2. QCM-D measurements of the adhesion of HEK001 cells onto the titanium-coated QCM-D sensors. (A) The Δ*D*-responses of the cells seeded in four different starting cell counts: 25k, 50k, 75k, and 100k. (B) The Δ*f*-response of cells seeded in four different starting cell counts: 25k, 50k, 75k, and 100k. (C) – (F) Images of the cells in four different starting cell counts: (C) 100k, (D) 75k, (E) 50k, and (F) 25k on the titanium coated QCM-D sensors after 20 h.

Table 5.1. Approximate counts of the cells adhered to the sensor surfaces after 20 h.

Starting count of the cells prior to seeding	Count of adhered cells
100,000	79000
75,000	65000
50,000	45000
25,000	23000

5.2.3. Identification of the Three Stages of Cell Adhesion

The process of cell adhesion to a substrate surface is a complex process and requires coordination of protein and membrane receptors. In the initial attachment step of cell adhesion, a cell settles down on the surface of a substrate and forms a loose contact with the substrate. Next the cell begins to flatten and spread its membrane over the substrate surface. Lastly, the cell forms adhesion complexes that connect to the substrate

with intracellular actin filaments through membrane receptors[31, 212]. The Δ*D*-response shown in Figure 5.3 exhibits a three-phase response profile: phase I, which occurs within the first hour, exhibits a sharp increase. Phase II, which occurs between 1 h and 3 h, exhibits a slightly less steep increase in Δ*D*-response. Lastly phase III, which occurs after 3 h, displays a gradual increase until it reaches a maximum. To verify the three phases of the cell adhesion process, live cell images were taken at various time points. At 0.5 h the cells were round and very loosely adsorbed, a clear indication of phase I initial attachment (Figure 5.4C). At 1.5 h, a small number of the cells were flattened, which is an indication of phase II cell spreading. However, the majority of cells were still round (Figure 5.4D), which is consistent with the appearance of phase I. This mixed cell morphology confirms that 1.5 h is likely a time point when the transition from phase I to II occurs. This is also the case for the image at 3 h (Figure 5.4E) where the transition from phase II to III occurs with many of the cells still in the phase II appearance. At 6 h, the majority of the cells were completely flattened, indicating the formation of focal adhesions and the appearance of the phase III (Figure 5.4F). Lastly at 20 h, all of the cells appeared in the phase III stage (Figure 5.4G). It is noteworthy that for the last three time points, 3 h, 6 h and 20 h, the number of cells adhered on the sensor remains virtually the same (Figure 5.4B). However, the Δ*D*-response continues to rise during this time and is nearly doubled between the responses at 3 h and 20 h. This clearly suggests that the change in energy dissipation in phase III is due to enhancement of the cells-substrate adhesion and not due to the increasing number of cells coming into contact with the sensor surface. The enhancement of the cell-sensor adhesion can be attributed to the formation of focal adhesion complexes, which increase the adhesion strength between the

cells and the sensor surface. The enhancement of cell adhesion also flattens the cells, resulting in a morphology that is consistent with those shown by the cells at 6 h and 20 h.

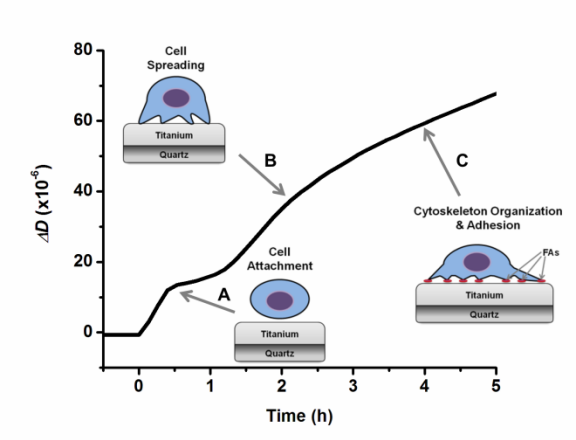

Figure 5.3. The Δ*D*-response profile of the three sequential stages of adhesion of HEK001 cells on the titanium-coated QCM-D sensor. (A) Phase I (0-1 h): initial attachment. (B) Phase II (1-3 h): cell spreading. (C) Phase III (> 3 h): cytoskeleton reorganization and formation of focal adhesion. (At least ten replicates were done of each experiment.)

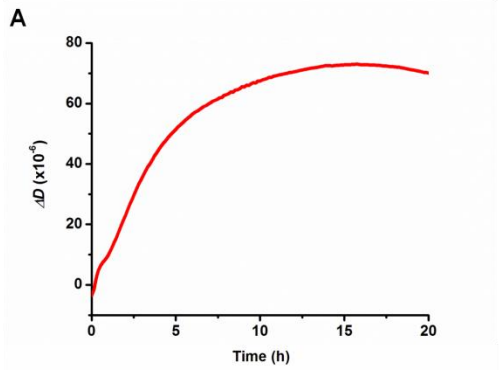

B

Time After Seeding (h)	Δf (Hz)	ΔD (x 10^{-6})	Number of Adhered Cells
0.5	-49.020	6.459	24833 ± 2728
1.5	-55.443	15.618	36000 ± 2179
3	-58.932	36.208	46500 ± 1443
6	-57.267	56.547	48167 ± 2522
20	-63.540	70.109	47000 ± 1732

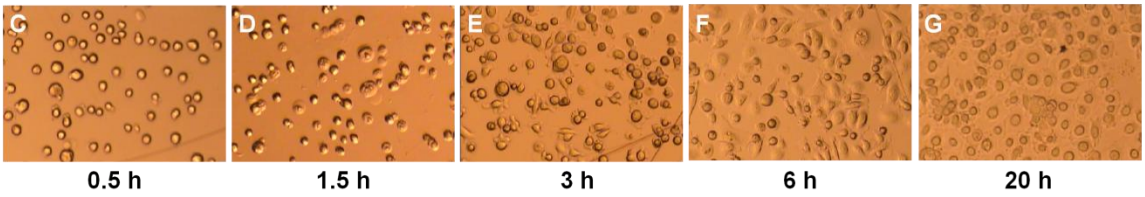

Figure 5.4. Live cell images at different time points of adhesion of HEK001 cells on the titanium-coated QCM-D sensor. (A) The Δ*D*-response of 75k cells seeded onto the sensor. (B) Numbers of the adhered cells and the corresponding QCM-D-responses at various incubation times. (C-G) Images of the adhered cells at time points: 0.5 h, 1.5 h, 3 h, 6 h, and 20 h after initial seeding.

5.2.4 Effects of Surface Coating on the Cell Adhesion Process

The adherence of cells to a biomaterial surface is determined by the material's surface properties. The ability to closely mimic the *in vivo* environment can potentially improve the biocompatibility of the material surface. In recent years, the QCM has been used as a tool for the evaluation of real-time cell-surface interactions of biomaterials[146-149] because of its ability to monitor the cell adhesion process in a non-invasive and real-time manner. When cells adhere to a substrate, cells first excrete a layer of extracellular matrix (ECM) proteins that are adsorbed onto the surface. Some of those ECM proteins include collagen I and IV, laminin, and fibronectin[213]. There have been studies conducted to determine which ECM proteins enhance keratinocyte attachment *in vitro*. Adam *et al.* studied the effects of the ECM proteins, collagen I and IV, laminin, and fibronectin, on

the attachment of keratinocytes onto a plastic surface[214]. Their studies demonstrated that fibronectin had the greatest enhancement on the attachment of keratinocytes and the best keratinocytes attachment took place between 3-4 h. Similar results were determined by Bush *et al*[215].

In this study, we monitored the process of cell adhesion to the sensor with either a bare titanium surface or a titanium surface coated with fibronectin. The surface coating was characterized with AFM imaging. The bare titanium sensor surface exhibited a smooth surface morphology indicated by minimal surface height represented by darker coloration (Figure 5.5A). The titanium sensor surface coated with fibronectin showed a rougher morphology displayed by a large variation of surface height represented by the combination of darker and lighter colored regions (Figure 5.5B). When HEK001 cells were adhering to the Ti sensor coated with fibronectin, the resulting Δ*D*-response showed a three-phase pattern that was very similar to the one shown by the Ti sensor without the fibronectin coating; however, the magnitude of the Δ*D*-response from the fibronectin-coated Ti sensor is significantly higher (Figure 5.6A), which indicates fibronectin coating enhances the adhesion of cells onto the Ti-coated surface. This result is verified by the cell images that show slightly flatter cell morphology on the fibronectin-coated sensor surface compared to the one without the fibronectin coating (Figures 5.6C and D). Additionally, the Δ*D*-response of the fibronectin-coated surface exhibited a shorter phase II and more rapid increase during the early stage of phase III compared with the one of the bare surface. This result suggests that the fibronectin coating accelerates the formation of cell-substrate adhesion, likely by the binding of integrin with the pre-existing fibronectin.

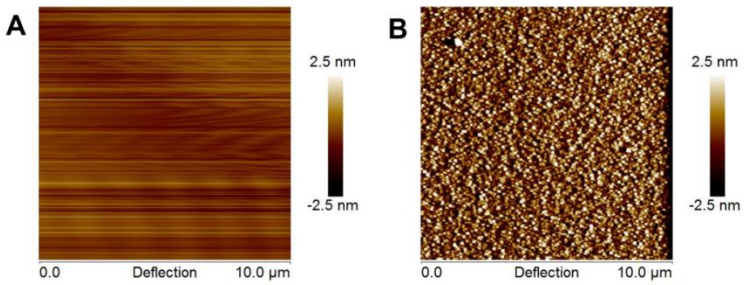

Figure 5.5. Comparison of surface coatings of QCM-D sensors. (A) AFM image of the bare titanium surface. (B) AFM image of the titanium surface coated with fibronectin.

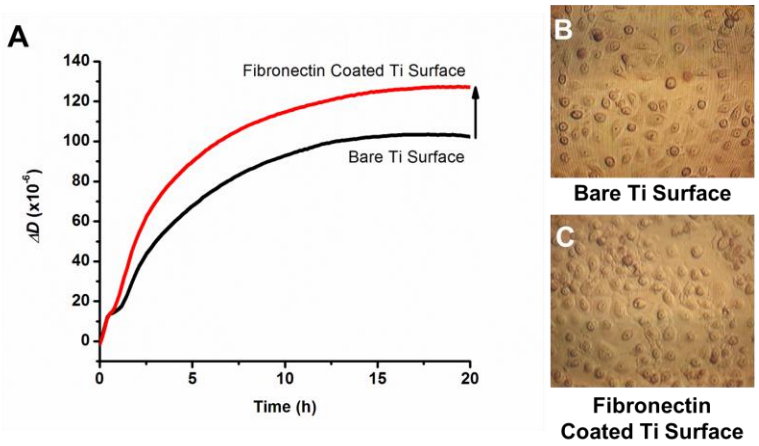

Figure 5.6. Comparison of the effect of fibronectin coating on the adhesion of HEK001 cells. (A) The Δ*D*-response profiles of adhesion of the cells on the sensor surfaces with and without the fibronectin coating. (B) Image of the cells adhered to a bare Ti-coated sensor surface. (C) Image of the cells adhered to a fibronectin coated Ti sensor surface.

5.2.5 Effects of Epidermal Growth Factor on the Cell Adhesion Process

Epidermal growth factor (EGF) is known to be able to induce mitogenic and motogenic responses in many cell types, including fibroblasts, keratinocytes, and epithelial cells[155, 174, 216], as well as impacting the cell-substratum adhesiveness, membrane activity, and/or contractile force generation.[216] When HEK001 cells were treated with 5 ng/mL EGF, the magnitude of the resulting Δ*D*-response was significantly reduced compared with the untreated cells (Figure 5.7A), suggesting a reduction of cell-

substrate adhesion by EGF. This reduction of cell adhesion was confirmed by a slightly less flat morphology displayed by the EGF-treated cells (Figures 5.7B and 5.7C). Maheshwari *et al.* have previously demonstrated that EGF is capable of modulating the strength of cell-substrate adhesion and allowing the cell to be in a migratory state so it is ready for attachment at the front of the cell and detachment at the rear of the cell[216]. Thus, EGF may play a critical role in mediating cell migration during wound healing of skin.

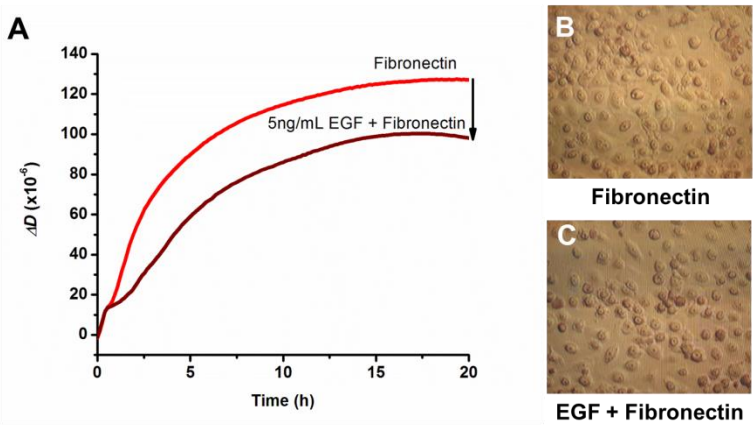

Figure 5.7. The effect of epidermal growth factor (EGF) on adhesion of HEK001 cells. (A) The Δ*D*-responses of the cells on the fibronectin-coated sensors with or without exposure to 10 nm EGF. (B) Image of the cells on a fibronectin-coated Ti sensor surface. (C) Image of the EGF-treated cells on a fibronectin coated Ti sensor surface.

5.2.6 Effects of Pathway Specific Modulators on the Cell Adhesion Process

The ERK/MAPK pathway is one of the principal signaling cascades by which cells respond to extracellular and intracellular cues. Abnormal activation of ERK/MAPK pathway is a common occurrence in many human cancers. In this study, we examined the effects of PD98059 and U0126 on adhesion of HEK001 cells onto the titanium-coated sensor surface, respectively (Figures 5.8A1 and 5.8B1). Both modulators are known

inhibitors of MAPK kinase 1, a key enzyme in the ERK/MAPK signaling pathway, which is responsible for the regulation of cell migration both *in vivo* and *in vitro*[217, 218]. The Δ*D*-response of HEK001 cells in the presence of 10 μM PD98059, showed an overall increase in magnitude over that of HEK001 cells in the absence of the modulator. A similar increase in Δ*D*-response was also observed with the cells in the presence of 10 μM U0126. The overall increases in Δ*D*-responses in the presence of MEK1 inhibitors imply that suppressing the ERK/MAPK pathway enhances the adhesiveness of the keratinocytes on the titanium surface. The enhanced adhesiveness is confirmed by the stronger cell adhesion and higher cell coverage shown in Figure 5.8. Thus, pharmacological modulation of the ERK/MAPK pathway could potentially provide an effective way to enhance osseointegration and minimize the infection caused by the medical implants.

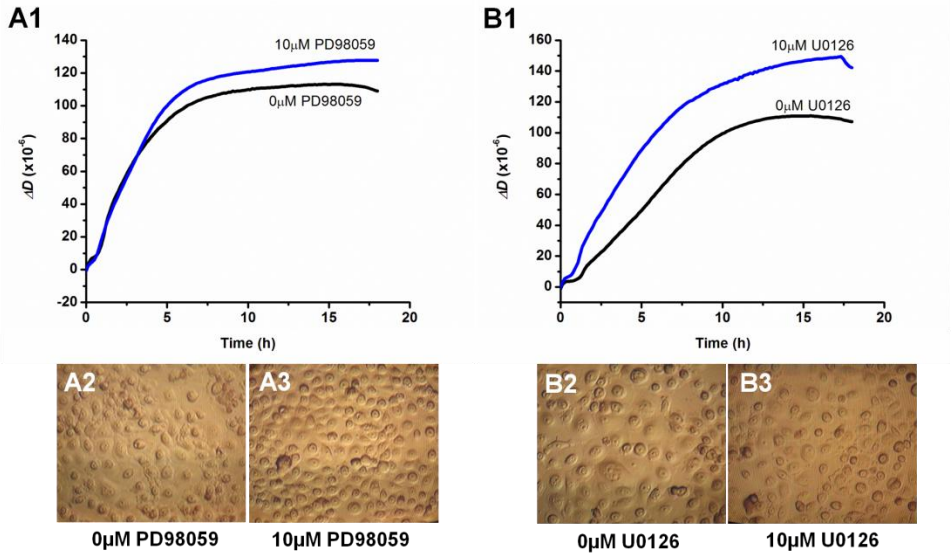

Figure 5.8. The effect of ERK/MAPKK pathway-specific modulators on adhesion of HEK001 cells. (A1) The Δ*D*-responses of HEK001 cells adhering onto the titanium-coated sensor surfaces in the presence and absence of 10 μM PD98059. Images of HEK001 cells adhered to the titanium-coated sensor surfaces in the absence (A2) and presence (A3) of 10 μM PD98059. (B1) The Δ*D*-responses of HEK001 cells adhering onto the titanium-coated sensor surfaces in the presence and absence of 10 μM U0126. (B2) Image of HEK001 cells adhered to the titanium-coated sensor surfaces in the absence (B2) and presence (B3) of 10 μM U0126.

The PI3K signaling pathway is responsible for the regulation of cellular survival, proliferation, and growth. When PI3K is activated, phospholipids are generated to further activate Akt, a serine/threonine kinase and other downstream effectors proteins[219]. In this study, we examined the effects of LY294002 and ZSTK474 on adhesion of HEK001 cells onto the titanium-coated sensor surfaces, respectively (Figure 5.9). Both modulators are known inhibitors of PI3K, a key enzyme in the PI3K signaling pathway[195, 220], which is involved in mediating cell adhesion in conjunction to promoting cell survival and proliferation. The Δ*D*-response of HEK001 cells in the presence of 1 μM LY294002, showed an overall increase in magnitude over that of HEK001 cells in the absence of the modulator. A similar increase in Δ*D*-response was also observed with the cells in the presence of 250 nM ZSTK474. The overall increases in Δ*D*-responses in the presence of

PI3K inhibitors imply that suppressing the PI3K pathway enhances the adhesiveness of the keratinocytes on the titanium surface. The enhanced adhesiveness is confirmed by the stronger cell adhesion and higher cell coverage shown in Figure 5.9. Overall the PI3K pathway has the effect on the cell adhesion process similar to the ERK/MAPK pathway.

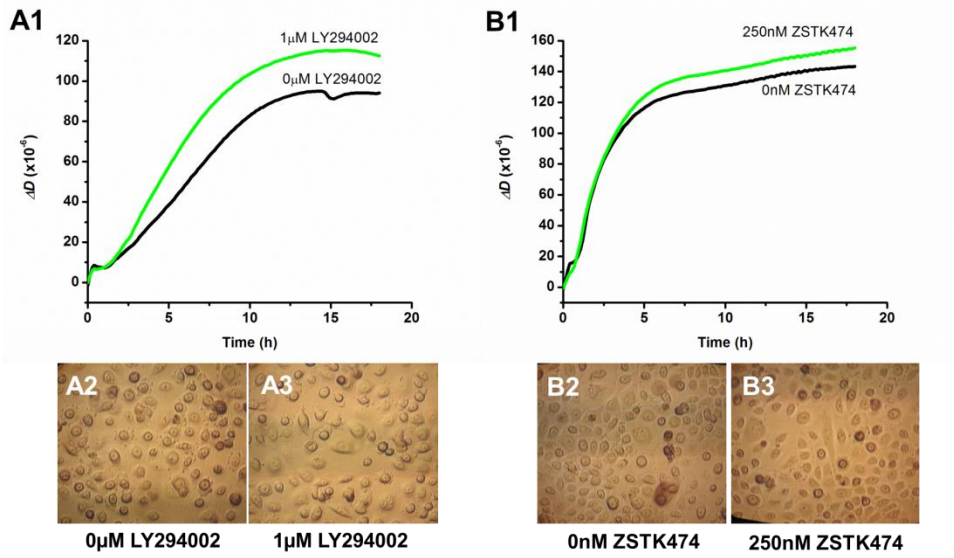

Figure 5.9. The effect of PI3K pathway-specific modulators on adhesion of HEK001 cells. (A1) The Δ*D*-responses of HEK001 cells adhering onto the titanium-coated sensor surfaces in the presence and absence of 1 μM LY294002. Images of HEK001 cells adhered to the titanium-coated sensor surfaces in the absence (A2) and presence (A3) of 1 μM LY294002. (B1) The Δ*D*-responses of HEK001 cells adhering onto the titanium-coated sensor surfaces in the presence and absence of 250 nM ZSTK474. (B2) Image of HEK001 cells adhered to titanium-coated sensor surfaces in the absence (B2) and presence (B3) of 250 nM ZSTK474.

The PLC pathway is responsible for the attachment of the cell onto the ECM[221]. Crooke *et al.* compared PLC-γ1-deficient fibroblast cells with normal fibroblast cells and showed the PLC-γ1-deficient cells to have decreased cell adhesion, spreading and migration[221, 222]. In this study, we examined the effects of U73122 and edelfosine on the adhesion of HEK001 cells onto the titanium-coated sensor surfaces, respectively (Figure 5.10). Both modulators are known inhibitors of phosphoinositide phospholipase C (PLC),

a key enzyme in the PLC signaling pathway[223, 224]. The Δ*D*-response of HEK001 cells in the presence of 10 μM U73122, showed an overall decrease in magnitude compared with that of HEK001 cells in the absence of the modulator. A substantial decrease in Δ*D*-response was also shown with the cells in the presence of 1 μM edelfosine. The overall decrease in the Δ*D*-response in the presence of PLC inhibitors imply that suppressing the PI3K pathway significantly reduces the adhesiveness of the keratinocytes on the titanium surface. The reduced adhesiveness is confirmed by the weaker cell adhesion and much lower cell coverage shown in Figure 5.10. This study indicates the PLC pathway has a significantly negative impact on the attachment of human epidermal keratinocytes onto an implant type surface.

If one reviews Figures 5.8-5.10, one sees that the controls (0.0 μM modulator) are nearly identical (vertical scales in the figures are different). The small differences are inherent in cell cultures done at different times under identical conditions.

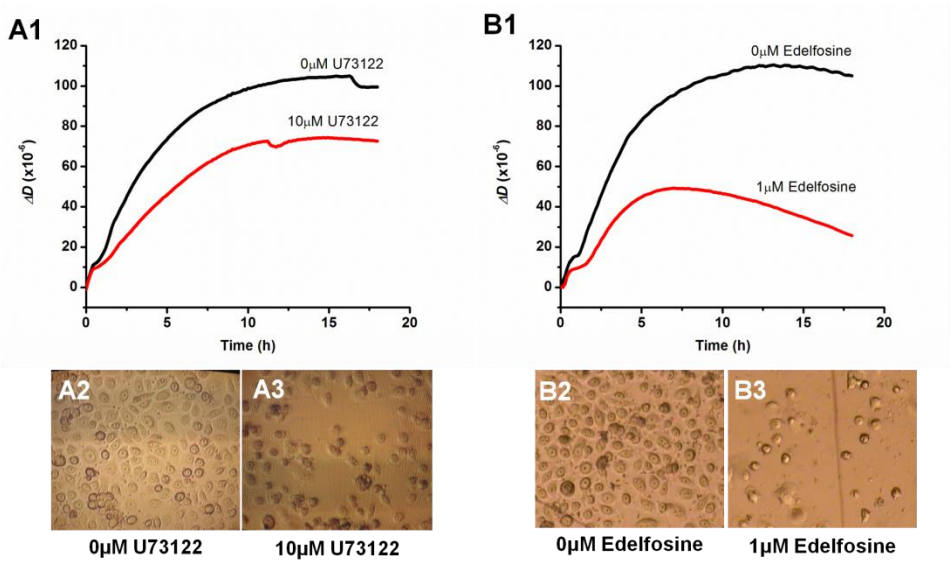

Figure 5.10. The effect of PLC pathway-specific modulators on adhesion of HEK001 cells. (A1) The Δ*D*-response of HEK001 cells adhering onto the titanium-coated sensor surfaces in the presence and absence of 10 μM U73122. Image of HEK001 cells adhered to the titanium-coated sensor surfaces in the absence (A2) and presence (A3) of 10 μM U73122. (B1) The Δ*D*-response of HEK001 cells adhering onto the titanium-coated sensor surfaces in the presence and absence of 1 μM edelfosine. Image of HEK001 cells adhered to the titanium-coated sensor surfaces in the absence (B2) and presence (B3) of 1 μM edelfosine. Both inhibitors reduced the overall level of the adhesion between HEK001 cells and the titanium surface, displayed by the decrease of the Δ*D*-response. Images show significantly fewer cells adhered to titanium sensor surface with PLC pathway modulators.

5.3 Conclusions

From this study, we have demonstrated that the QCM-D is an effective technique for detection of the adhesion process of human epidermal keratinocytes under physiological conditions. The effectiveness of the QCM-D relies not only on the ability for monitoring the cell adhesion process in a real-time and non-invasive manner, but also the sensitivity and time resolution for examining the fine details of the time-dependent Δ*D*-response to provide a mechanistic insight into the adhesion process. For example, we have established the three-stage adhesion process of human epidermal keratinocytes based on the profile of the time-dependent Δ*D*-response. Also from this study, we have further established that the Δ*D*-response is a far more sensitive and specific measure of

cell-substrate adhesion than the Δf-response, in part due to the viscoelastic property of the cell.

We have shown that the adhesion of human epidermal keratinocytes on an implant type of surface can be modulated in a variety of ways, such as surface coating with fibronectin, growth factor stimulation, or pharmacological modulation. Overall we have established the QCM-D as an effective technique to characterize the effectiveness of biomaterials for prostheses and to aid in the identification of therapies that are capable of enhancing cell adhesion to promote wound healing.

Chapter 6: Assessing GPCR-Mediated Cell Adhesion Using Dissipation Monitoring of the QCM-D

6.1 Introduction

G protein-coupled receptors (GPCRs) are a large family of receptors responsible for the transduction of information from the extracellular environment to the intracellular environment[225]. GPCRs account for approximately 2-4 % of the human genome and are characterized by its seven transmembrane (7TM) domain configuration[226, 227]. When a ligand binds to the GPCR, it results in the dissociation of the heterotrimeric G protein into active G_{α} and $G_{\beta\gamma}$ subunits[228]. The disassociated α-subunit then couples with a specific effector protein to influence a diverse set of downstream signaling cascades[229]. The downstream signaling cascade is directly dependent on the α-subunit type (G_s, $G_{i/o}$, $G_{q/11}$, and $G_{12/13}$)[229] (Figure 6.1).

GPCRs control many physiological functions, such as sensory transduction[230], cell-cell communication[231], muscle contraction[232], neurotransmission[233], immune response[234], and hormonal signaling[235]. The dysfunction of GPCRs contributes to health conditions and diseases, such as inflammatory disease[236], cardiovascular disease[237], and cancer[226]. More than 50 % of the current therapeutics target GPCRs directly or indirectly making this family of receptors one of the largest groups of receptors targeted for drugs[226, 238]. Two major foci of GPCR research are the development of GPCR screening assays and understanding the mechanism of the GPCR receptors.

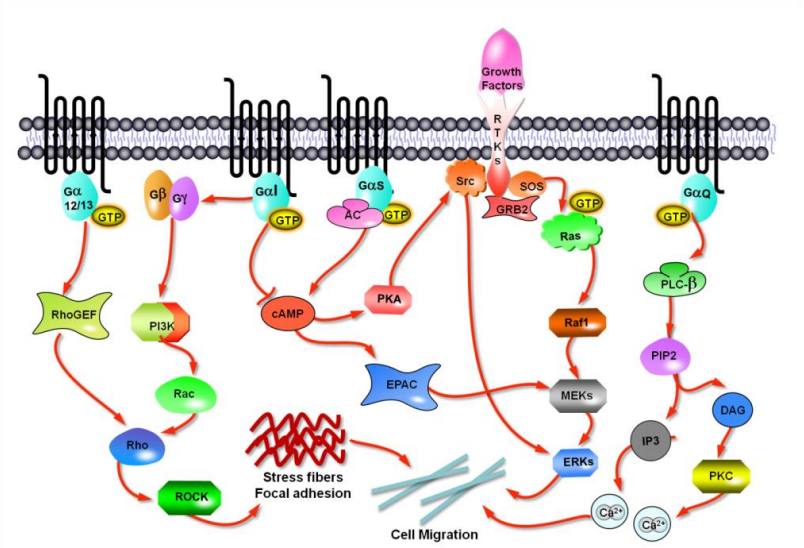

Figure 6.1. The GPCR signaling pathway. This map was created based on the original pathway map from SABiosciences (Valencia, CA).

Some stimuli that can activate GPCRs, include proteins, lipids, peptides, hormones, small biomolecules, and light[239]. The endogenous ligands are known for about 20 % of GPCRs and for the remaining GPCRs, the endogenous ligands are unknown. These GPCRs with unidentified endogenous ligands are known as "orphan" GPCRs[240, 241]. In this study, we will look at some endogenous ligands and small biomolecules that have been shown to activate specific GPCRs. For the activation of specific GPCRs of the $G_{\alpha s}$ pathway, we analyzed the following ligands: epinephrine (Epi)[242, 243], 5'-N-Ethylcarboxamidoadenosine (NECA) [244, 245], and isoproterenol (ISO)[246, 247]. For the activation of specific GPCRs of $G_{\alpha i}$ pathway, we examined lysophosphatidic acid (LPA)[63, 248] and nicotinic acid (NA)[249, 250]. For the activation of specific GPCRs of $G_{\alpha q}$ pathway, we studied adenosine triphosphate (ATP)[251, 252], bradykinin (BK)[253, 254], thrombin (Thr) [255-257], and histamine (Hist)[258, 259].

It has been shown ligands can signal through GPCRs via a preferred signaling pathway, but can activate other signaling pathways[260]. Crosstalking of multiple pathways can potentially have an effect on the binding specificity and efficacy of the ligands. Such crosstalk interactions may have a significant impact on the physiological outcomes of the receptor and therefore can potentially provide novel targets for therapeutics and provide a new perspective on the signaling pathways[261]. Crosstalk can occur at various levels of the signaling pathway, it can occur at the receptor level and at the effector/second messenger level[260]. At the receptor level, crosstalk can occur through receptor dimerization[262]. A ligand can bind at one receptor of the formed receptor dimer, and this will affect the ligand binding to the second receptor causing different downstream effects[262]. There is also evidence crosstalk can occur when there are multiple conformations of the receptor, where the G protein favors a specific conformations and this leads to the activation of multiple G protein signaling pathways[149, 263, 264]. Lastly the more conventional signaling crosstalk is through downstream activation of effector molecules and the production of secondary messengers. Many have studied the crosstalk mediated through G_i pathway's $\beta\gamma$ subunit on the activation phospholipase C (PLC) of the G_q pathway[260]. Another well-established crosstalk is stimulation of adendylyl cyclase of the G_s pathway induced by the $\beta\gamma$ subunit of the G_i pathway[260].

Currently there are many methods for screening the GPCR pathway. Some of these methods, include receptor binding, G protein dependent/independent functional, real-time fluorescence, and label-free whole cell assays[66]. Receptor binding assay is a method for studying and characterizing the interaction between the receptor and the ligand[265]. Receptor binding assay is a cell-free method where purified receptors and the

radiolabeled ligands are mixed together to allow ligands to bind to the receptors. The sample is then washed, filtered, and measured for radioactivity. The receptor binding assay is a very high throughput screening method, but it cannot provide information about the downstream signaling of the receptor, and therefore it does not provide a complete understanding of the signaling mechanism of the receptor[266]. The G protein functional assay analyzes the biological responses of a ligand binding to a GPCR by quantifying the downstream production concentrations of second messengers and/or effectors, such as cAMP, Ca^{2+}, IP_3, and β-arrestin[267]. Similarly, G protein functional assays are very high throughput screening methods, but these assays are very pathway specific. The high specificity of these assays makes them not suitable for studying orphan GPCRs because their coupled pathways are unknown. In addition, many GPCRs activate more than one signaling pathway and since functional assays are very pathway specific, it can potentially miss information about the other pathways that are activated due to crosstalk or multi-pathway activation[267]. Lastly, these functional assays are not real-time assays, and this can result in missed information about the kinetics of cellular responses.

A more advanced technique for GPCR screening and analysis is real-time fluorescence. In real-time fluorescence assays, cell lines that express protein targets labeled with auto-fluorescent proteins (e.g., the green fluorescent protein (GFP)) are first generated[268]. Then a ligand or compound of interest induces a response in the cells to promote protein translocation. The response is then monitored by using an optical microscope-based instrument to image or record the fluorescently tagged proteins. Real-time fluorescence assays can provide information on the kinetics of receptor activation and signaling and also on the spatial distribution of the receptors[60]. Fluorescence assays

allows physical visualization of the mechanisms of GPCR signaling; it allows analysis of kinetics of individual steps, and it provides spatial locations of signal proteins within the cells[12, 60]. Although optical techniques using fluorescent labels allow more comprehensive study of receptor binding and signaling, the presence of fluorescent labels can potentially modify the physiological cellular environment of the targeted molecules of interest, which may lead to altered and uncertain results.

Lastly, label-free whole cell assay is a dynamic and integrated method where the overall signal transduction response is measured and not a single transduction pathway[61]. Furthermore, these assays are label-free and do not introduce foreign molecules that can potentially alter the physiological cellular environment for the targets of interest. Current label-free whole cell methods are based on impedance and optical sensor technologies. Both of these sensor technologies can detect the changes in cellular features, such as cell adhesion, cell morphology, cell proliferation, and cell death[62-64]. GPCR signaling has been detected using these technologies and the signals are highly sensitive where it can detect endogenous ligand-induced responses[61]. Both technologies have the ability to record responses in real-time and provide profiles of the kinetics of cellular responses. In addition, these profiles can be quantified to give potency values or EC_{50} values[61, 66]. The combination of the results obtained through label-free whole cell technologies and results obtained from traditional cell signaling methods can potentially provide new information about cellular pathways and cellular responses mediated through GPCRs.

In the work reported here, we used the real-time ΔD-response of QCM-D as a way to monitor the cellular response of GPCR activation in human carcinoma A431 cells. First, we examined the ΔD-response mediated through the activation of G protein

receptors to cell adhesion. Then a series of GPCR ligands that are specific to the $G_{\alpha q}$, $G_{\alpha s}$, and $G_{\alpha i}$ signaling pathways were examined to provide common Δ*D*-response features for the three well-known and studied of G protein signaling pathways. To determine the sensitivity of the Δ*D*-response to detect GPCR mediated response, the EC_{50} values were obtained for these ligands and were compared to the values determined through traditional methods. To confirm that the Δ*D*-response is mediated through the respective GPCR pathway, modulation experiments were performed. Lastly, using modulation experiments, we examined signal coordination and crosstalk among multiple signaling pathways, and we obtained information on the order of activation in a multiple signaling system.

6.2 Results

6.2.1 Detection of Δ*D*-Response Mediated Through the Activation of G protein Receptors

When a ligand binds to a G protein receptor, it can induce a variety of intracellular responses. The intracellular response is dependent on the GTP protein bond to the receptor. The three main subtypes in which we are mainly interested are G_s-coupled, G_i-coupled, and G_q-coupled (Figure 6.2). Each subtype of protein can activate different downstream effector proteins and in turn produce a different cellular response including change in cell adhesion.

Epinephrine (Epi) is known to bind the G_s-coupled beta-2 adrenergic receptor (A_{2B}) and induces $G_{\alpha s}$ pathway. The cellular response was recorded as a function of time. The Epi-induced Δ*D*-response profile consists of three phases. The first phase is a sharp increase in the Δ*D*-response to about 3-min (S1 to S2), followed by a 1-minute short and

rapid decrease in phase II (S2 to S3), and ending with a gradual level off of the Δ*D*-response in phase III (S3 to S4) (Figure 6.2A).

Lysophosphatidic acid (LPA) is identified as an agonist for G_i-coupled LPA receptor and induces $G_{\alpha i}$ pathway. The LPA-mediated cellular response profile also consists of three phases. The initial phase is a quick and steep increase (I1 to I2) and reaching a peak at 6 min (I2), followed by a steep decline below the baseline ($\Delta D = 0$) at 20 min (I2 to I3) in phase II and ending in a gradual incline in phase III (I3 to I4) (Figure 6.2B).

With the adenosine triphosphate (ATP) stimulation, the Δ*D*-response of the G_q-coupled P2Y receptor was obtained. ATP-induced response profile consists of three phases. The ATP-induced response begins with a fast and steep increase for 10 minutes in phase I (Q1 to Q2); secondly, there is a transition phase that includes a short steep decrease phase (Q2 to Q3) for 5 minutes and followed by shoulder phase for another 5 minutes in phase II (Q3 to Q4). Lastly the ATP-induced Δ*D*-response terminates with a gradual level off in phase III (Q4 to Q5) (Figure 6.2C). The three GPCR class agonists examined provided three different Δ*D*-response profiles. The differences in Δ*D*-response profiles can potentially detect downstream signaling of different G- protein classes.

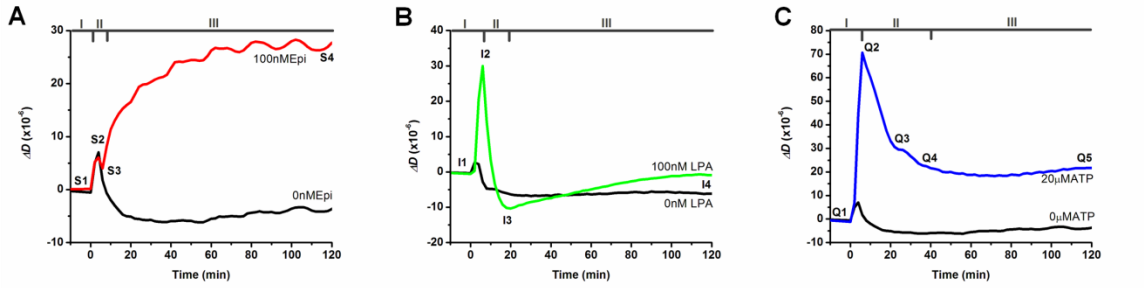

Figure 6.2. Real-time QCM-D measurements (at the order of vibrational mode n = 3) of the responses of A431 cells to GPCR ligands at 37 °C. (A) The signature Δ*D*-response of G_s signaling pathway induced by 100 nM epinephrine (Epi). (B) The signature Δ*D*-response of G_i signaling pathway induced by 100 nM lysophosphatidic acid (LPA). (C) The signature Δ*D*-response of G_q signaling pathway induced by 20 μM adenosine triphosphate (ATP).

6.2.2 Correlation of the Δ*D*-Response Mediated Through the Activation of G protein Receptors to Cell Adhesion

In previous studies, we found that the Δ*D*-response induced by EGF through the EGFR pathways was correlated with de-adhesion and re-adhesion of focal adhesions. The decrease in Δ*D*-response is correlated with weaker cell adhesion and increase in the Δ*D*-response associates with stronger cell adhesion. We visually examined GPCR ligand-induced changes in the number and size of focal adhesions as a function of time with the aid of immunostained vinculin. Figure 6.3 A1-A4 shows the images of immunostained vinculin of different exposure times of Epi. Our data reveal an increase in the number of vinculin spots with increasing exposure time, which is correlated with the Epi-induced increase of Δ*D*-responses over time (Figure 6.3A). Similar experiments were performed with LPA (Figure 6.3 B1-B4). After 10 minutes of exposure of LPA, we observed an increase in the number of vinculin. At 30 min and 60 min we observed vinculin levels decrease. These results correspond with the rapid increase and rapid decrease observed in the LPA-induced Δ*D*-response. Finally, cells were stained after increasing exposure times of ATP (Figure 6.3 C1-C4). We observed the highest levels of vinculin at 10 minutes and

weaker levels of vinculin at 30 min and 60 min. These showed similar patterns compared to the Δ*D*-response, where the ATP-induced response increases rapidly within the first 10 minutes and then gradually decreases. Figures 6.3A-C shows the correlation of the normalized dissipation and normalized fluorescence intensities of vinculin with exposure of Epi, LPA, and ATP. The comparison between the fluorescence levels of vinculin and the Δ*D*-response for each ligand show when the Δ*D*-response response increases, the cell adhesion increases and when the Δ*D*-response response decreases, the cell adhesion decreases.

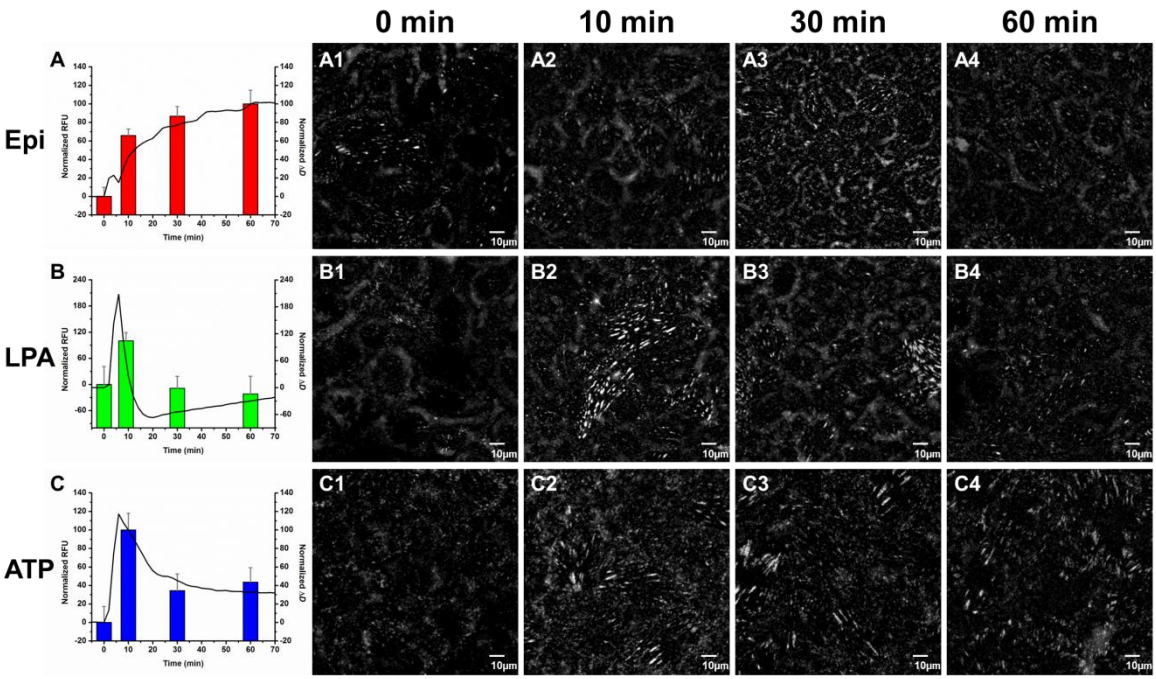

Figure 6.3. The correlation between the Δ*D*-response and the cell adhesion. Quantitation of the density of focal adhesion in relative fluorescence unit (RFU) as a measure of cell adhesion strength (mean ± SEM; N = 10). All correlations determined are highly statistically significant ($p < 0.005$). (A) A correlation is shown between the normalized intensity of the Δ*D*-response of 100 nM Epi and the normalized RFU of focal adhesion induced by 100 nM Epi. (A1) to (A4) show the fluorescence images of focal adhesion by immunostained vinculin in a monolayer of cells after various lengths of time of exposure to 100 nM Epi: 0 min, 10 min, 30 min, 60 min, respectively. (B) A correlation is shown between the normalized intensity of the Δ*D*-response of 100 nM LPA and the normalized RFU of focal adhesion induced by 100 nM LPA. (B1) to (B4) show the fluorescence images of focal adhesion in a monolayer of cells after various lengths of time of exposure to 100 nM LPA: 0 min, 10 min, 30 min, 60 min, respectively. (C) A correlation is shown between the normalized intensity of the Δ*D*-response of 20 μM ATP and the normalized RFU of focal adhesion induced by 20 μM ATP. (C1) to (C4) shows the fluorescence images of focal adhesion by immunostained vinculin in a monolayer of cells after various lengths of time of exposure to 20 μM ATP: 0 min, 10 min, 30 min, and 60 min, respectively.

6.2.3 Examination of GPCR-Mediated QCM-D-Response in MCF10A

Endogenous G protein coupled receptors can be expressed in various cell lines. To determine if the Δ*D*-response profile of each GPCR subtype is similar in various cell lines, a set of GPCR-inducing ligands was studied in MCF10A cells and compared with the Δ*D*-response of A431 cells. NECA was used to induce the G_s-coupled adenosine A_{2A}/A_{2B} receptors in MCF10A cells. The Δ*D*-response profile obtained in MCF10A cells

(Figure 6.4A) showed an overall increase in the Δ*D*-response similar to that of A431 cells (Figure 6.4D), but there are differences in the shape of the Δ*D*-response profile. LPA was used to induce LPA1 receptors in MCF10A cells. The Δ*D*-response profile of MCF10A displayed a different profile than that of the LPA-induced Δ*D*-response in A431 cells. The LPA-induced Δ*D*-response in MCF10A shifted below the control response where the LPA-induced Δ*D*-response in A431 does not (Figure 6.4B and 6.4E). ATP was used to induce the P2Y receptors in MCF10A cells. In MCF10A cells the Δ*D*-response profile does not exhibit a gradual phase II, whereas the Δ*D*-response in A431 cells has a distinct shoulder (Figure 6.4C and 6.4F). These differences in the Δ*D*-response demonstrate the ligand-induced response is specific to the cell type. (The possible causes of these differences in response are discussed after Figure 8.3 in chapter 8.) These experiments demonstrate that the QCM-D is sensitive enough to detect such differences, which can potentially be beneficial in differentiating abnormal and normal cellular responses.

If one reviews Figure 6.4, one sees that the controls (0.0 μM ligand) are very similar within each cell type (vertical scales in the figures are different). The small differences observed are due to inherent difference in cell cultures done at different times under identical conditions.

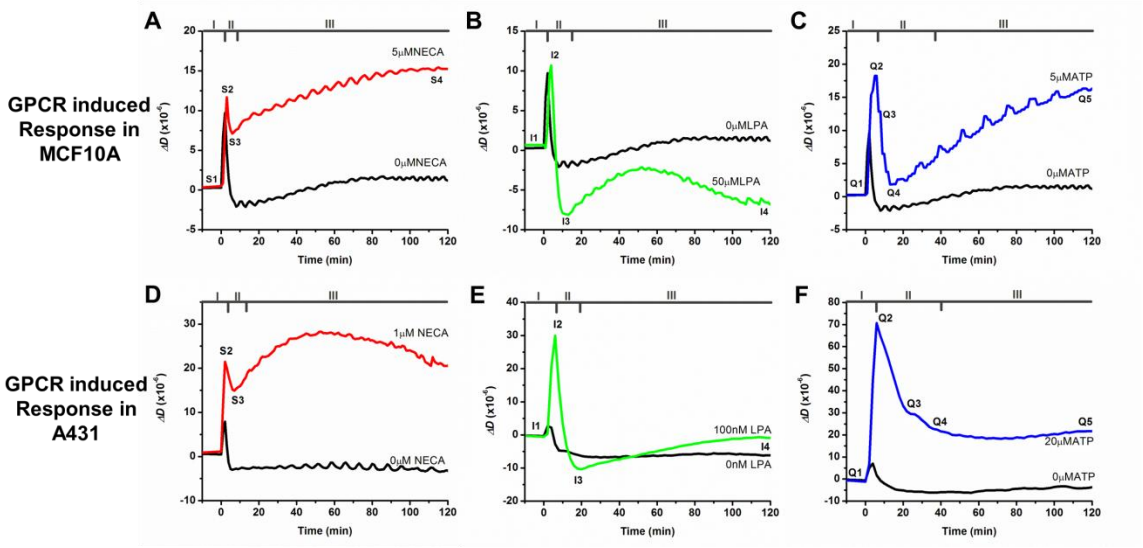

Figure 6.4. Comparison of GPCR ligand-induced QCM-D measurements in MCF10A and A431 cells. (A) The Δ*D*-response of G_s signaling pathway induced by 5 μM NECA in MCF10A. (B) The Δ*D*-response of G_i signaling pathway induced by 10 μM LPA in MCF10A. (C) The Δ*D*-response of G_q signaling pathway induced by 5 μM ATP in MCF10A. (D) The Δ*D*-response of G_s signaling pathway induced by 1 μM NECA in A431. (E) The Δ*D*-response of G_i signaling pathway induced by 100 nM LPA in A431. (F) The Δ*D*-response of G_q signaling pathway induced by 20 μM ATP in A431.

6.2.4 Characterization of the Δ*D*-Response Mediated Through the Activation of G protein-Coupled Receptor Subtype

To determine specific patterns in the Δ*D*-response mediated through different G protein coupled receptor families, a series of G_s-coupled, G_i-coupled, and G_q-coupled inducing ligands were tested. For the response mediated through the $G_{\alpha s}$ pathway, we tested two other ligands, 5'-N-ethylcarboxamidoadenosine (NECA) and isoproterenol (ISO). They are known to bind to the adenosine receptor and adrenergic receptor, respectively. The Δ*D*-response of the $G_{\alpha s}$ pathway-inducing ligands showed a Δ*D*-response pattern with a similar initial steep increase followed by an overall increase (Figure 6.5).

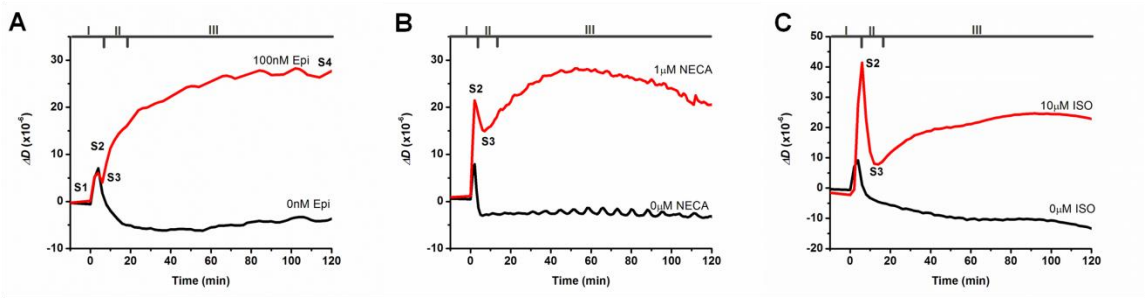

Figure 6.5. Comparison of the elevated QCM-D-response induced by G_s stimulated ligands in A431 cells. (A) The Δ*D*-response induced by epinephrine (Epi). (B) The Δ*D*-response induced by 5'-N-ethylcaroxamidoadenosine (NECA). (C) The Δ*D*-response induced by isoproterenol (ISO). (At least ten replicates were done of each experiment.)

For the response mediated through the $G_{\alpha i}$ pathway, we examined nicotinic acid (NA) mediated through the HM74A receptor. Nicotinic acid-induced Δ*D*-response showed a quick and steep peak at 6-min (I2), followed by a steep decline below the initial starting position at 20-min (I3) and ending in a gradual stabilization (Figure 6.6). The Δ*D*-responses of LPA and NA showed very similar response patterns.

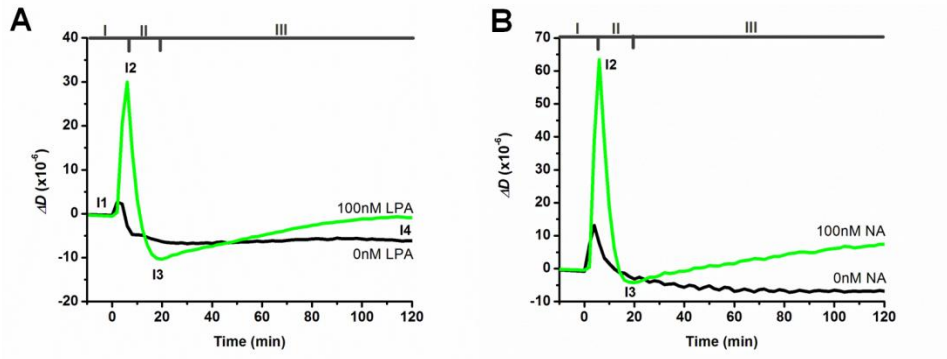

Figure 6.6. Comparison of the steep initial QCM-D-response peak induced by G_i stimulated ligands in A431 cells. (A) The Δ*D*-response induced by lysophosphatidic acid (LPA). (B) The Δ*D*-response induced by nicotinic acid (NA). (At least ten replicates were done of each experiment.)

For examination of the response mediated through the $G_{\alpha q}$ pathway, we also studied bradykinin (BK), thrombin (Thr), and histamine (Hist) through the G_q-coupled bradykinin B2 receptor (BDKRB2), protease-activated receptor 1 (PAR1), and histamine H1 receptor, respectively. The Δ*D*-response of these three ligands have similar profile of a steep initial increasing phase, followed by a short steep decreasing phase with a shoulder phase, and ending with a gradual level-off phase (Figure 6.7).

From these studies of different ligands of each different G protein receptor subtype, we can establish ligands of the same G protein subtype have similar Δ*D*-response pattern. These common Δ*D*-response features can potentially be used to characterize the G protein subtype of orphan GPCRs. The common Δ*D*-response feature shared among G_s ligands occurs in phase III, where there is a gradual increase. The common Δ*D*-response features shared among G_i ligands occur in phase I and II, where there is a steep increase and followed by a rapid decrease to baseline levels. The common Δ*D*-response feature determined for the G_q ligands is a quick and steep increase that occurs in phase I and a slow and gradual decrease in phases II and III of the Δ*D*-response. These common features due to each G protein subtype may suggest that each pathway can induce different cellular response detected by the QCM-D and these common features are summarized in Figure 6.8.

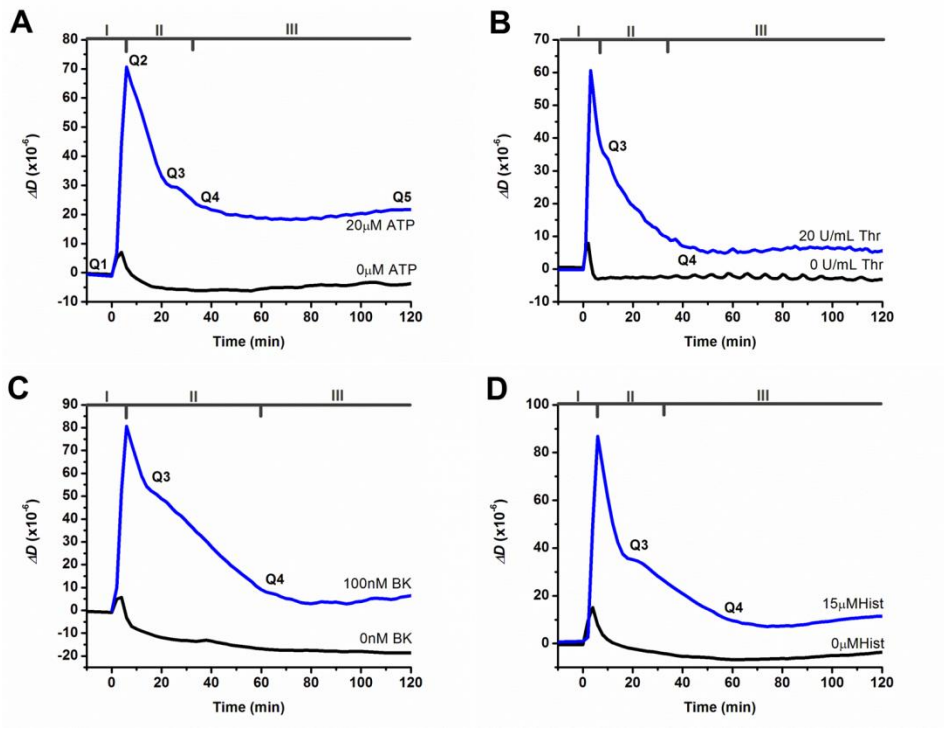

Figure 6.7. Comparison of the steep initial QCM-D-response peak with shoulder induced by G_q stimulated ligands in A431 cells. (A) The Δ*D*-response induced by adenosine triphosphate (ATP). (B) The Δ*D*-response induced by thrombin (Thr). (C) The Δ*D*-response induced by bradykinin (BK). (D) The Δ*D*-response induced by histamine (Hist). (At least ten replicates were done of each experiment.)

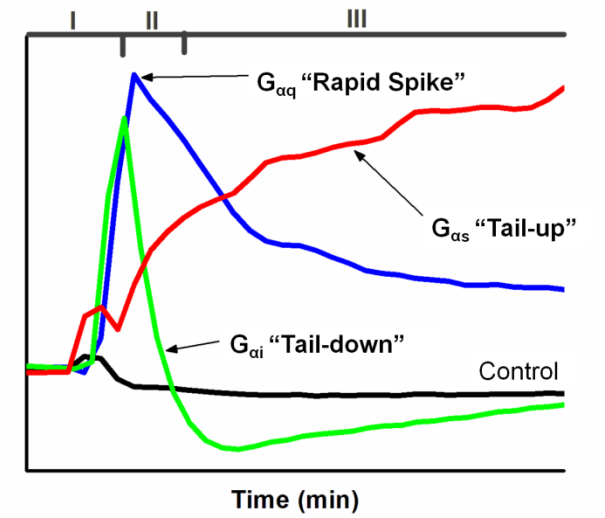

Figure 6.8. Illustration of common features in the Δ*D*-response of each GPCR subtype.

6.2.5 Analysis of the Dose Dependence of the Δ*D*-Response Induced by the G protein Receptors

Many current methods in screening the GPCR pathway provide quantitative values that can be used to compare with other methods. To provide a quantitative assessment of the QCM-D-responses of the GPCR ligands, an EC_{50} value was determined for each ligand. EC_{50} is the concentration of agonist that induces a response halfway between the maximum and baseline response of the agonist[269]. The EC_{50} values can also be used as an approximation of the binding affinity of a ligand (K_d)[190].

To determine the EC_{50} values of the GPCR ligands in this study, the Δ*D*-responses were acquired at various concentrations for each ligand. Each ligand showed a dose dependent increase in the Δ*D*-response (Figure 6.9). The magnitude of the Δ*D*-response at a specific time point was used to determine the EC_{50}. The chosen time point for the magnitude measurements was based on the location of the common feature of the Δ*D*-response that was described in the previous section. For the G_s-inducing ligands, Epi, NECA, and ISO, the magnitude of the dose response was taken between 20 to 30 minutes. For the G_i-inducing ligands, LPA, and NA, the magnitude of the dose response was taken between 10 to 15 minutes. For the G_q-inducing ligands, ATP, Thr, BK and Hist, the magnitude of the dose response was taken between 8 to 10 minutes. The dose response curves were generated and fitted to obtain the EC_{50} values for each ligand (Figure 6.10). The calculated EC_{50} values determined are listed in Table 6.1 and are compared to literature EC_{50} values others have obtained using current methods in screening GPCRs. The EC_{50} values determined with Δ*D*-response showed less than 10-fold difference compared with the EC_{50} values obtained by others using conventional methods and techniques. There have been publications comparing data of optical and

impedance sensor technologies to traditional GPCR labeling screening methods and most comparisons showed a 10-fold difference in EC_{50} values[61]. Our comparable EC_{50} values to traditional method values demonstrate the QCM-D is a very sensitive instrument compared to other label-free biosensors. The EC_{50} values determined with the ΔD-response also showed lower EC_{50} values compared with those determined by conventional methods. One reason could be that the time point selected for determination of the EC_{50} value is the maximum in the real-time and continuous ΔD-response, whereas conventional methods take data at discrete time points, typically missing the maximum response of the a cell to a ligand by a slight amount. The maximum response comes fairly quickly after dosing, and is easy to miss if data are taken at discrete time points; any data taken slightly after the actual maximum lead to higher EC_{50} values.

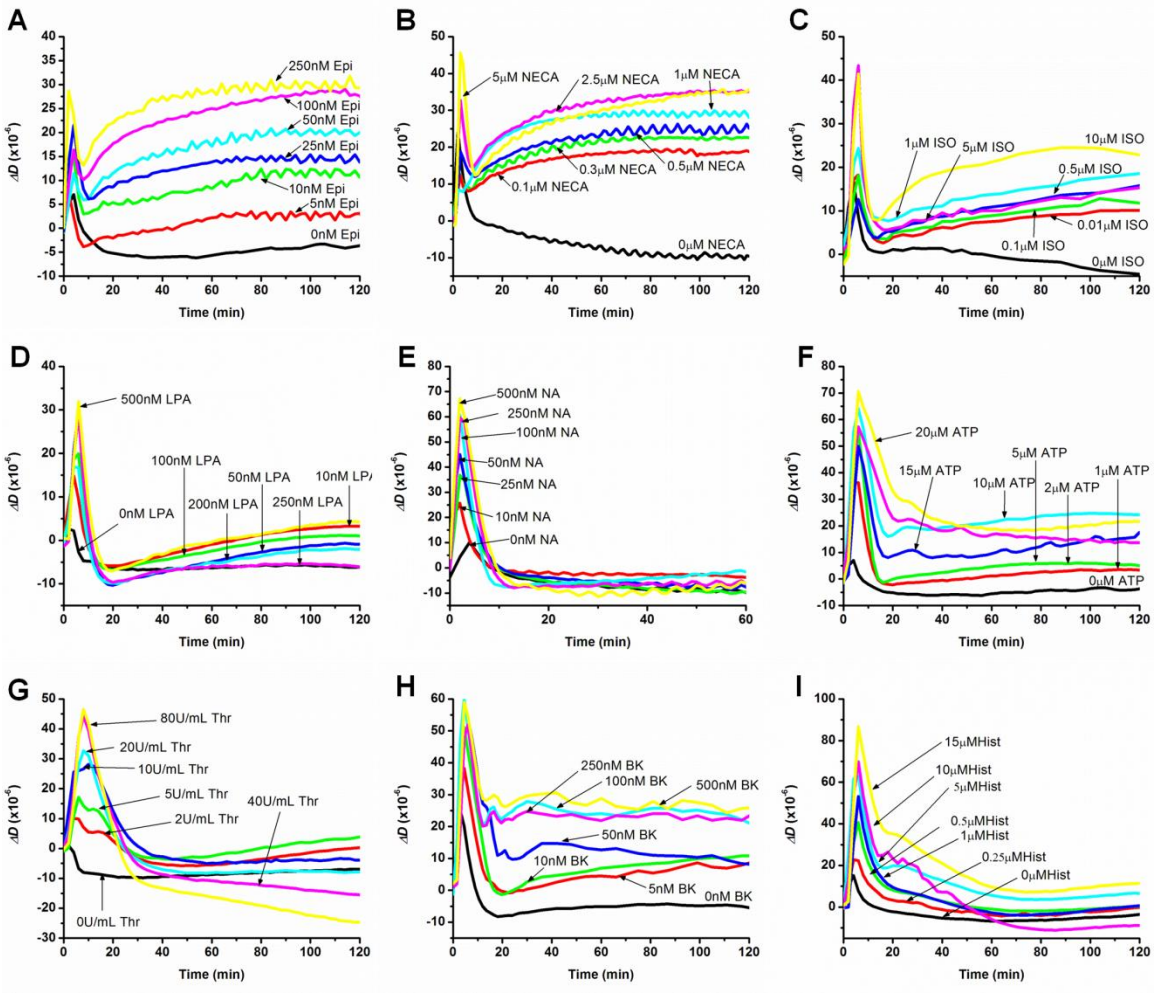

Figure 6.9. Δ*D*-response vs time for GPCR-induced ligands in A431 cells, showing dose response. (A, B, C) G_s-mediated ligands: Epi, NECA, and ISO, respectively. (D, E) G_i-induced ligands: LPA and NA, respectively. (F, G, H, I) G_q-mediated ligands: ATP, Thr, BK, and Hist, respectively.

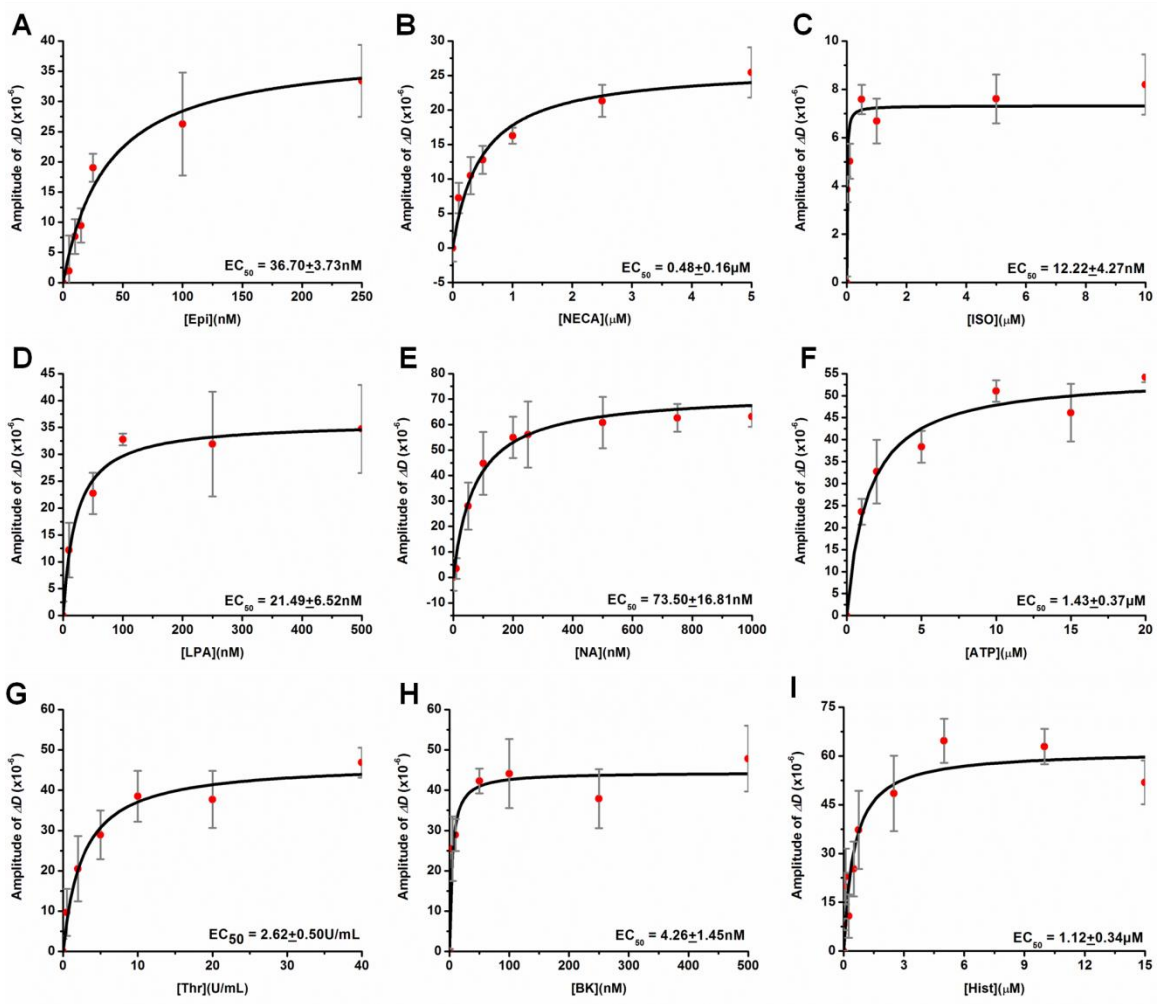

Figure 6.10. Δ*D*-response vs. concentration of GPCR-inducing ligands in A431 cells. (A) Δ*D*-responses determined at 8 min as a function of Epi concentration. (B) Δ*D*-responses at 10 min as a function of NECA concentration. (C) Δ*D*-responses at 9 min as a function of ISO concentration. (D) Δ*D*-responses at 6min as a function of LPA concentration. (E) Δ*D*-responses at 6min as a function of NA concentration. (F) Δ*D*-responses at 6 min as a function of ATP concentration. (G) Δ*D*-responses at 8 min as a function of Thr concentration. (H) Δ*D*-responses at 6 min as a function of BK concentration. (I) Δ*D*-responses at 8 min as a function of Hist concentration. The EC_{50} value is shown on each plot.

Table 6.1. Summary of EC_{50} values determined using the amplitudes of Δ*D*-responses of each ligand.

GPCR Ligand	G-Protein	EC_{50} (determined w/ Δ*D*)	EC_{50} (literature)	Method of Detection
Epi	G_s	36.70 ± 3.73 nM	54.96 nM [270]	cAMP
NECA	G_s	0.48 ± 0.16 µM	1.0–1.4 µM [244, 271]	cAMP
ISO	G_s	12.22 ± 4.27 nM	19.8 nM [270]	cAMP
LPA	G_i	21.49 ± 6.52 nM	52 nM (IC_{50}) [272]	cAMP
NA	G_i	73.50 ± 16.81 nM	67–128 nM (IC_{50}) [273, 274]	cAMP
ATP	G_q	1.43 ± 0.37 µM	1.5–5.8 µM [275]	Ca^{2+}
Thr	G_q	2.62 ± 0.50 U/mL	6.0±1.0 U/mL [257, 276, 277]	Ca^{2+}
BK	G_q	4.26 ± 1.45 nM	6 nM [278, 279]	Ca^{2+}
Hist	G_q	1.12 ± 0.34 µM	1-3 µM [258, 259]	Ca^{2+}

6.2.6 Confirmation of the GPCR Signaling Pathways Through Modulation Studies

To further validate that the GPCR mediated Δ*D*-responses can be related to specific subtype of GPCRs, pathway specific modulators were used to suppress the response of each GPCR signaling pathway. These modulation studies help to confirm the Δ*D*-response produced is due a specific GPCR signaling pathway and to provide information on signal coordination of multiple pathways.

Pertussis toxin (PTX), from *Bordetella pertussis,* catalyzes the ADP-ribosylation of the α subunits of the $G_{\alpha i/o}$ protein subtype. ADP-ribosylation of the α subunit of the $G_{i/o}$ proteins locks the α subunits into an inactive state and hinders the α subunits to inhibit adenylyl cyclase (AC)[280]. This modification of the $G_{\alpha i/o}$ results in the increased accumulation of cAMP and therefore alters pathological response to the $G_{\alpha i/o}$ agonist. Cholera toxin (CTX), from *Vibrio cholerae,* catalyzes the ADP-ribosylation of the α subunit of the $G_{\alpha s}$ protein subtype using cellular NAD^+ [58]. This modulation locks the α subunits in the active state causing elevated cAMP, and therefore over stimulates and masks the responses to $G_{\alpha s}$ agonists. YM-254890 (YM), from the bacteria *Chromobacterium sp. QS3666,* selectively blocks GDP release from the $G_{\alpha q}$ protein[281].

This inhibits the mobilization of intracellular calcium ion and transcription mediated through serum response element (SRE)-stimulated by receptors coupled to $G_{\alpha q}$[282-284]. Pertussis toxin, cholera toxin, and YM-254980 pretreatment have been used by others to suppress the responses of the $G_{\alpha i}$, $G_{\alpha s,}$ and $G_{\alpha q}$ signaling pathway, respectively[285].

For modulator studies of the $G_{\alpha s}$ pathway, cells were pretreated with CTX (a modulator) and then were induced with the G_s ligands. In the Epi-induced and the ISO-induced Δ*D*-responses showed a suppression of phase III of the Δ*D*-responses with CTX (Figures 6.11A and 6.11C). In the NECA-induced Δ*D*-response, there was similar suppression of phase III of the Δ*D*-response with pretreatment of CTX. However, phases I and II in the NECA-induced Δ*D*-responses were not inhibited by the CTX (Figure 6.11B). From these modulation studies on G_s-inducing ligands, we were able to confirm the increase in phase III of the Δ*D*-response is mediated by the $G_{\alpha s}$ pathway.

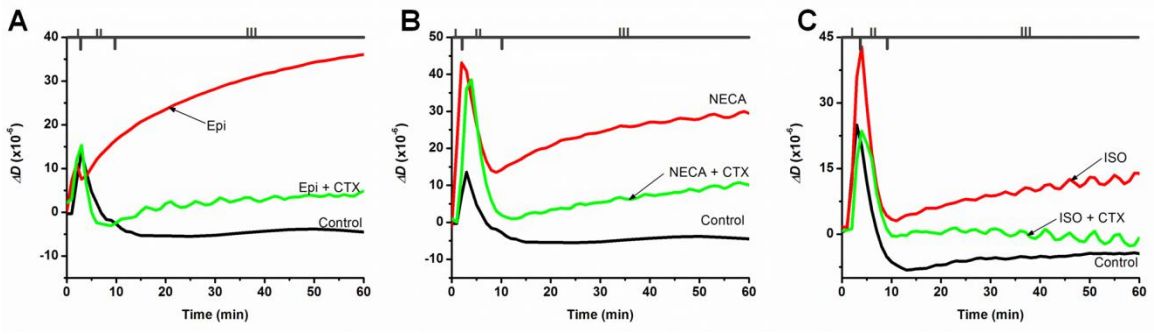

Figure 6.11. Δ*D*-response vs. time showing the effects of CTX on G_s-inducing ligands in A431 cells. (A) 250 ng/mL CTX pretreatment on 250 nM Epi-induced Δ*D*-response. (B) 250 ng/mL CTX pretreatment on 1 μM NECA-induced Δ*D*-response. (C) 250 ng/mL CTX pretreatment on 250 nM ISO-induced Δ*D*-response.

To modulate the $G_{\alpha i}$ pathway, cells were exposed to PTX and then stimulated with G_i-inducing ligands, LPA and NA. The LPA-induced Δ*D*-response showed a significant reduction of the peak in between phases I and II and little change in phase III when modulated with PTX (Figure 6.12A). Comparable effects were established with NA, where there was significant peak suppression of the peak between phases I and II with PTX pretreatment (Figure 6.12B). These studies confirmed the sharp peak in phase I and II of the Δ*D*-response of the G_i-inducing ligands is mediated through the $G_{\alpha i}$ pathway.

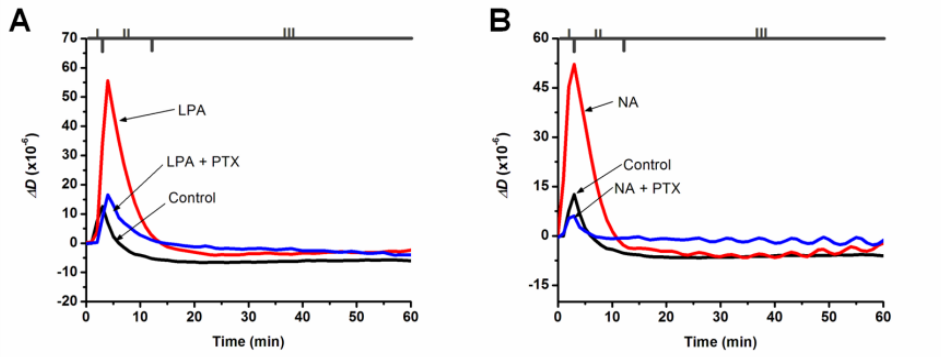

Figure 6.12 Δ*D*-response vs. time showing the effects of PTX on G_i-inducing ligands in A431 cells. (A) 250 ng/mL PTX pretreatment on 500 nM LPA-induced Δ*D*-response. (B) 250 ng/mL PTX pretreatment on 125 nM NA-induced Δ*D*-response.

Finally, experiments were performed with YM-254890 to inhibit the G_q response of the G_q-inducing ligands, ATP, Thr, BK and Hist. The ATP-induced Δ*D*-response of cells pretreated with YM showed a suppression of the peak in between phases I and II. However, in phase III of the ATP-induced Δ*D*-response with YM inhibition showed an increase to similar magnitude to the Δ*D*-response with no pretreatment (Figure 6.13A). Pretreatment with YM showed a significant suppression of the entire Δ*D*-response of the

Thr-induced, BK-induced, and Hist-induced Δ*D*-responses (Figures 6.13B-C). These studies confirmed the sharp peak with a gradual decrease is the common Δ*D*-response feature of the $G_{\alpha q}$ pathway.

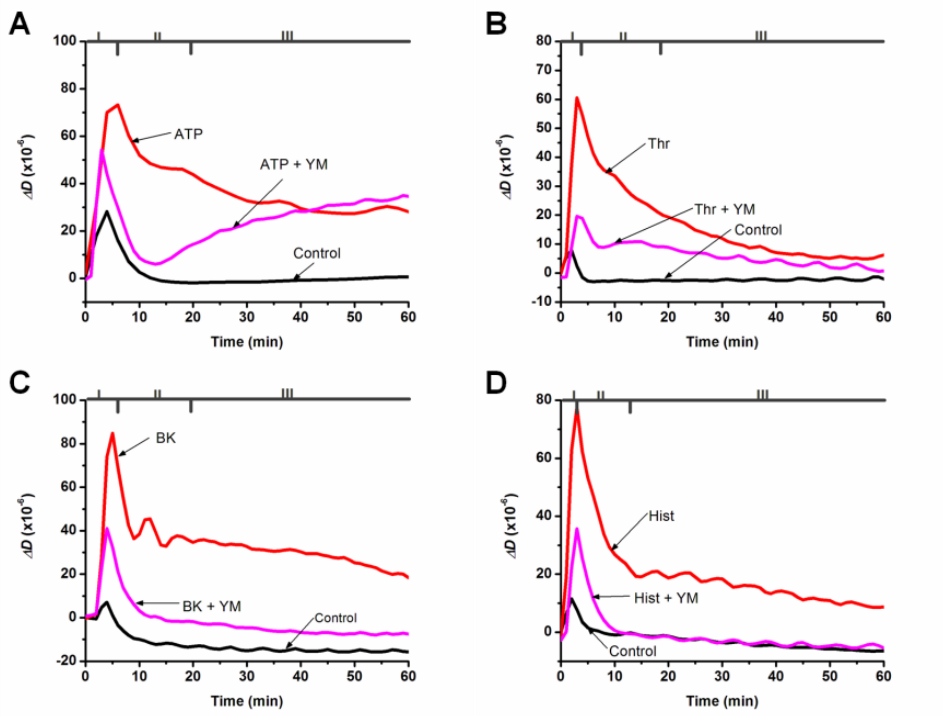

Figure 6.13. Δ*D*-response vs. time showing the effects of PTX on G_q-inducing ligands in A431 cells. (A) 300 nM YM pretreatment on 20 μM ATP-induced Δ*D*-response. (B) 300 nM YM pretreatment on 20 U/mL Thr-induced Δ*D*-response. (C) 300 nM YM pretreatment on 50 nM BK-induced Δ*D*-response. (D) 300 nM YM pretreatment on 15 μM Hist-induced Δ*D*-response.

6.2.7 Analysis of Multiple Pathway Activation via Modulation Studies

From the previous modulation studies, the Δ*D*-response of ATP and NECA revealed incomplete inhibition in response to pathway specific modulators. This incomplete inhibition of the Δ*D*-response may be due to activation of multiple GPCR pathways. Others have shown that GPCRs can couple to more than one G protein and can activate multiple signaling pathways[286]. In these studies, all three pathway modulators

were used on each ligand to determine the activation of multiple GPCR signaling pathways.

It has been shown by others that A431 cell expresses $G_{q/s}$-coupled P_2Y_{11} receptors, G_q-coupled P_2Y_1 (weakly), G_q-coupled P_2Y_4, and G_q-coupled P_2Y_6 [287, 288]. It has also been shown ATP is a non-specific P_2Y agonist and can activate any of the receptors expressed in A431 cells[289]. In the ATP-induced Δ*D*-response pretreated with CTX exhibited significant suppression of the phase III, but not the initial peak in phase I and II. This suggests that phase III reflects the activation $G_{\alpha s}$ pathway, and it is likely activated through the P_2Y_{11} receptor. The modulation with PTX did not cause a change to the ATP-induced Δ*D*-response, which confirms that the P_2Y subtypes expressed in A431 do not couple to the $G_{\alpha i}$ pathway (Figure 6.14A). Lastly, the initial peak in phase I and II is the portion of the Δ*D*-response mediated by the $G_{\alpha q}$ pathway through a combination of the G_q-coupled receptors expressed in A431 cells. This demonstrates that the Δ*D*-response induced by ATP in A431 cells is a combination of the cellular response mediated through early phase activation of the $G_{\alpha q}$ pathway and a late phase activation of the $G_{\alpha s}$ signaling pathway.

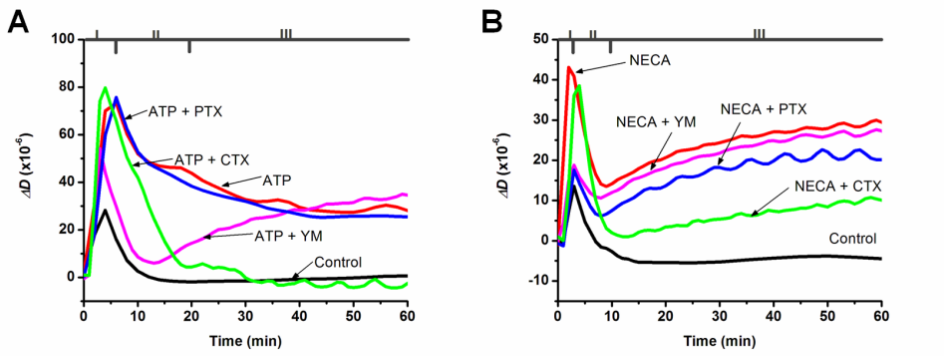

Figure 6.14. Real-time QCM-D measurements of the GPCR modulator responses on G_s-inducing ligands of A431 cells. (A) Effects comparison of 250 ng/mL PTX, 250 ng/mL CTX, and 300 nM YM pretreatments on 250 nM ATP-induced Δ*D*-response. (B) Comparison of 250 ng/mL PTX, 250 ng/mL CTX, and 300 nM YM pretreatments on 1 μM NECA-induced Δ*D*-response.

It has been shown that A431 cell expresses A_{2A}, A_{2B}, and A_1 subtypes of adenosine receptors[290]. NECA is a non-specific adenosine agonist and can bind to adenosine receptor $G_{s/q}$-coupled $A_{2A,}$ G_s-coupled A_{2B}, and G_i-coupled A_1 and A_3. The NECA-induced Δ*D*-response with PTX and YM pretreatments showed significant reduction of the initial peak in phase I and II, but little to no reduction of phase III. These results suggest that the initial peak could be due to $G_{\alpha i}$ and $G_{\alpha q}$ signaling through the A_1 receptor and A_{2A} receptor, respectively. Phase III of the Δ*D*-response inhibited by CTX suggests that it reflects the response of the $G_{\alpha s}$ signaling through the A_{2A} receptor and A_{2B} receptor. The dissection of the Δ*D*-response induced by NECA suggests the cellular response is mediated through a combination of the $G_{\alpha s,}$ $G_{\alpha q,}$ and $G_{\alpha i}$ signaling pathway in A431 cells. The modulator studies provide evidence the Δ*D*-response can be used to dissect signaling pathways and potentially provide information about the signal coordination, crosstalk between signaling pathways, and stimulation of multiple pathways.

6.3 Discussion/Conclusions

GPCRs are of great interest because of their large involvement in numerous physiological and pathological roles in transducing extracellular signals of a broad range of biomolecules, including proteins, peptides, and organic compounds, into intracellular effector pathway responses. Due to their large influence on physiological functions, such as blood pressure regulation, allergic response, hormonal regulation, and progression of cancer, this makes them important targets for a variety of therapeutics[235]. There are more than 140 orphan GPCRs, for which the endogenous ligands for these GPCRs remain unidentified and their natural functions remain unknown[226]. These orphan GPCRs are a great source of potential drug targets. Therefore the development of screening assays for GPCR has been a major focus to provide insight on the role and mechanism of these GPCRs.

This study demonstrates the QCM-D can be a useful label-free, real-time, whole cell technique in detecting GPCR-induced cellular responses. The QCM-D allows biomolecules to operate in a more native-like and physiological-like state compared to traditional biochemical assays. Most traditional biochemical assays utilize non-native fluorescent labels to track cell signaling pathways and produce foreign environment for the molecule of interest, which may lead to uncertainty in the results. We demonstrated the ΔD-response induced by specific G protein coupled receptor ligands is dose sensitive and allows for quantification. The EC_{50} values determined for the ΔD-response induced by GPCR ligands have a less than 10-fold difference compared to traditional second messenger assays (Table 6.1).

The Δ*D*-response has been shown to provide sensitive measurements of the cellular response induced by specific G-coupled receptor ligands in A431 cells. The QCM-D can capture unique real-time Δ*D*-responses of different G protein coupling receptors ($G_{\alpha s,}$ $G_{\alpha i}$, and $G_{\alpha q}$). In the present study, each G protein coupling receptor subtype, when activated, exhibited common features in the Δ*D*-response, which can therefore be used as a qualitative indicator for differentiating the cellular responses of G protein coupling receptors. The common feature of Δ*D*-response for the $G_{\alpha s}$ signaling cascade is a gradual increase in the third phase of the response. The common Δ*D*-response feature of the $G_{\alpha i}$ signaling is a steep peak in phases I and II. The common Δ*D*-response pattern determined for the $G_{\alpha q}$-induced signaling is the initial steep peak phase I and a gradual decrease in phases II and III (Figure 6.8).

Due to the QCM-D's ability to detect changes in cell adhesion, a cellular process induced by many pathways allows for non-specific pathway detection. In traditional methods, pathway-specific secondary messengers or effectors, such as cAMP, Ca^{2+}, IP_3, and β-arrestin, are detected and do not provide information about the effects on other signaling pathways. On the other hand, the QCM-D allows for an objective detection of the GPCR-mediated signaling for the reason that cell adhesion can be mediated through multiple pathways and not a single specific G protein-coupled pathway. Many studies completed by others show that cell adhesion can be affected through stimulation of GPCRs[61]. To further confirm this notion, a correlation between the Δ*D*-response and levels of cell adhesion was sought (Figure 6.3). The correlation shown in Figure 6.3, between cell adhesion and the Δ*D*-response, allows for a better understanding of the nature of the Δ*D*-response and provides fundamental information about the cellular

response. From this correlation, we demonstrated that the activation of the $G_{\alpha s}$ pathway by epinephrine and isoproterenol causes an overall increased Δ*D*-response, which suggests an increase in cell adhesion. This observation is in line with reports of other research groups stating that cAMP induces integrin-mediated cell adhesion through the stimulation $G_{\alpha s}$-coupled beta-2 adrenergic receptor[291-293]. G_q protein-coupled receptors, when activated, result in PIP_2 hydrolysis and Ca^{2+} release from intracellular stores via the PLC-IP_3 signaling pathway[294]. Findings reported in the literature suggest that calcium mobilization regulates cell adhesion[295-297]. We also established that the G_q pathway induced by thrombin, bradykinin, and histamine resulted in a steep increase in the Δ*D*-response that can be interpreted as a rapid increase in cell adhesion. In our studies the G_i pathway induced by LPA and NA caused a rapid increase and subsequently a rapid decrease in the Δ*D*-response, which reflects an initial rapid increase in cell adhesion followed by a rapid decrease. Other studies have shown LPA causes cell dispersal of epithelial cell colonies[298, 299]. The quick increase and decrease in the Δ*D*-response can be due to stimulation of lamellipodia formation and enhanced migration of the cells demonstrated by Yamashita *et al*[299].

The Δ*D*-response is an integrated response to the cellular response mediated through the GPCR pathway. The QCM-D can display the overall cellular response of multiple downstream cellular events, unlike many traditional second messenger assays that can only quantify specific second messengers, which allows for only partial display of the cellular events of a cellular response. The modulation studies revealed multiple signaling pathway activation mediated through multiple receptor subtypes of ATP and NECA. The deconvolution of ATP-induced and NECA-induced Δ*D*-responses facilitated

the identification of signal coordination in multiple signaling pathways. With the combination of the appropriate pharmacological modulators or gene-silencing techniques, the QCM-D readout induced by G protein specific ligands can provide novel insight in the dynamics of cell signaling. The integrated Δ*D*-response allows for detections of subtle changes that traditional methods cannot detect. In this study, we have successfully separated the signaling pathways with the use of modulators, such as PTX, CTX and YM.

In summary, the QCM-D technique has been demonstrated to be a potentially useful label-free and real-time detection of the GPCR-induced cellular responses. The Δ*D*-response induced by G protein specific ligand can provide comparable quantitative results to conventional biochemical methods. The QCM-D allows for non-specific pathway detection through the detection of changes in cell adhesion. In addition, the time-resolved detection of the QCM-D provides insight on the kinetics of the GPCR signaling pathway. Lastly, with the appropriate modulators the Δ*D*-response can be deconvoluted to give insight on signaling dynamics, such as multiple pathway stimulation and pathway crosstalk. The QCM-D can potentially provide insight on the role and the mechanism of known GPCRs and orphan GPCRs. Lastly the QCM-D can potentially be a useful platform in screening novel drug targets.

Chapter 7: Real-Time Detection of Cellular Response Mediated by Distinct Subclasses of Epidermal Growth Factor Receptors**

7.1 Introduction

Epidermal growth factor receptor regulates cell growth, proliferation, motility, and differentiation through its downstream signaling pathways[183, 184]. Ligand binding to the extracellular domain of EGFR induces receptor dimerization, activates its kinase domain to induce its downstream signaling cascades[300]. Ligand binding studies with the use of radiolabeled EGF, the natural ligand of EGFR, suggest that there are two subclasses of EGFR[301, 302]: high-affinity EGFR, which exhibits K_d-values of a few nM or less, and low-affinity EGFR, which exhibits K_d-values of 10 nM or above. High-affinity EGFR accounts for less than 10 % of the total EGFR; however, it is the subclass that is most responsible for the regulation of cell growth, proliferation, motility, and differentiation[183, 184]. In contrast, low-affinity EGFR controls Ca^{2+} influx and fluid-phase pinocytosis[303], but contributes little to the regulation of cell growth, proliferation, motility, and differentiation. It has been originally suggested by Macdonald and Pike that the two subclasses of EGFR arise from negative cooperativity[304]. A ligand binds and forms an asymmetric EGFR dimer in which only one binding site is occupied[305, 306]. The unoccupied site in this dimer is structurally restrained and leads to a reduced affinity for binding of the second ligand[305, 306].

** Parts of this chapter are adapted from:
Chen, J.Y., Li, M., Penn, L.S. & Xi, J. Real-Time and Label-Free Detection of Cellular Response to Signaling Mediated by Distinct Subclasses of Epidermal Growth Factor Receptors. *Anal. Chem.* **83**, 3141-3146 (2011).

It is known that an abnormal EGFR signaling can induce uncontrolled cell growth and a malignant phenotype, such as tumors[307]. In fact, EGFR is highly expressed in a variety of human tumors, including head and neck squamous cell cancer, colorectal cancer, non-small cell lung cancer, and breast cancer[43]. Because of the critical role of high-affinity EGFR in regulation of cell growth, proliferation, motility, and differentiation, the extent of cell signaling mediated by high-affinity EGFR can therefore be very informative for assessing the role of EGFR in cancer development and cancer diagnosis[308]. This requires a detection system that is capable of tracking cellular responses specifically to high-affinity EGFR signaling.

This chapter describes a QCM-D-based approach that specifically assesses the individual cellular response of both high-affinity and low-affinity EGFR signaling. With this approach, we were able to distinguish and detect cellular responses mediated by high-affinity and low-affinity EGFR signaling. Various real-time and label-free sensor technologies have been developed to examine EGFR-mediated cell signaling[309, 310]. However, none of those technologies has been able to simultaneously detect the individual responses mediated by each of these two subclasses of EGFR and distinguish the cell signaling mediated by high-affinity EGFR from that mediated by low-affinity EGFR.

7.2 Results/Discussion

7.2.1 Establishing the EGF-Induced ΔD- and Δf- Responses

In the present study, QCM-D was used to monitor the short-term, EGF-induced response of a confluent monolayer of human carcinoma A431 cells. Figure 7.1 shows

Δ*D*- and Δ*f*- responses of the cells as a function of time under three different sets of experimental conditions. Figure 7.1A shows the effect of 10 nM EGF on the Δ*D*-response of the cells. The cells treated with EGF or without EGF (buffer) show an initial sharp increase in Δ*D* (peak DM), which is due to mechanical perturbation of the cells by the transfer of liquid by pipetting. After an initial rise, a rapid decrease in Δ*D*-response is shown by both cell samples. However, the EGF-treated cells exhibited a much greater decrease in Δ*D*-response than the buffer-treated cells did. This difference represents the EGF-induced Δ*D*-response of the cells. The observed large decrease in Δ*D*-response of the EGF-treated cells indicates a decrease in adhesion of the cell monolayer on the sensor surface. This is consistent with the known stiffening and rounding of A431 cells in response to the EGF treatment[311]. The lowest value of Δ*D*-response was reached at about 50 min (at dotted line H), which agrees well with previous observations that A431 cells develop the most extreme rounding around 45 min[312]. The Δ*f*-responses of the cells from the same experiment are shown in Figure 7.1B. The initial response of both the EGF-treated and buffer-treated cells was a sharp decrease (peak fM), resulting from the above-mentioned mechanical perturbation. After this, the Δ*f*-response of the buffer-treated cells increased and leveled off at a constant value, while the Δ*f*-response of the EGF-treated cells continued to rise to produce peak L. Thus peak L represents the EGF-induced Δ*f*-response of the cells. The increase in Δ*f*-response shown by the rising of peak L reflects a decrease in mass, which could arise from the transport of ions or liquid medium out of the shallow pockets underneath of the cells into the cytoplasm[114].

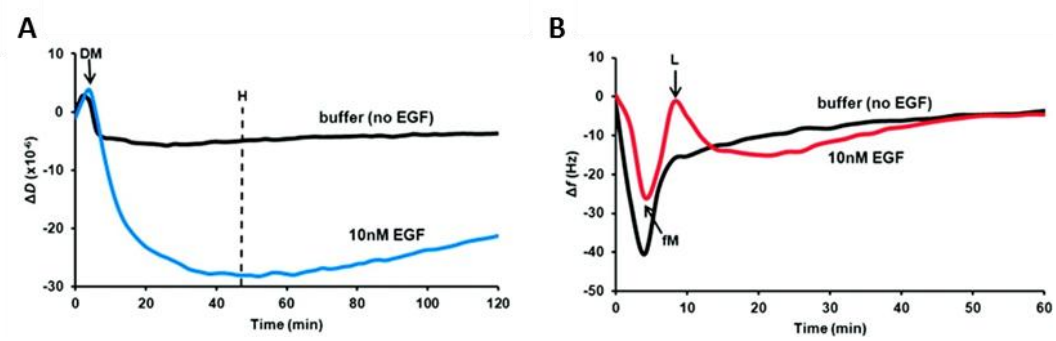

Figure 7.1. Δ*D*- and Δ*f*- responses vs. time for A431 cells exposed to EGF. (A) Δ*D*-response in the presence and absence of 10 nM EGF. Peak DM is indicated by the arrow. Minima in the Δ*D*-responses are indicated by dotted line H. (B) Δ*f*-response in the presence and absence of 10 nM EGF. Peak L and peak fM are indicated by arrows[154]. (At least ten replicates were done of each experiment.)

7.2.2 Validation of the EGF-Induced Δ*D*- and Δ*f*- Responses

Next, we conducted an experiment to determine if both the EGF-induced Δ*D*- and Δ*f*- responses observed were truly the cellular responses induced by EGFR-mediated cell signaling. Figures 7.2A and 7.2B show the results for the cells exposed to 10 nM EGF pretreated and not pretreated with PD158780, a potent inhibitor of EGFR tyrosine kinase which initiates all the downstream signaling pathways of EGFR[192]. The cells without the pretreatment showed the expected decrease in Δ*D*-response (Figure 7.2A) and the expected appearance of peak L (Figure 7.2B). The pretreatment with the inhibitor suppressed the decrease in Δ*D*-response (Figure 7.2A) and suppressed the peak L in the Δ*f*-response (Figure 7.2B). The results of this experiment showed that EGFR tyrosine kinase is responsible for the large decrease in the Δ*D*-response observed in Figure 7.2A and also for peak L in the Δ*f*-response in Figure 7.2B. Thus the Δ*D*- and Δ*f*- responses observed were due to EGFR-mediated cell signaling.

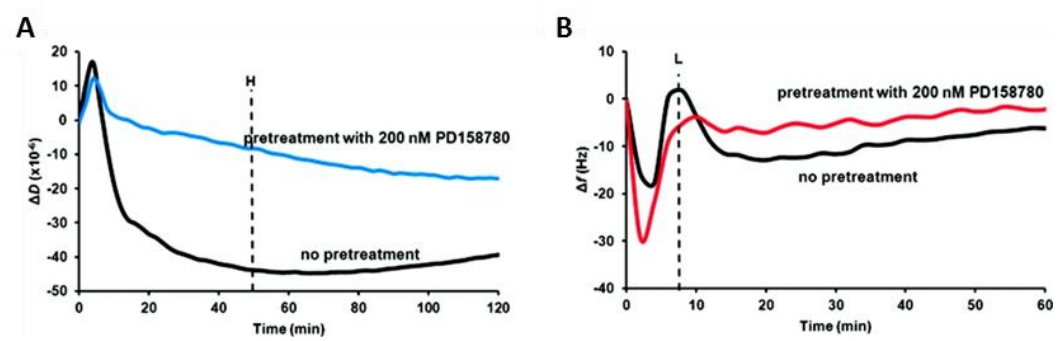

Figure 7.2. Δ*D*- and Δ*f*- responses vs. time showing the effect of inhibitor on A431 cells exposed to EGF. (A) The Δ*D*-response of the cells pretreated with EGFR tyrosine kinase inhibitor, PD158780, showing suppression of EGF-induced response. (B) The Δ*f*-response (peak L) of the cells pretreated with EGFR tyrosine kinase inhibitor, PD158780, showing suppression of EGF-induced response[154].

7.2.3 Distinguishing of Responses Mediated by High-Affinity and Low-Affinity EGFR

The third experiment was done to determine which subclass of EGFR, the low-affinity or the high-affinity, was responsible for Δ*D*- and Δ*f*- responses to EGF observed in Figures 7.1A and 7.1B. To determine this, we used EGFR monoclonal antibody mAb 2E9 (333 nM), an antibody that is known to block the cell signaling mediated by low-affinity EGFR, but not to affect high-affinity EGFR signaling[303]. Figure 7.3A shows that the cells with and without pretreatment gave nearly identical decreases in the Δ*D*-response. Since the antibody had no effect on the Δ*D*-response of the cells, the Δ*D*-response is therefore due to cell signaling mediated by high-affinity EGFR alone. However, the Δ*f*-response of the cells pretreated with the antibody shows that peak L was nearly abolished by the antibody pretreatment (Figure 7.3B), leading to the conclusion that peak L reflects the cellular response to low-affinity EGFR signaling.

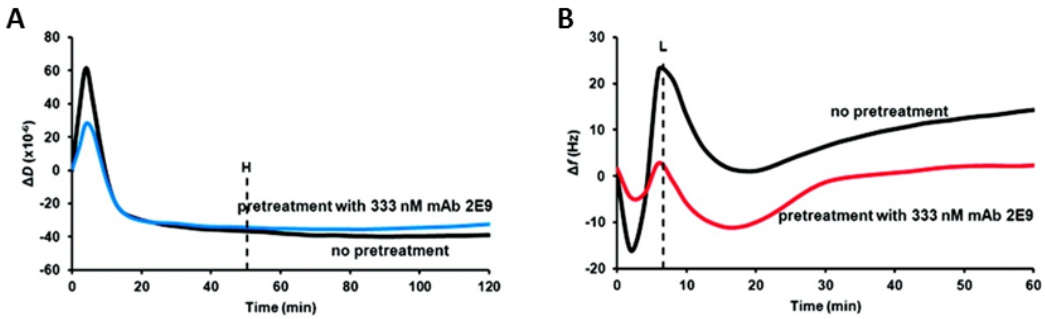

Figure 7.3. Δ*D*- and Δ*f*- responses vs. time showing the effects antibody on A431 cells to exposed to EGF. (A) The Δ*D*-response of the cells pretreated with EGFR monoclonal antibody mAb 2E9, showing no suppression of EGF-induced response. (B) The Δ*f*-response (peak L) of the cells pretreated with mAb 2E9, showing a significant suppression of EGF-induced response[154].

7.2.4 Validation of Responses Mediated by High-Affinity and Low-Affinity EGFR

To further verify the specificity of the QCM-D signal toward the individual subclass of EGFR, the dose-response of EGF was examined. As shown in Figures 7.4A and 7.4B, the higher the concentrations of EGF, the greater the amplitudes of the Δ*D*-response at dotted line H and Δ*f*-response at peak L, respectively. From the dose-response curves (normalized amplitudes of QCM-D signals vs. EGF concentrations) shown in Figures 7.4C and 7.4D, the EC_{50} values were determined to be 2.1 nM for the high-affinity EGFR (Figure 7.4C) and 39 nM for the low-affinity EGFR (Figure 7.4D). If the EC_{50} values are used as approximate measures of binding affinity[190], our values for high-affinity and low-affinity EGFRs are consistent with K_d-values obtained by others. Overall, the results of our dose-response study further validate that the QCM-D signals, Δ*D* and Δ*f*, are specific for the high-affinity and low-affinity EGFR, respectively.

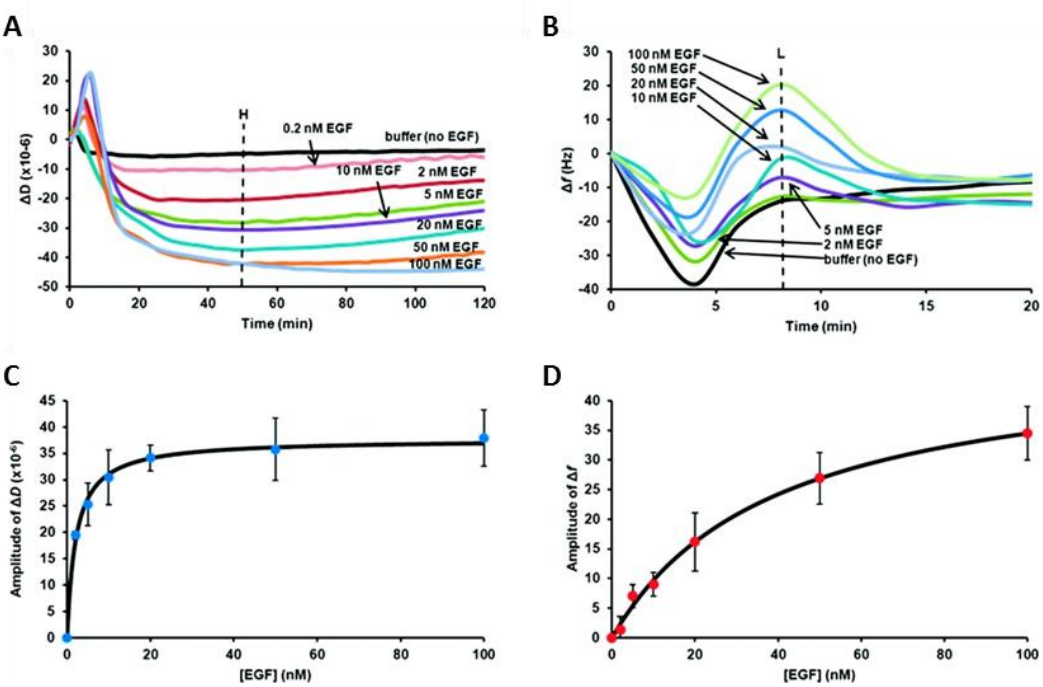

Figure 7.4. Dose-dependent, EGF-induced responses of A431 cells. (A) Dose-dependent Δ*D*-responses versus time. (B) Dose-dependent Δ*f*-responses versus time. (C) The amplitudes of Δ*D*-responses at dotted line H, average ±1 std deviation of at least ten replicate experiments, as a function of EGF concentration. (D) The amplitudes of Δ*f*-responses at peak L, average ±1 std deviation of at least three replicate experiments, as a function of EGF concentration[154].

7.2.5 The Identification of EGF-Induced Cellular Processes Responsible for Δ*D*- and Δ*f*- Responses

To verify whether the Δ*D*-response is mediated through high-affinity EGFR, we examined the remodeling of the cytoskeleton, a process that is integral to high-affinity EGFR cell signaling. Cytochalasin D (CD), a potent, cell-permeable inhibitor of actin polymerization was used. CD is capable of attenuating the remodeling of the cytoskeleton[313]. In Figure 7.5A, pretreatment with CD significantly suppressed the Δ*D*-response of the cells to EGF, confirming that cytoskeleton remodeling is the major cause of the Δ*D*-response to EGF. This is similar to the findings of Heitmann and coworkers' that a change in the cytoskeleton is a major contributor to the dissipation-related QCM response of cells[114].

Lastly we wanted to determine the specific cellular response responsible for peak L in the Δ*f*-response. It has been determined by others that the activation of low-affinity EGFR in A431 cells induces Ca^{2+} influx and/or fluid-phase pinocytosis[303]. The increase in Δ*f* is indicative of a decrease in mass within the sensing volume. This suggests that this loss of mass could be due to the transport of extracellular ions and/or liquid medium from underneath the cell layer into the cytoplasm above. To verify if either of these processes is responsible for peak L, we measured the EGF-induced response of the cells pretreated with 3 mM of EGTA (ethylene glycol tetraacetic acid). EGTA, a divalent ion chelator, blocks calcium influx by trapping Ca^{2+} and preventing its entry into cells[314, 315]. Figure 7.5B shows that the presence of 3 mM of EGTA significantly suppressed peak L, which confirms that the EGF-induced Ca^{2+} influx indeed gives rise to peak L.

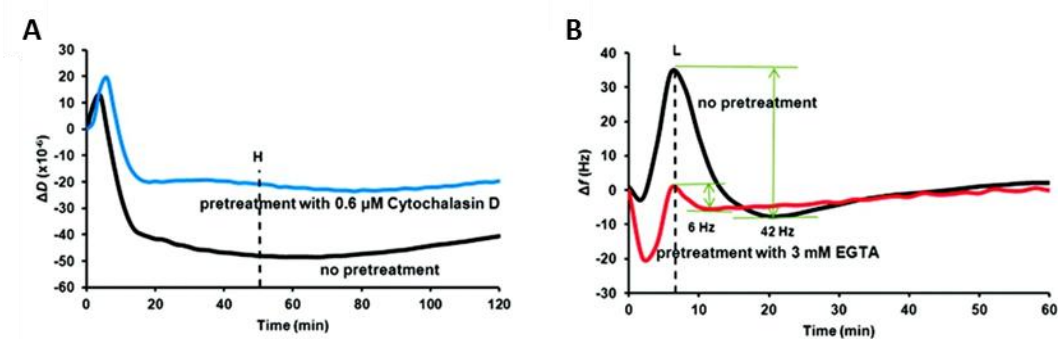

Figure 7.5. The identification of EGF-induced cellular processes that are primarily responsible for Δ*D*- and Δ*f*- responses. (A) Δ*D*-response was suppressed substantially for the cells pretreated with an inhibitor of actin polymerization, cytochalasin D. (B) Δ*f*-response at peak L was almost abolished for the cells pretreated with a calcium chelator, EGTA; peak L of the EGTA treated cells is only 6 Hz while that of the control (with no EGTA pretreatment) is 42 Hz[154].

7.3 Conclusions

In conclusion, QCM-D provides a novel approach for monitoring the early responses of cells to EGFR-mediated signaling by real-time tracking of changes in the energy dissipation and resonance frequency responses of cells. Our study revealed that the ΔD-response is associated with the remodeling of the cytoskeleton and represents the cellular response to signaling mediated by high-affinity EGFR. The Δf-response is associated with the calcium influx and represents the cellular response to signaling mediated by low-affinity EGFR. The unique capability of QCM-D can be further exploited to investigate the role of activated, high-affinity EGFR in cancer development and can potentially complement the existing approaches for biomarker detection and prognosis of cancer.

Chapter 8: Detection of Cancer Cell Signaling Biomarkers with the Quartz Crystal Microbalance with Dissipation Monitoring

8.1 Introduction

Ovarian cancer is one of the four major gynecological cancers, and the survival rate for ovarian cancer patients is the poorest[316]. The five-year relative survival rate is 44 % for all stages of ovarian cancer patients[317]. The main reason for such a poor survival rate is due to the lack of an effective method for early detection since all of ovarian carcinomas are often composed of a variety of histopathological features that exhibit distinct biological behaviors[318, 319]. Ovarian cancer is a heterogeneous disease where the expressed mutations and/or gene amplifications occur in multiple signaling pathways and varies across population of patients[68]. Thus ovarian cancer has not been linked to one specific defect in any single protein or signaling pathway. However, two signaling pathways have been explicitly studied in mediating the initiation and progression of ovarian carcinomas: they are the downstream pathways mediated through epidermal growth factor receptor (EGFR)[320, 321] and lysophophatidic acid (LPA) G protein coupled receptor[322, 323].

The EGFR signaling pathway regulates cell growth, proliferation, motility and differentiation through downstream signaling cascades of the MAPK pathway, the PI3K pathway and the PLCγ pathway[324]. An abnormal level of EGFR has been reported to be present in between 33 % and 75 % of ovarian cancers and has been shown as an important factor in both the growth and the progression of ovarian cancer[325, 326]. Due to its importance in cancer development, approaches of blocking the activation of EGFR,

including receptor-specific inhibitors and anti-EGFR monoclonal antibodies, have been developed[41, 326].

Another well-studied factor linked to ovarian cancer is LPA, an autocrine growth signal produced from ovarian cancer cells[327]. Studies have shown LPA accumulates at abnormally high micromolar concentrations in malignant ascites[328, 329]. LPA affects many cellular functions, such as cell proliferation, cytoskeletal reorganization, cell survival/apoptosis, cell adhesion/migration, and ion transport, through the activation of the G_i, G_q, and $G_{12/13}$ subfamilies of the G protein[330]. Recent studies have demonstrated that LPA can transactivate EGFR through protein kinase C (PKC) and matrix metalloproteinase (MMP) activation[68] and affect cell growth through the PI3K pathway[330].

There have been reports demonstrating thrombin[331] and histamine[332] to be over expressed in ovarian cancer. Thrombin interacts with specific G protein-coupled protease activated receptors (PARs) and mediates the coagulation cascade[331]. It has been shown that cancer coagulation factors play a role in the progression and metastasis of cancer through a number of growth factors, cytokines and extracellular matrix (ECM) proteins[333]. Histamine has been shown to modulate proliferation of many normal and malignant tissues through the G protein-coupled histamine receptors. High concentrations of histamine have been found in melanoma, colon, breast, and ovarian cancers[334]. The association of histamine to malignant tumors remains controversial, but some studies have shown that histamine is an important paracrine and autocrine regulator of cell growth of tumor cells[335, 336]. To improve survival rate amongst ovarian cancer patients, a sensitive assay platform for detection of those potential biomarkers, such as EGFR, LPA,

thrombin, and histamine, could be an effective approach for early detection of the disease.

Biomarkers play an important role in disease detection and treatment. There are a variety of biomolecules that are considered biomarkers, including antigens, DNA, mRNA, and enzymes[337]. The detection of the biomarkers in body fluids, such as blood and urine, is a powerful medical tool for early diagnosis and treatment of diseases. Early detection of biomarkers is very important in the case of cancer, cardiovascular disorders, and other pathological conditions[337]. However at early stages of disease, biomarkers are often present in very low concentration making them troublesome to detect[338]. Additionally, body fluid samples are a mixture of various proteins, which can make specific biomarkers even more difficult to identify. There are many biomarker detection methods that have been developed, including enzyme-linked immunosorbent assay (ELISA)[339], gel electrophoresis[340], mass-sensing bio-optical compact disc (BioCD) protein array[341], colorimetric assay[342], electrochemical assay[343], and fluorescence methods[344]. Many of these methods are based on the conventional immunoassays where antibodies are functionalized on a solid support for target protein capture. Among many of these technologies, a common problem is these assays allow for nonspecific adsorption of non-target proteins, which can provide inaccurate results. Therefore, the current biomarker detection methods lack specificity, accuracy and sensitivity needed for clinical application[337].

The QCM-D has shown its capabilities in monitoring the process of cell adhesion and detecting cellular responses to ligands and drugs[155, 174]. In recent years, the QCM has found its niche in biomarker detection because of its unique capability of providing the

functional readout of cells that undergo processes, including signaling transduction[154, 155, 345], growth[150, 346, 347], apoptosis[34], exocytoses[348], migration[156], morphological change[151, 152], cell cycles[153], etc. Such information is indicative of the physiological state of cells under normal or pathological conditions and has the potential for applications in diagnosis and prognosis of human diseases.

In this work, we used the QCM-D to probe the response of ovarian carcinoma (SKOV-3) cells to biomolecules, such as EGF, LPA, thrombin, and histamine. These molecules have been identified as crucial players in the progression of ovarian cancer. The main focus of the study was to determine the sensitivity of this cell-based platform for detection of these molecules. We also examined the pharmacological effects of LY294002 and wortmannin on the EGF-induced response of SKOV-3 cells. These studies will provide evidence that the QCM-D can potentially be a useful analytical tool in examining disease progression and evaluating responsiveness to drug therapies.

8.2 Results

Membrane-bound proteins or surface receptors comprise about a third of all cellular proteins and are highly important in signal transductions. Receptors are the basis of signal transduction due to their location, and they are responsible for converting an extracellular signal into an intracellular signal to allow the cell to respond and communicate with neighboring cells[349]. In cancer, many of these receptors are often deregulated[350]. The ability to probe these overexpressed and/or mutated surface receptors can potentially be useful in probing of tumors, in monitoring disease progression, and assessing responsiveness to drug therapies[351].

8.2.1 Probing Surface Receptors of Ovarian Cancer Cells

Studies have shown that the major pathways involved in development of ovarian cancer are the downstream pathways mediated by EGFR and LPAR (LPA receptor), a G_i-coupled receptor[41, 352]. In this study, we used the QCM-D to examine the ligand-induced cellular response of EGFR and LPAR. When treated with 50 nM EGF, the SKOV-3 cells exhibited a time-dependent Δ*D*-response, which begins with a small initial increase, followed by a rapid decrease and then quickly transitions into a sharp increase until around 30 min. For the remaining time, the response virtually levels off (Figure 8.1A). The pattern of the EGF-induced Δ*D*-response of the SKOV-3 cells is similar to those of A431 cells and MCF10A cells obtained in previous studies[154, 155]. When treated with 1 μM LPA, the SKOV-3 cells exhibited a time-dependent Δ*D*-response that was very distinct from the EGF-induced response: The profile first began with a large and steep increase for ~5 min, followed by a sharp decrease for ~10 min, and finally ended with a stable response close to the initial baseline level of the control, where the cells were not exposed to any LPA (Figure 8.1B).

There have been reports suggesting abnormal levels of thrombin and histamine found in ovarian cancer[333, 334]. Thrombin and histamine are small biomolecules that bind to PAR and histamine receptors, respectively, and both activate the G_q-coupled signaling pathway. Thus it is not surprising that both thrombin- and histamine-induced Δ*D*-response profiles were very similar: They both begin with a rapid increase for 5 min, then a sharp decline in the next 5 min, then after a quick transition, a slow rise up to a stable level of response for the rest of the time (Figures 8.1C and 8.1D).

The distinct Δ*D*-response profiles exhibited by these three types of receptors, EGFR (EGF), G_i-coupled receptor (LPA) and G_q-coupled receptor (thrombin and histamine) imply that the QCM-D has the ability to detect and differentiate cellular response mediated by various types of surface receptors. The fact that both thrombin and histamine belong to the same type of receptors and show similar Δ*D*-response profiles indicates that these response profiles represent the signature response of each type of receptor. These signature responses will be compared to the responses obtained by other label-free cell-based assays[102] for the future study.

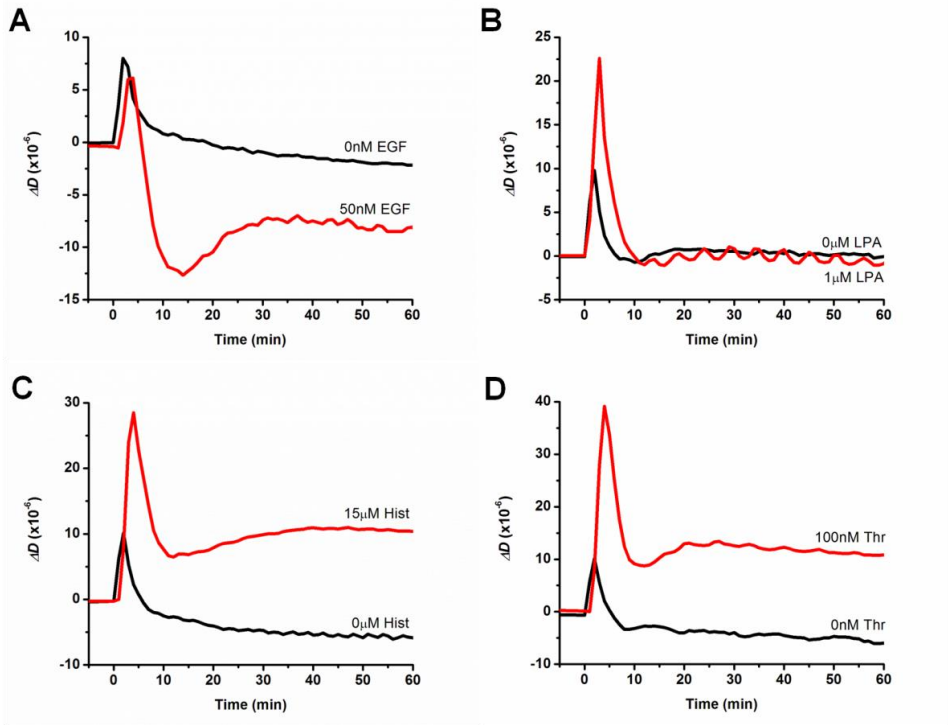

Figure 8.1. Real-time QCM-D measurements (at the third mode of vibration) of the responses of SKOV-3 cells to biomolecules at 37 °C. (A) The signature Δ*D*-response induced by 50 nM epidermal growth factor (EGF). (B) The signature Δ*D*-response induced by 1 μM lysophosphatidic acid (LPA). (C) The signature Δ*D*-response induced by 15 μM histamine (Hist). (D) The signature Δ*D*-response induced by 100 nM thrombin (Thr). (At least ten replicates were done of each experiment.)

8.2.2 Sensitivity of the Δ*D*-Response to Endogenous Biomolecules in Ovarian Cancer Cells

There is a need for highly sensitive and quantitative technologies to detect and characterize tumor tissue samples to provide faster reliable information on the diagnosis, prognosis, and targeted therapy for the patient. In this study, we tested biomolecules in the ranges of the physiological concentrations determined by others to explore the potential of the QCM-D for providing sensitive and quantitative information of specific biomarkers of ovarian cancer cells (Table 8.1). Both EGF and thrombin have been found in human serum in nanomolar levels, and we have successfully detected the Δ*D*-response induced by both EGF and thrombin in the range of 5-100 nM (Figures 8.2A and 8.2D). The physiological concentrations for LPA and histamine in human serum are in the micromolar range and we have successfully detected LPA and histamine in the range of 0.5-20 μM and 0.25-15 μM, respectively (Figures 8.2B and 8.2C). In summary, we have demonstrated that the QCM-D is capable of detecting the cellular response in the form of a time-dependent Δ*D*-response profile induced by those endogenous biomolecules at the corresponding physiological concentration ranges. The QCM-D-based cell assay platform is highly sensitive toward the detection of the potential biomarkers so that a slightly abnormal change of the concentration of these biomarkers in the early stage of the disease development can be readily identified. This platform is also mechanistically informative because the Δ*D*-response profile is capable of revealing the type of signaling mechanism that biomarker could be involved. Overall, the ability to detect cellular responses within physiological concentration range can potentially be useful in studying patient samples and providing more accurate analysis of the main cause of the illness.

In addition, the dose dependence of the Δ*D*-response of SKOV-3 cells allows us to derive the efficacy information for each biomarker in its role of activation of the membrane receptors for medical diagnosis and prognosis purposes.

Table 8.1. Physiological concentration ranges of EGF, LPA, histamine and thrombin in human plasma and detection range of the QCM-D tested in the study.

Biomolecule	Physiological Concentration Range	QCM-D Test Range	Lowest Concentration Detected
EGF	Low nM [353]	0-100 nM	1 nM
LPA	μM [354]	0-20 μM	10 nM
Histamine	Low μM [355]	0-15 μM	250 nM
Thrombin	nM [356]	0-100 nM	5 nM

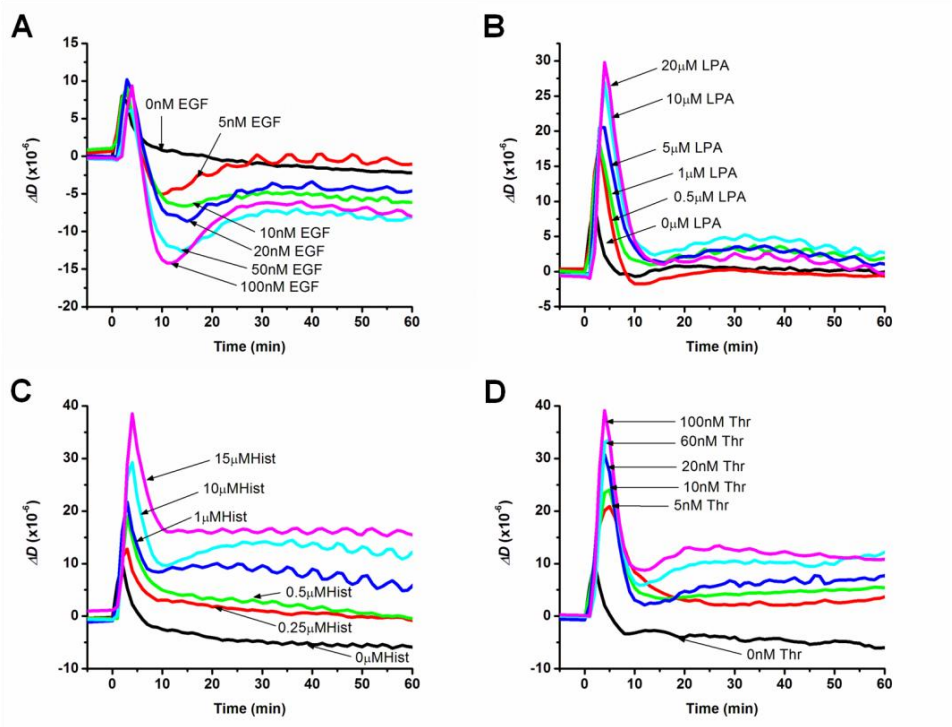

Figure 8.2. Real-time QCM-D measurements of in the dose response of SKOV-3 cells. (A) Dose-dependent Δ*D*-response induced by EGF. (B) Dose-dependent Δ*D*-response induced by LPA. (C) Dose-dependent Δ*D*-response induced by histamine. (D) Dose-dependent Δ*D*-response induced by thrombin.

8.2.3 Comparison of Ligand-Induced Δ*D*-Responses in Various Cell Lines

It is known that various cell lines respond to stimulation differently. In this study, we compared the ligand-induced Δ*D*-responses of SKOV-3 cells, with those of MCF-10A and A431 cells, to assess their similarities and differences that are important for biomarker detection. First of all, the EGF-induced Δ*D*-responses of all three cell lines show a similar initial sharp rise followed by a rapid decline down to a large negative level. The major difference of the three response profiles lies in the rise that occurs immediately after the large decline. For SKOV-3 cells, the response has a quick transition that leads to a sharp rise. For MCF10A cell and A431 cells, they both have a longer transition that leads to a gradual rise (Figures 8.3A-8.3C).

As G_q-coupled ligands, histamine and thrombin were able to induce all three cell lines to give a Δ*D*-response profile with a sharp peak right from the beginning (Figures 8.3G- 8.3L). This sharp peak also displays a signature decline phase, where the response drops down rapidly to about one half or two thirds of the peak height, then transitions to a more gradual decrease towards the baseline level. Overall, the initial sharp peak with a two-phase decline is the key feature for a typical G_q-coupled response. Whether being induced with histamine or thrombin, the response profile of each cell line shows very little difference. Between different cell lines, however, the response profiles exhibit a substantial difference in their transitions between the rapid and slow decline. For SKOV-3 cells, the transition is very distinct and appears as a shallow valley. For MCF10A and A431 cells, there is no obvious transition and the slow decline appears immediately after the rapid one.

As a G_i-coupled ligand, LPA induced the cells to give a Δ*D*-response profile with a sharp peak right from the beginning (Figures 8.3D-8.3F), similar to the key feature of the typical G_q-coupled response (Figures 8.3G-8.3L). Unlike the G_q-coupled response, the G_i-coupled response has only a single decline phase with a deeper drop that may reach either at or far below the baseline level. The depth of the drop is cell-type dependent.

In summary, the controls for all cell types responded very similarly to the biomarkers used. By contrast, the ligand-induced Δ*D*-responses are different for each specific cell type. These cell-type-specific Δ*D*-responses could be due to different receptor expression level and diversity of the receptor conformations and organizations in the different cell types[206]. Another reason for the different Δ*D*-responses could be the heterogeneity in the expression, organization, and interaction of the cytosolic components in the different cell types[357]. There are many examples in literature that a given receptor may prefer different signaling pathways in different cell types[357, 358]. Such signature QCM-D-response is highly sensitive and reliable for biomarker detection. The use of the QCM-D may provide an effective platform for medical diagnosis and prognosis.

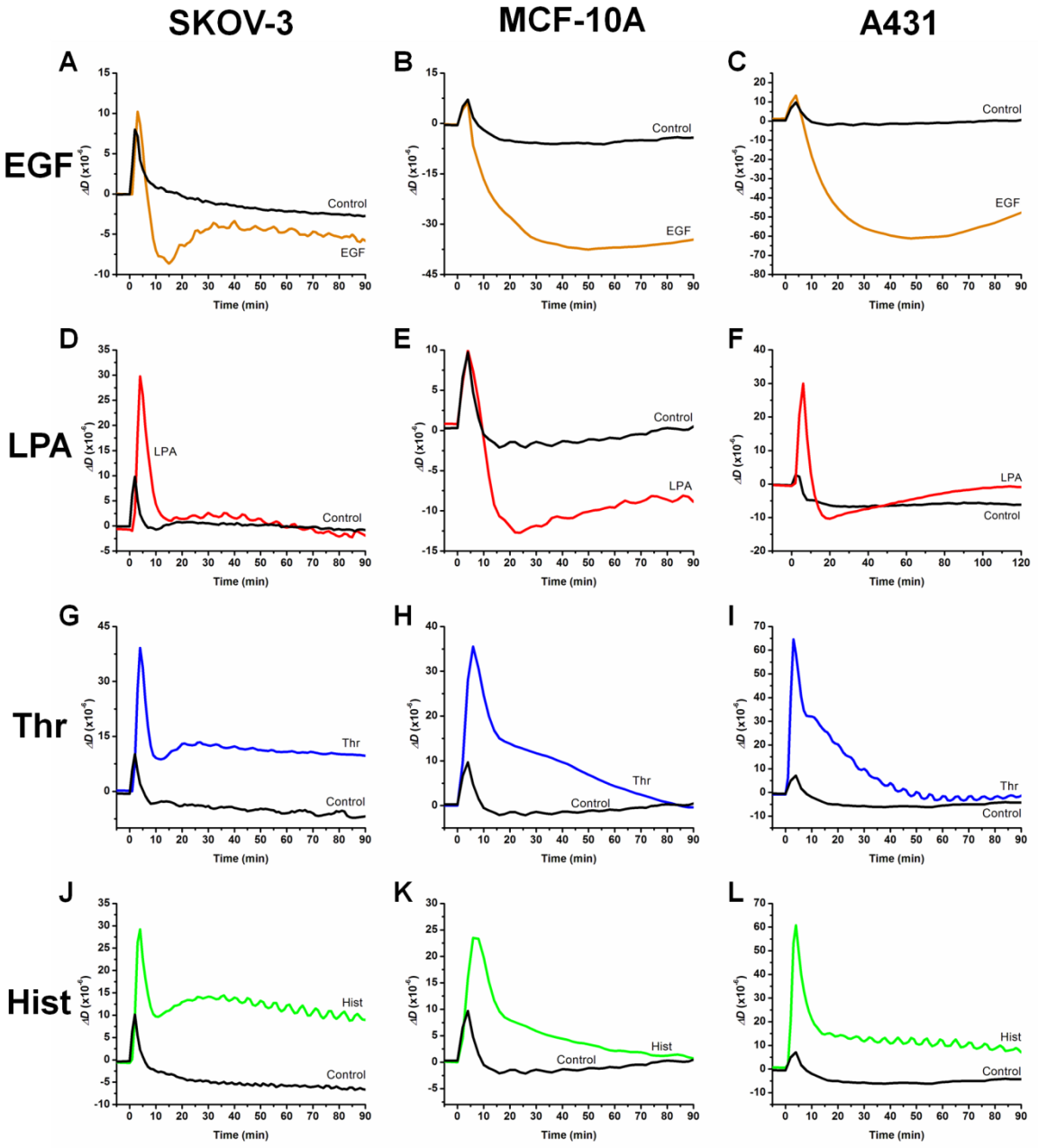

Figure 8.3. Comparison of ligand-induced Δ*D*-responses of SKOV-3 cells, MCF-10A cells, and A431 cells. (A-C) EGF-induced Δ*D*-responses in SKOV-3 cells, MCF-10A cells, and A431 cells, respectively. (D-F) LPA-induced Δ*D*-responses in SKOV-3 cells, MCF-10A cells, and A431 cells, respectively. (G-I) Thrombin-induced Δ*D*-responses in SKOV-3 cells, MCF-10A cells, and A431 cells, respectively. (J-L) Histamine-induced Δ*D*-responses in SKOV-3 cells, MCF-10A cells, and A431cells, respectively. In each figure above the black Δ*D*-responses is the control, which is cells in assay buffer. (At least ten replicates were done of each experiment.)

8.2.4 Assessing the Responsiveness to Pharmacological Modulators

Among the EGFR mediated pathways, the PI3K pathway is known to regulate cell adhesion. To obtain some insight into how the downstream PI3K pathway affects the EGF-induced cellular response, we inhibited the activity of specific signaling proteins in the PI3K pathway and assessed the effects of such inhibition on the EGF-induced Δ*D*-responses.

First we probed the PI3K pathway by treating the SKOV-3 cells with LY294002 and wortmannin, both are potent inhibitors of PI3K signaling protein. Figure 8.4 shows inhibition studies of the PI3K pathway. When the SKOV-3 cells were treated with LY294002, the EGF-induced Δ*D*-response showed a dose dependent reduction of the magnitude (Figure 8.4A). When the SKOV-3 cells were treated with wortmannin, the EGF-induced Δ*D*-response showed a dose dependent suppression of the Δ*D*-response between 5min – 30min (Figure 8.4D). From these results, we conclude that the QCM-D has the sensitivity to probe the effects of pharmacological modulators on the adhered cells within the range of concentration used in typical biochemical assays[52]. Next, we compared the effects of LY294002 and wortmannin on the EGFR mediated response in SKOV-3 cells with those of MCF-10A cells and A431 cells (Figure 8.4). Both LY294002 and wortmannin were able to suppress the EGFR-mediated cellular responses in a dose-dependent manner in all three cell lines. However, each of the three cell lines shows a unique inhibition pattern that appears to be cell-type dependent (Figure 8.4). We attribute this finding to the intricate difference in the signaling network of each individual cell type, even though both modulators target the PI3K pathway. For the same cell lines, inhibition patterns by either LY294002 or wortmannin are quite similar. This result is

consistent with the fact that both inhibitors target the same protein molecule PI3K of the same signaling pathway. Thus the QCM-D is capable of providing mechanistic information on how a drug molecule affects cellular function.

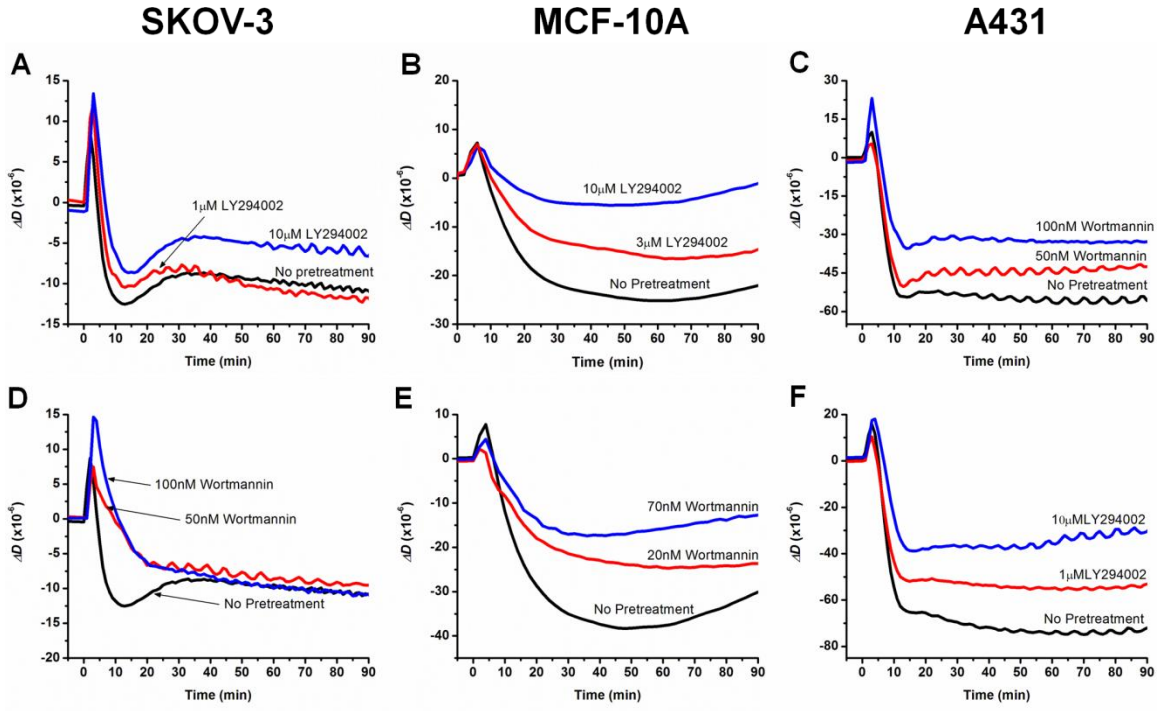

Figure 8.4. Δ*D*-response vs. time showing the effect of two different pharmacological modulators (LY294002, top row and wortmannin, bottom row) on three different cell lines (SKOV-3 cells, MCF-10A cells and A431 cells) exposed to 10nM EGF. (A) SKOV-3 cells induced by EGF and suppressed by 1 μM and by 10 μM LY294002. (B) MCF10A cells induced by EGF and suppressed by 3 μM and by 10 μM LY294002. (C) A431 cells induced by EGF and suppressed by 1 μM and by 10 μM LY294002. (D) SKOV-3 cells induced by EGF and suppressed by 50 nM and by 100 nM wortmannin. (E) MCF10A cells induced by EGF and suppressed by 20 nM and by 70 nM wortmannin. (F) A431 cells induced by EGF and suppressed by 50 nM and by 100 nM wortmannin.

8.3 Summary

Ovarian carcinoma consists of a variety of tumor cells with various histopathological features and varied biological behaviors[318]. Various reports have linked biomolecules, such as EGF, LPA, thrombin, and histamine, with the development of a

variety of ovarian cancers. In this study, we have demonstrated that the whole cell-based QCM-D assay has the sensitivity and specificity to assess the cellular response induced by these potential biomarkers of ovarian cancer. The QCM-D relies on the ΔD-response profiles induced by these biomarkers at physiological concentrations to reveal the signature of these biomarkers (Table 8.1). These sensitive, reliable, and informative signatures can be used for detecting biomarkers at relevant physiological concentrations and for providing mechanistic insight into their effects on ligand-receptor binding and/or specific type of cell signaling. A more accurate and reliable early detection of these and other biomarker may pave the way for the future development of an effective therapeutic treatment of ovarian cancer.

Chapter 9: Overall Summary

The overall objective of this project was to apply the quartz crystal microbalance with dissipation monitoring (QCM-D) to the investigation of the properties of biological systems that are relevant to fundamental biology and future medical applications. The QCM-D is an ultrasensitive mechanical sensing device that is capable of providing real-time, non-invasive measurements of the changes in frequency and energy dissipation of adhered cells. Over the past few decades, acoustic instruments, such as the QCM, have been used in biological and biomedical research. Much of these studies have been limited to a few areas of biological and biomedical research, such cell interaction with various surfaces and the effects of pharmaceuticals of cells. The capabilities of acoustic sensors can be further exploited to provide more insight into fundamental cell biology and to suggest future applications. The work reported in this dissertation describes the use of the QCM-D as a platform for the study of biological systems at cellular and tissue levels.

Chapters 1, 2, and 3 gave an introduction to cell adhesion, presented basic principles of the QCM-D technology, and describe the materials and methods used in the experiments, respectively.

Chapter 4 describes an examination of the cell de-adhesion process induced by epidermal growth factor receptor (EGFR) signaling. We revealed that this de-adhesion process is a complex process, including an initial fast cell de-adhesion, a transition, and finally, a slow re-adhesion. We found that three downstream pathways (MAPK/ERK, PI3K, and PLC) of EGFR signaling mediate the de-adhesion process. These results established a quantitative framework for the analysis of cell adhesion and established a functional output for studying cell signaling.

Chapter 5 describes an investigation of the adhesion process of cells to surfaces coated with titanium, a material commonly used for medical implants. In this chapter, a correlation of the *ΔD*-response and the three-stage adhesion process is demonstrated. We demonstrated that the adhesion of human epidermal keratinocytes can be affected in a variety of ways, such as coating the surface with fibronectin, stimulating the cells with growth factor, and modulating the cell signaling pathways with pharmacological molecules.

Chapter 6 describes the examination of the cellular response mediated through the GPCR signaling. Characteristic patterns in the *ΔD*-response were found to each of the three signaling pathways ($G_{\alpha q}$, $G_{\alpha s}$, and $G_{\alpha i}$). These characteristic *ΔD*-responses were then used to demonstrate signal coordination among pairs of GPCR signaling pathways. The EC_{50} values determined from the *ΔD*-response induced by GPCR ligands were compared with EC_{50} values obtained with other methods.

Chapter 7 describes the investigation of the use of the QCM-D to detect and distinguish between subclasses of EGFR. Our study revealed that the Δ*D*-response is associated with the remodeling of the cytoskeleton and represents the cellular response to signaling mediated by high-affinity EGFR. The Δ*f*-response is associated with the calcium influx and represents the cellular response to signaling mediated by low-affinity EGFR.

Chapter 8 describes the detection of potential biomarkers of ovarian cancer with the QCM-D. Here we demonstrated that the cell-based QCM-D assay has the sensitivity and specificity to assess the cellular response induced by specific subclasses of EGFR and potential biomarkers of ovarian cancer.

The results presented demonstrated that the QCM-D is a highly sensitive, non-invasive, and label-free technique that has the capabilities to explore a wide range of cellular processes, such as cell signaling and mechanotransduction. Conventional cell biology uses a simplified approach for the examination of cellular structure and function by examining one component at a time. This approach has not been very effective in dealing with the complexity of the cell. The ΔD-response is an integrated functional output of the cell that is regulated by the network of cell signaling. This makes the ΔD-response of the QCM-D a novel approach for dealing with the complexity of the cell and for tracking the response of the signaling reaction that are responsible for the regulation of a particular cellular function. Another advantage of using the QCM-D as an approach to study cellular responses is the QCM-D can offer lots of information with one experiment that is because the QCM is a continuous monitor of cellular response in real-time. This capability can potentially save money and on reagents, such as ligands and modulators. Therefore, with careful experimental design the QCM-D can probe cellular responses and combined with other conventional techniques can potentially provide further insight on cellular events. Further development of QCM-D as a cell sensing platform can also potentially advance its use in clinical applications such as biomarker detection and testing for personalized treatment of a disease.

Chapter 10: Future Work

Although the work described in this dissertation demonstrated the QCM-D is a useful technique in studying cell adhesion, there are still numerous experiments that should be done. Some future experiments are described below.

In order to confirm the reliability of the QCM-D as a sensing platform for screening drugs, other inhibitors that affect the EGFR downstream signaling pathways should be tested. The inhibitors selected should target various signaling molecules within each downstream signaling pathway.

In order to verify the dependability of the QCM-D as a sensing platform for the adhesion of cells on implant materials, a future study of other surface coatings and other pharmacological modulators that specifically target cell adhesion molecules should be examined. Different metal, polymer, and ceramic substrates should be tested.

Many of the GPCR ligands examined in this study can potentially induce off-target effects. Future studies using genetically altered cells would be expected to shed light on off-target effects on the ligand-induced ΔD-responses.

To further validate the specificity and sensitivity of the QCM-D for biomarker detection, a study on a mixture of biomarkers and proteins as a mock body fluid sample should be conducted.

References

1. Bendas, G. & Borsig, L. Cancer cell adhesion and metastasis: selectins, integrins, and the inhibitory potential of heparins. *Int. J. Biochem. Cell Biol.* **2012**, 10 (2012).

2. Cavallaro, U. & Christofori, G. Cell adhesion in tumor invasion and metastasis: loss of the glue is not enough. *Biochim. Biophys. Acta.* **1552**, 39-45 (2001).

3. Veale, D.J. & Maple, C. Cell adhesion molecules in rheumatoid arthritis. *Drugs Aging.* **9**, 87-92 (1996).

4. Morel, J.C.M. et al. Signal transduction pathways involved in rheumatoid arthritis synovial fibroblast interleukin-18-induced vascular cell adhesion molecule-1 expression. *J. Biol. Chem.* **277**, 34679-34691 (2002).

5. Blankenberg, S., Barbaux, S. & Tiret, L. Adhesion molecules and atherosclerosis. *Atherosclerosis.* **170**, 191-203 (2003).

6. Galkina, E. & Ley, K. Vascular adhesion molecules in atherosclerosis. *Arterioscler. Thromb. Vasc. Biol.* **27**, 2292-2301 (2007).

7. Miura, Y. et al. Defective osteogenesis of the stromal stem cells predisposes CD18-null mice to osteoporosis. *Proc. Natl. Acad. Sci. U. S. A.* **102**, 14022-14027 (2005).

8. Perinpanayagam, H. et al. Early cell adhesion events differ between osteoporotic and non-osteoporotic osteoblasts *J. Orthoped. Res.* **19**, 993-1000 (2001).

9. Lodish H, B.A., Zipursky SL, Matsudaira P, Baltimore D, Darnell J in Mol. Cell Biol., Edn. 4th edition (W. H. Freeman, New York; 2000).

10. Gonzalez-Amaro, R. & Sanchez-Madrid, F. Cell adhesion molecules: selectins and integrins. *Crit. Rev. Immunol.* **19**, 389-429 (1999).

11. Juliano, R.L. Signal transduction by cell adhesion receptors and the cytoskeleton: functions of integrins, cadherins, selectins, and immunoglobulin-superfamily members. *Annu. Rev. Pharmacol. Toxicol.* **42**, 283-323 (2002).

12. Gales, C. et al. Real-time monitoring of receptor and G-protein interactions in living cells. *Nat. Meth.* **2**, 177-184 (2005).

13. van Roy, F. & Berx, G. The cell-cell adhesion molecule E-cadherin. *Cell. Mol. Life Sci.* **65**, 3756-3788 (2008).

14. Maître, J.-L. & Heisenberg, C.-P. Three functions of cadherins in cell adhesion. *Curr. Biol.* **23**, R626-R633 (2013).

15. Wai Wong, C., Dye, D.E. & Coombe, D.R. The role of immunoglobulin superfamily cell adhesion molecules in cancer metastasis. *Int. J. Cell Biol.* **2012** (2012).

16. Vaughn, D.E. & Bjorkman, P.J. The (Greek) key to structures of neural adhesion molecules. *Neuron* **16**, 261-273 (1996).

17. Lasky, L.A. Selectin-carbohydrate interactions and the initiation of the inflammatory response. *Annu. Rev. Biochem.* **64**, 113-139 (1995).

18. Springer, T.A. Traffic signals on endothelium for lymphocyte recirculation and leukocyte emigration. *Annu. Rev. Physiol.* **57**, 827-872 (1995).

19. Case, L.B. & Waterman, C.M. Integration of actin dynamics and cell adhesion by a three-dimensional, mechanosensitive molecular clutch. *Nat. Cell Biol.* **17**, 955-963 (2015).

20. Hynes, R.O. Cell adhesion: old and new questions. *Trends Cell Biol.* **9**, M33-37 (1999).

21. Arnaout, M.A., Goodman, S. & Xiong, J.-P. Structure and mechanics of integrin-based cell adhesion. *Curr. Opin. Cell Biol.* **19**, 495-507 (2007).

22. Loftus, J.C. & Liddington, R.C. New insights into integrin-ligand interaction. *J. Clin. Invest.* **100**, S77-81 (1997).

23. Humphries, M.J. & Newham, P. The structure of cell-adhesion molecules. *Trends Cell Biol* **8**, 78-83 (1998).

24. Carter, W.G., Kaur, P., Gil, S.G., Gahr, P.J. & Wayner, E.A. Distinct functions for integrins alpha 3 beta 1 in focal adhesions and alpha 6 beta 4/bullous pemphigoid antigen in a new stable anchoring contact (SAC) of keratinocytes: relation to hemidesmosomes. *J. Cell Biol.* **111**, 3141-3154 (1990).

25. Jockusch, B.M. et al. The molecular architecture of focal adhesions. *Annu. Rev. Cell. Dev. Biol.* **11**, 379-416 (1995).

26. Borradori, L. & Sonnenberg, A. Structure and function of hemidesmosomes: more than simple adhesion complexes. *J. Invest. Dermatol.* **112**, 411-418 (1999).

27. Nievers, M.G., Schaapveld, R.Q. & Sonnenberg, A. Biology and function of hemidesmosomes. *Matrix Biol.* **18**, 5-17 (1999).

28. Tsuruta, D., Hashimoto, T., Hamill, K.J. & Jones, J.C. Hemidesmosomes and focal contact proteins: functions and cross-talk in keratinocytes, bullous diseases and wound healing. *J. Dermatol. Sci.* **62**, 1-7 (2011).

29. Zillikens, D. Acquired skin disease of hemidesmosomes. *J. Dermatol. Sci.* **20**, 134-154 (1999).

30. Chen, J.Y., Penn, L.S. & Xi, J. Quartz Crystal Microbalance: Sensing Cell-Substrate Adhesion and Beyond. *Biosens. Bioelectron.* **99**, 593-602 (2018).

31. Geiger, T. & Zaidel-Bar, R. Opening the floodgates: proteomics and the integrin adhesome. *Curr. Opin. Cell Biol.* **24**, 562-568 (2012).

32. Nowacki, L. et al. Real-time QCM-D monitoring of cancer cell death early events in a dynamic context. *Biosens. Bioelectron.* **64**, 469-476 (2015).

33. Fatisson, J., Azari, F. & Tufenkji, N. Real-time QCM-D monitoring of cellular responses to different cytomorphic agents. *Biosens. Bioelectron.* **26**, 3207-3212 (2011).

34. Braunhut, S.J., McIntosh, D., Vorotnikova, E., Zhou, T. & Marx, K.A. Detection of apoptosis and drug resistance of human breast cancer cells to taxane treatments using quartz crystal microbalance biosensor technology. *Assay Drug. Dev. Technol.* **3**, 77-88 (2005).

35. Humphries, M.J. Integrin cell adhesion receptors and the concept of agonism. *Trends Pharmacol. Sci.* **21**, 29-32.

36. Wozniak, M.A., Modzelewska, K., Kwong, L. & Keely, P.J. Focal adhesion regulation of cell behavior. *Biochim. Biophys. Acta* **1692**, 103-119 (2004).

37. Nyati, M.K., Morgan, M.A., Feng, F.Y. & Lawrence, T.S. Integration of EGFR inhibitors with radiochemotherapy. *Nat. Rev. Cancer* **6**, 876-885 (2006).

38. Bill, H.M. et al. Epidermal growth factor receptor-dependent regulation of integrin-mediated signaling and cell cycle entry in epithelial cells. *Mol. Cell. Biol.* **24**, 8586-8599 (2004).

39. Herbst, R.S. Review of epidermal growth factor receptor biology. *Int. J. Radiat. Oncol. Biol. Phys.* **59**, 21-26 (2004).

40. Schneider, M.R. & Wolf, E. The epidermal growth factor receptor ligands at a glance. *J. Cell Physiol.* **218**, 460-466 (2009).

41. Lafky, J.M., Wilken, J.A., Baron, A.T. & Maihle, N.J. Clinical implications of the ErbB/epidermal growth factor (EGF) receptor family and its ligands in ovarian cancer. *Biochim. Biophys. Acta* **1785**, 232-265 (2008).

42. Arteaga, C.L. The epidermal growth factor receptor: from mutant oncogene in nonhuman cancers to therapeutic target in human neoplasia. *J. Clin. Oncol.* **19**, 32s-40s (2001).

43. Dei Tos, A.P. & Ellis, I. Assessing epidermal growth factor receptor expression in tumours: What is the value of current test methods. *Eur. J. Cancer.* **41**, 1383-1392 (2005).

44. Cain, R.J. & Ridley, A.J. Phosphoinositide 3-kinases in cell migration. *Biol. Cell* **101**, 13-29 (2009).

45. Allen, F.D. et al. Epidermal growth factor induces acute matrix contraction and subsequent calpain-modulated relaxation. *Wound Repair Regen.* **10**, 67-76 (2002).

46. Gollob, J.A., Wilhelm, S., Carter, C. & Kelley, S.L. Role of Raf kinase in cancer: therapeutic potential of targeting the Raf/MEK/ERK signal transduction pathway. *Semin. Oncol.* **33**, 392-406 (2006).

47. Cuevas, B.D. et al. MEKK1 regulates calpain-dependent proteolysis of focal adhesion proteins for rear-end detachment of migrating fibroblasts. *EMBO J.* **22**, 3346-3355 (2003).

48. Stähle, M. et al. Mechanisms in LPA-induced tumor cell migration: critical role of phosphorylated ERK. *J. Cell Sci.* **116**, 3835-3846 (2003).

49. Osaki, M., Oshimura, M. & Ito, H. PI3K-Akt pathway: its functions and alterations in human cancer. *Apoptosis* **9**, 667-676 (2004).

50. Kharait, S., Tran, K., Yates, C. & Wells, A. in Cell Motility in Cancer Invasion and Metastasis, Vol. 8. (ed. A. Wells) 301-338 (Springer Netherlands, Heidelberg, Germany; 2006).

51. Fujita, K. et al. Myosin light chain kinase from skeletal muscle regulates an ATP-dependent interaction between actin and myosin by binding to actin. *Mol. Cell. Biochem.* **190**, 85-90 (1999).

52. Gharbi, Severine I. et al. Exploring the specificity of the PI3K family inhibitor LY294002. *Biochem. J.* **404**, 15-21 (2007).

53. Xie, W. et al. 3β-Hydroxy-6-aza-cholestane and related analogues as phosphatidylinositol specific phospholipase C (PI-PLC) inhibitors with antitumor activity. *Bioorganic Med. Chem.* **8**, 699-706 (2000).

54. Xie, H. et al. EGF receptor regulation of cell motility: EGF induces disassembly of focal adhesions independently of the motility-associated PLCgamma signaling pathway. *J. Cell Sci.* **111**, 615-624 (1998).

55. Cheng, Z. et al. Luciferase reporter assay system for deciphering GPCR pathways. *Curr. Chem. Genomics Transl. Med.* **4**, 84-91 (2010).

56. Katritch, V., Cherezov, V. & Stevens, R.C. Structure-function of the G-protein-coupled receptor superfamily. *Annu. Rev. Pharmacol. Toxicol.* **53**, 531-556 (2013).

57. Wu, J., Xie, N., Zhao, X., Nice, E.C. & Huang, C. Dissection of aberrant GPCR signaling in tumorigenesis - a systems biology approach. *Cancer Genomics Proteomics* **9**, 37-50 (2012).

58. Landry, Y., Niederhoffer, N., Sick, E. & Gies, J.P. Heptahelical and other G-protein-coupled receptors (GPCRs) signaling. *Curr. Med. Chem.* **13**, 51-63 (2006).

59. Kobilka, B.K. G protein coupled receptor structure and activation. *Biochim. Biophys. Acta* **1768**, 794-807 (2007).

60. Lohse, M.J. et al. Optical techniques to analyze real-time activation and signaling of G-protein-coupled receptors. *Trends Pharmacol. Sci.* **29**, 159-165 (2008).

61. Scott, C.W. & Peters, M.F. Label-free whole-cell assays: expanding the scope of GPCR screening. *Drug Discov. Today* **15**, 704-716 (2010).

62. Xi, B., Naichen, Y., Xiaobo, W., Xiao, X. & Yama, A. The application of cell-based label-free technology in drug discovery. *Biotechnol. J.* **3**, 484-495 (2008).

63. Fang, Y., Frutos, A.G. & Verklereen, R. Label-free cell-based assays for GPCR screening. *Comb. Chem. High Throughput Screen.* **11**, 357-369 (2008).

64. Peters, M.F. & Scott, C.W. Evaluating cellular impedance assays for detection of GPCR pleiotropic signaling and functional selectivity. *J. Biomol. Screen.* **14**, 246-255 (2009).

65. Tuteja, N. Signaling through G protein coupled receptors. *Plant Signal. & Behav.* **4**, 942-947 (2009).

66. Zhang, R. & Xie, X. Tools for GPCR drug discovery. *Acta Pharmacol. Sin.* **33**, 372-384 (2012).

67. Cheng, C.I., Chang, Y.-P. & Chu, Y.-H. Biomolecular interactions and tools for their recognition: focus on the quartz crystal microbalance and its diverse surface chemistries and applications. *Chem. Soc. Rev.* **41** (2012).

68. Hurst, J.H. & Hooks, S.B. Lysophosphatidic acid stimulates cell growth by different mechanisms in SKOV-3 and Caov-3 ovarian cancer cells: distinct roles for Gi- and Rho-dependent pathways. *Pharmacology* **83**, 333-347 (2009).

69. Lania, A., Mantovani, G. & Spada, A. Genetics of pituitary tumors: Focus on G-Protein mutations. *Exp. Biol. Med.* **228**, 1004-1017 (2003).

70. Trejo, J. in Signal Transduction: Pathways, Mechanisms and Diseases. (ed. A. Sitaramayya) 83-98 (Springer Berlin Heidelberg, Berlin, Heidelberg; 2010).

71. Urbakh, M., Tsionsky, V., Gileadi, E. & Daikhin, L. in Piezoelectric Sensors, Vol. 5. (eds. C. Steinem & A. Janshoff) 111-149 (Springer Berlin Heidelberg, 2007).

72. Höök, F. & Kasemo, B. in Piezoelectric Sensors 425-447 (2007).

73. Marx, K.A. The quartz crystal microbalance and the electrochemical QCM: Applications to studies of thin polymer films, electron transfer systems, biological macromolecules, biosensors, and cells. *Springer Ser. Chem. Sens. Biosens.* **5**, 371-424 (2007).

74. Hunter, A.C. Application of the quartz crystal microbalance to nanomedicine. *J. Biomed. Nanotechnol.* **5**, 669-675 (2009).

75. Cargnello, M. & Roux, P.P. Activation and function of the MAPKs and their substrates, the MAPK-activated protein kinases. *Microbiol. Mol .Biol. Rev.* **75**, 50-83 (2011).

76. Kedziora, K.M. et al. Rapid remodeling of invadosomes by Gi-coupled Receptors: Dissecting the role of Rho GTPases. *J. Biol. Chem.* **291**, 4323-4333 (2016).

77. Erb, L. & Weisman, G.A. Coupling of P2Y receptors to G proteins and other signaling pathways. *Wiley Interdiscip. Rev. Membr. Transp. Signal.* **1**, 789-803 (2012).

78. Khalili, A. & Ahmad, M. A review of cell adhesion studies for biomedical and biological applications. *Int. J. Mol. Sci.* **16**, 18149 (2015).

79. Puech, P.-H. et al. Measuring cell adhesion forces of primary gastrulating cells from zebrafish using atomic force microscopy. *J. Cell Sci.* **118**, 4199-4206 (2005).

80. Bao, G. et al. USNCTAM perspectives on mechanics in medicine. *J. R. Soc. Interface* **11**, . (2014).

81. Athanasiou, K.A. et al. Development of the cytodetachment technique to quantify mechanical adhesiveness of the single cell. *Biomaterials* **20**, 2405-2415 (1999).

82. Christ, K.V. & Turner, K.T. Methods to measure the strength of cell adhesion to substrates. *J. Adhes. Sci. Technol.* **24**, 2027-2058 (2010).

83. Hochmuth, R.M. Micropipette aspiration of living cells. *J. Biomech.* **33**, 15-22 (2000).

84. Merkel, R., Nassoy, P., Leung, A., Ritchie, K. & Evans, E. Energy landscapes of receptor-ligand bonds explored with dynamic force spectroscopy. *Nature* **397**, 50-53 (1999).

85. Helenius, J., Heisenberg, C.P., Gaub, H.E. & Muller, D.J. Single-cell force spectroscopy. *J. Cell Sci.* **121**, 1785-1791 (2008).

86. Sen, S., Subramanian, S. & Discher, D.E. Indentation and adhesive probing of a cell membrane with AFM: theoretical model and experiments. *Biophys. J.* **89**, 3203-3213 (2005).

87. Shao, J.-Y. Measuring piconewton forces and its application in cellular and molecular biomechanics. *Advs. Biomech.*, 47-51 (2001).

88. Zhang, H. & Liu, K.-K. Optical tweezers for single cells. *J. R. Soc. Interface* **5**, 671-690 (2008).

89. Lee, G.Y.H. & Lim, C.T. Biomechanics approaches to studying human diseases. *Trends Biotechnol.* **25**, 111-118.

90. Reyes, C.D. & García, A.J. A centrifugation cell adhesion assay for high‐throughput screening of biomaterial surfaces. *J. Biomed. Mater. Res. A* **67**, 328-333 (2003).

91. García, A.J., Ducheyne, P. & Boettiger, D. Quantification of cell adhesion using a spinning disc device and application to surface-reactive materials. *Biomaterials* **18**, 1091-1098 (1997).

92. Van Kooten, T., Schakenraad, J., Van der Mei, H. & Busscher, H. Development and use of a parallel‐plate flow chamber for studying cellular adhesion to solid surfaces. *J. Biomed. Mater. Res. A* **26**, 725-738 (1992).

93. Roy, P., Rajfur, Z., Pomorski, P. & Jacobson, K. Microscope-based techniques to study cell adhesion and migration. *Nat. Cell Biol.* **4**, E91-E96 (2002).

94. Mui, K.L., Chen, C.S. & Assoian, R.K. The mechanical regulation of integrin-cadherin crosstalk organizes cells, signaling and forces. *J. Cell Sci.* **129**, 1093-1100 (2016).

95. Munevar, S., Wang, Y.-l. & Dembo, M. Traction force microscopy of migrating normal and H-ras transformed 3T3 fibroblasts. *Biophys. J.* **80**, 1744-1757 (2001).

96. Jiang, J., Qin, J., Li, H. & Cai, S. Cell micropatterning techniques. *Gaojishu Tongxun* **13**, 101-107 (2003).

97. Velve-Casquillas, G., Le Berre, M., Piel, M. & Tran, P.T. Microfluidic tools for cell biological research *Nano today* **5**, 28-47 (2010).

98. Park, Y.I., Lee, K.T., Suh, Y.D. & Hyeon, T. Upconverting nanoparticles: a versatile platform for wide-field two-photon microscopy and multi-modal in vivo imaging. *Chem. Soc. Rev.* **44**, 1302-1317 (2015).

99. Webb, D.J. & Brown, C.M. Epi-fluorescence microscopy. *Methods Mol. Biol.* **931**, 29-59 (2013).

100. Stephens, D.J. & Allan, V.J. Light microscopy techniques for live cell imaging. *Science* **300**, 82-86 (2003).

101. Axelrod, D. Cell-substrate contacts illuminated by total internal reflection fluorescence. *J. Cell Biol.* **89**, 141-145 (1981).

102. Lieb, S. et al. Label-free analysis of GPCR-stimulation: The critical impact of cell adhesion. *Pharmacol. Res.* **108**, 65-74 (2016).

103. Giaever, I. & Keese, C.R. A morphological biosensor for mammalian cells. *Nature* **366**, 591-592 (1993).

104. Xi, B., Yu, N., Wang, X., Xu, X. & Abassi, Y. The application of cell-based label-free technology in drug discovery. *Biotechnol. J.* **3**, 484-495 (2008).

105. Benson, K., Cramer, S. & Galla, H.-J. Impedance-based cell monitoring: barrier properties and beyond. *Fluids Barriers CNS* **10**, 5-5 (2013).

106. Asphahani, F. et al. Influence of cell adhesion and spreading on impedance characteristics of cell-based sensors. *Biosens. Bioelectron.* **23**, 1307-1313 (2008).

107. Giaever, I. & Keese, C.R. Micromotion of mammalian cells measured electrically. *Proc. Natl. Acad. Sci. U. S. A.* **88**, 7896-7900 (1991).

108. Diemert, S. et al. Impedance measurement for real time detection of neuronal cell death. *J. Neurosci. Methods* **203**, 69-77 (2012).

109. Asphahani, F. & Zhang, M. Cellular impedance biosensors for drug screening and toxin detection. *Analyst* **132**, 835-841 (2007).

110. Stahelin, R.V. Surface plasmon resonance: a useful technique for cell biologists to characterize biomolecular interactions. *Mol. Biol. Cell* **24**, 883-886 (2013).

111. Patching, S.G. Surface plasmon resonance spectroscopy for characterisation of membrane protein–ligand interactions and its potential for drug discovery. *Biochim. Biophys. Acta* **1838**, 43-55 (2014).

112. van der Merwe, P.A. & Barclay, A.N. Analysis of cell-adhesion molecule interactions using surface plasmon resonance. *Curr. Opin. Immunol.* **8**, 257-261 (1996).

113. Yashunsky, V., Lirtsman, V., Golosovsky, M., Davidov, D. & Aroeti, B. Real-time monitoring of epithelial cell-cell and cell-substrate interactions by infrared surface plasmon spectroscopy. *Biophys. J.* **99**, 4028-4036 (2010).

114. Heitmann, V., Reiss, B. & Wegener, J. The quartz crystal microbalance in cell biology: Basics and applications. *Springer Ser. Chem. Sens. Biosens.* **5**, 303-338 (2007).

115. Saitakis, M. & Gizeli, E. Acoustic sensors as a biophysical tool for probing cell attachment and cell/surface interactions. *Cell. Mol. Life Sci.*, 1-15 (2011).

116. Wegener, J., Janshoff, A. & Steinem, C. The quartz crystal microbalance as a novel means to study cell-substrate interactions in situ. *Cell Biochem. Biophys.* **34**, 121-151 (2001).

117. Dixon, M.C. Quartz crystal microbalance with dissipation monitoring: Enabling real-time characterization of biological materials and their interactions. *J. Biomol. Tech.* **19**, 151-158 (2008).

118. Şeke, Ş. & Elçin, Y.M. in Biol. Med. Sensor Technologies. (ed. K. Iniewski) 105-124 (CRC Press, 2012).

119. Marx, K.A. Quartz crystal microbalance: a useful tool for studying thin polymer films and complex biomolecular systems at the solution-surface interface. *Biomacromolecules* **4**, 1099-1120 (2003).

120. Cavic, B.A., Thompson, M. & Hayward, G.L. Acoustic waves and the study of biochemical macromolecules and cells at the sensor-liquid interface. *Analyst* **124**, 1405-1420 (1999).

121. Gufflet, N. Quartz crystal resonators - brief overview. *KVG Quartz Crystal Technology GmbH* (2011).

122. Janata, J. Principles of chemical sensors. (Springer Science & Business Media, 2010).

123. Lack, F.R., Willard, G.W. & Fair, I.E. Some improvements in quartz crystal circuit elements. *Bell Syst. Tech. J.* **13**, 453-463 (1934).

124. Rodahl, M. & Kasemo, B. Frequency and dissipation-factor responses to localized liquid deposits on a QCM electrode. *Sens. Actuators B Chem.* **37**, 111-116 (1996).

125. Sauerbrey, G. Verwendung von Schwingquarzen zur Wägung dünner Schichten und zur Mikrowägung. *Zeitschrift für Physik A Hadrons and Nuclei* **155**, 206-222 (1959).

126. King, W.H. Piezoelectric sorption detector. *Anal. Chem.* **36**, 1735-1739 (1964).

127. Rodahl, M., Hook, F., Krozer, A., Brzezinski, P. & Kasemo, B. Quartz crystal microbalance setup for frequency and Q-factor measurements in gaseous and liquid environments. *Rev. Sci. Instrum.* **66**, 3924-3930 (1995).

128. Johannsmann, D. Viscoelastic, mechanical, and dielectric measurements on complex samples with the quartz crystal microbalance. *Phys. Chem. Chem. Phys.* **10**, 4516-4534 (2008).

129. Zhang, Y., Du, B., Chen, X. & Ma, H. Convergence of dissipation and impedance analysis of quartz crystal microbalance studies. *Anal. Chem.* **81**, 642-648 (2009).

130. Heitmann, V. & Wegener, J. Monitoring cell adhesion by piezoresonators: Impact of increasing oscillation amplitudes. *Anal. Chem.* **79**, 3392-3400 (2007).

131. Le Guillou-Buffello, D., Gindre, M., Johnson, P., Laugier, P. & Migonney, V. An alternative quantitative acoustical and electrical method for detection of cell adhesion process in real-time. *Biotechnol. Bioeng.* **108**, 947-962 (2011).

132. Kanchanawong, P. et al. Nanoscale architecture of integrin-based cell adhesions. *Nature* **468**, 580-584 (2010).

133. Wegener, J., Seebach, J., Janshoff, A. & Galla, H.-J. Analysis of the composite response of shear wave resonators to the attachment of mammalian cells. *Biophys. J.* **78**, 2821-2833 (2000).

134. Bicknese, S., Periasamy, N., Shohet, S.B. & Verkman, A.S. Cytoplasmic viscosity near the cell plasma membrane: measurement by evanescent field frequency-domain microfluorimetry. *Biophys. J.* **65**, 1272-1282 (1993).

135. Redepenning, J., Schlesinger, T.K., Mechalke, E.J., Puleo, D.A. & Bizios, R. Osteoblast attachment monitored with a quartz crystal microbalance. *Anal. Chem.* **65**, 3378-3381 (1993).

136. Gryte, D.M., Ward, M.D. & Hu, W.-S. Real-time measurement of anchorage-dependent cell adhesion using a quartz crystal microbalance. *Biotechnol. Prog.* **9**, 105-108 (1993).

137. Wegener, J., Janshoff, A. & Galla, H.J. Cell adhesion monitoring using a quartz crystal microbalance: comparative analysis of different mammalian cell lines. *Eur. Biophys. J.* **28**, 26-37 (1998).

138. Lord, M.S. et al. Monitoring cell adhesion on tantalum and oxidised polystyrene using a quartz crystal microbalance with dissipation. *Biomaterials* **27**, 4529-4537 (2006).

139. Modin, C. et al. QCM-D studies of attachment and differential spreading of pre-osteoblastic cells on Ta and Cr surfaces. *Biomaterials* **27**, 1346-1354 (2006).

140. Wegener, J., Zink, S., Rösen, P. & Galla, H.J. Use of electrochemical impedance measurements to monitor β-adrenergic stimulation of bovine aortic endothelial cells. *Pflugers Arch* **437**, 925-934 (1999).

141. Rodahl, M. et al. Simultaneous frequency and dissipation factor QCM measurements of biomolecular adsorption and cell adhesion. *Farad. Discuss*, 229-246 (1997).

142. Fredriksson, C., Kihlman, S., Rodahl, M. & Kasemo, B. The piezoelectric quartz crystal mass and dissipation sensor: A means of studying cell adhesion. *Langmuir* **14**, 248-251 (1998).

143. Marx, K.A., Zhou, T., Montrone, A., McIntosh, D. & Braunhut, S.J. Quartz crystal microbalance biosensor study of endothelial cells and their extracellular matrix following cell removal: Evidence for transient cellular stress and viscoelastic changes during detachment and the elastic behavior of the pure matrix. *Anal. Biochem.* **343**, 23-34 (2005).

144. Molino, P.J., Hodson, O.M., Quinn, J.F. & Wetherbee, R. The quartz crystal microbalance: a new tool for the investigation of the bioadhesion of diatoms to surfaces of differing surface energies. *Langmuir* **24**, 6730-6737 (2008).

145. Saravia, V. & Toca-Herrera, J.L. Substrate influence on cell shape and cell mechanics: HepG2 cells spread on positively charged surfaces. *Microsc. Res. Tech.* **72**, 957-964 (2009).

146. Şeker, Ş., Elçin, A.E. & Elçin, Y.M. Real-time monitoring of mesenchymal stem cell responses to biomaterial surfaces and to a model drug by using quartz crystal microbalance. *Artif. Cells Nanomed. Biotechnol.* **44**, 1722-1732 (2016).

147. Tagaya, M. In situ QCM-D study of nano-bio interfaces with enhanced biocompatibility. *Polym. J.* **47**, 599-608 (2015).

148. Westas, E. et al. Using QCM-D to study the adhesion of human gingival fibroblasts on implant surfaces. *J. Biomed. Mater. Res. A* **103**, 3139-3147 (2015).

149. Guo, M. et al. Enhanced adhesion/spreading and proliferation of mammalian cells on electropolymerized porphyrin film for biosensing applications. *Biosens. Bioelectron.* **23**, 865-871 (2008).

150. Zhou, T., Kenneth, A.M., Michael, W., Heather, S. & Susan, J.B. The Quartz Crystal Microbalance as a Continuous Monitoring Tool for the Study of Endothelial Cell Surface Attachment and Growth. *Biotechnol. Prog.* **16**, 268-277 (2000).

151. Tymchenko, N. et al. Reversible changes in cell morphology due to cytoskeletal rearrangements measured in real-time by QCM-D. *Biointerphases* **7**, 1-9 (2012).

152. Zhou, T., Marx, K.A., Dewilde, A.H., McIntosh, D. & Braunhut, S.J. Dynamic cell adhesion and viscoelastic signatures distinguish normal from malignant human mammary cells using quartz crystal microbalance. *Anal. Biochem.* **421**, 164-171 (2012).

153. Alessandrini, A., Croce, M.A., Tiozzo, R. & Facci, P. Monitoring cell-cycle-related viscoelasticity by a quartz crystal microbalance. *Appl. Phys. Lett.* **88**, 083905/083901-083905/083903 (2006).

154. Chen, J.Y., Li, M., Penn, L.S. & Xi, J. Real-time and label-free detection of cellular response to signaling mediated by distinct subclasses of epidermal growth factor receptors. *Anal. Chem.* **83**, 3141-3146 (2011).

155. Chen, J.Y., Shahid, A., Garcia, M.P., Penn, L.S. & Xi, J. Dissipation monitoring for assessing EGF-induced changes of cell adhesion. *Biosens. Bioelectron.* **38**, 375-381 (2012).

156. Tarantola, M. et al. Dynamics of human cancer cell lines monitored by electrical and acoustic fluctuation analysis. *Integr. Biol.* **2**, 139-150 (2010).

157. Suresh, S. Biomechanics and biophysics of cancer cells. *Acta Biomater.* **3**, 413-438 (2007).

158. Cross, S.E., Jin, Y.-S., Rao, J. & Gimzewski, J.K. Nanomechanical analysis of cells from cancer patients. *Nat Nano* **2**, 780-783 (2007).

159. Li, Q.S., Lee, G.Y.H., Ong, C.N. & Lim, C.T. AFM indentation study of breast cancer cells. *Biochem. Biophys. Res. Commun.* **374**, 609-613 (2008).

160. Zhang, S., Bai, H. & Yang, P. Real-time monitoring of mechanical changes during dynamic adhesion of erythrocytes to endothelial cells by QCM-D. *Chem. Commun.* **51**, 11449-11451 (2015).

161. Yang, J., Zhang, L., Yu, C., Yang, X.-F. & Wang, H. Monocyte and Macrophage Differentiation: Circulation Inflammatory Monocyte as Biomarker for Inflammatory Diseases. *Biomark. Res.* **2**, 1 (2014).

162. Garcia, M.P., Shahid, A., Chen, J.Y. & Xi, J. Effects of the expression level of epidermal growth factor receptor on the ligand-induced restructuring of focal adhesions: a QCM-D study. *Anal. Bioanal. Chem.* **405**, 1153-1158 (2013).

163. Zandi, R., Larsen, A.B., Andersen, P., Stockhausen, M.-T. & Poulsen, H.S. Mechanisms for oncogenic activation of the epidermal growth factor receptor. *Cell. Signal.* **19**, 2013-2023 (2007).

164. Sebastian, S. et al. The complexity of targeting EGFR signalling in cancer: From expression to turnover. *Biochim. Biophys. Acta* **1766**, 120 (2006).

165. Wells, A., Kassis, J., Solava, J., Turner, T. & Lauffenburger, D.A. Growth factor-induced cell motility in tumor invasion. *Acta Oncol.* **41**, 124 - 130 (2002).

166. Chronaki, D., Stratiotis, D.I., Tsortos, A., Anastasiadou, E. & Gizeli, E. Screening between normal and cancer human thyroid cells through comparative adhesion studies using the quartz crystal microbalance. *Sens. Biosensing Res.* **11, Part 2**, 99-106 (2016).

167. Han, L., Liu, P., Petrenko, V.A. & Liu, A. A label-free electrochemical impedance cytosensor based on specific peptide-fused phage selected from landscape phage library. *Sci. Rep.* **6**, 22199 (2016).

168. Shan, W. et al. An aptamer-based quartz crystal microbalance biosensor for sensitive and selective detection of leukemia cells using silver-enhanced gold nanoparticle label. *Talanta* **126**, 130-135 (2014).

169. Zhang, S., Bai, H., Luo, J., Yang, P. & Cai, J. A recyclable chitosan-based QCM biosensor for sensitive and selective detection of breast cancer cells in real time. *Analyst* **139**, 6259-6265 (2014).

170. Atay, S. et al. Quartz crystal microbalance based biosensors for detecting highly metastatic breast cancer cells via their transferrin receptors. *Anal. Methods* **8**, 153-161 (2016).

171. Trinder, D., Zak, O. & Aisen, P. Transferrin receptor-independent uptake of differic transferrin by human hepatoma cells with antisense inhibition of receptor expression. *Hepatology* **23**, 1512-1520 (1996).

172. Marques, O., da Silva, B.M., Porto, G. & Lopes, C. Iron homeostasis in breast cancer. *Cancer Lett.* **347**, 1-14 (2014).

173. Ranjan, R., Esimbekova, E.N. & Kratasyuk, V.A. Rapid biosensing tools for cancer biomarkers. *Biosens. Bioelectron.* **87**, 918-930 (2017).

174. Garcia, M., Shahid, A., Chen, J. & Xi, J. Evaluating inhibition of the epidermal growth factor (EGF)-induced response of mutant MCF10A cells with an acoustic sensor. *Biosensors* **2**, 448-464 (2012).

175. Elmlund, L., Käck, C., Aastrup, T. & Nicholls, I. Study of the interaction of trastuzumab and SKOV3 epithelial cancer cells using a quartz crystal microbalance sensor. *Sensors* **15**, 5884 (2015).

176. Wei, X.-L., Mo, Z.-H., Li, B. & Wei, J.-M. Disruption of HepG2 cell adhesion by gold nanoparticle and Paclitaxel disclosed by in situ QCM measurement. *Colloids Surf. B Biointerfaces* **59**, 100-104 (2007).

177. Tan, L. et al. In vitro study on the individual and synergistic cytotoxicity of adriamycin and selenium nanoparticles against Bel7402 cells with a quartz crystal microbalance. *Biosens. Bioelectron.* **24**, 2268-2272 (2009).

178. Zhou, Y. et al. Magnetically enhanced cytotoxicity of paramagnetic selenium-ferroferric oxide nanocomposites on human osteoblast-like MG-63 cells. *Biosens. Bioelectron.* **25**, 1116-1121 (2010).

179. Fohlerová, Z., Turánek, J. & Skládal, P. The cell adhesion and cytotoxicity effects of the derivate of vitamin E compared for two cell lines using a piezoelectric biosensor. *Sens. Actuator B Chem.* **174**, 153-157 (2012).

180. Costa, P. & Parsons, M. in International Review of Cell and Molecular Biology, Vol. Volume 283. (ed. J. Kwang) 57-91 (Academic Press, 2010).

181. Berrier, A.L. & Yamada, K.M. Cell–matrix adhesion. *J. Cell. Physio.* **213**, 565-573 (2007).

182. Vial, D. & McKeown-Longo, P.J. Epidermal growth factor (EGF) regulates α5β1 integrin activation state in human cancer cell lines through the p90RSK-dependent phosphorylation of filamin A. *J. Biol. Chem.* **287**, 40371-40380 (2012).

183. Carpenter, G. Receptors for Epidermal Growth Factor and Other Polypeptide Mitogens. *Annu. Rev. Biochem.* **56**, 881-914 (1987).

184. Lemmon, M.A. & Schlessinger, J. Cell signaling by receptor tyrosine kinases. *Cell* **141**, 1117-1134 (2010).

185. Scaltriti, M. & Baselga, J. The epidermal growth factor receptor pathway: a model for targeted therapy. *Clin. Cancer Res.* **12**, 5268-5272 (2006).

186. Welsh, J.B., Gill, G.N., Rosenfeld, M.G. & Wells, A. A negative feedback loop attenuates EGF-induced morphological changes. *J. Cell Biol.* **114**, 533-543 (1991).

187. Murphy-Ullrich, J.E. The de-adhesive activity of matricellular proteins: is intermediate cell adhesion an adaptive state. *J. Clin. Invest.* **107**, 785-790 (2001).

188. Palecek, S.P., Huttenlocher, A., Horwitz, A.F. & Lauffenburger, D.A. Physical and biochemical regulation of integrin release during rear detachment of migrating cells. *J. Cell Sci.* **111**, 929-940 (1998).

189. Lauffenburger, D.A. & Horwitz, A.F. Cell migration: A physically integrated molecular process. *Cell* **84**, 359-369 (1996).

190. Limbird, L.E. Cell surface receptors: A short course on theory and methods, Edn. 3rd. (Springer Science+Business Media, New York; 2005).

191. Martin-Fernandez, M., Clarke, D.T., Tobin, M.J., Jones, S.V. & Jones, G.R. Preformed oligomeric epidermal growth factor receptors undergo an ectodomain structure change during signaling *Biophys. J.* **82**, 2415-2427 (2002).

192. Rewcastle, G.W. et al. Tyrosine kinase inhibitors. 10. isomeric 4-[(3-bromophenyl)amino]pyrido[d]- pyrimidines are potent ATP binding site inhibitors of the tyrosine kinase function of the epidermal growth factor receptor. *J. Med. Chem.* **39**, 1823-1835 (1996).

193. Legate, K.R., Wickström, S.A. & Fässler, R. Genetic and cell biological analysis of integrin outside-in signaling. *Genes Dev.* **23**, 397-418 (2009).

194. Sen, S. & Kumar, S. Cell–matrix de-adhesion dynamics reflect contractile mechanics. *Cell. Mol. Bioeng.* **2**, 218-230 (2009).

195. Vlahos, C.J., Matter, W.F., Hui, K.Y. & Brown, R.F. A specific inhibitor of phosphatidylinositol 3-kinase, 2-(4-morpholinyl)-8-phenyl-4H-1-benzopyran-4-one (LY294002). *J. Biol. Chem.* **269**, 5241-5248 (1994).

196. Smith, R.J. et al. Receptor-coupled signal transduction in human polymorphonuclear neutrophils: effects of a novel inhibitor of phospholipase C-dependent processes on cell responsiveness. *J. Pharmacol. Exp. Ther.* **253**, 688-697 (1990).

197. Pirouzi, G. et al. Review of the socket design and interface pressure measurement for transtibial prosthesis. *Sci. World J.* **2014**, 9 (2014).

198. Ali, S. et al. Qualitative study of prosthetic suspension systems on transtibial amputees' satisfaction and perceived problems with their prosthetic devices. *Arch. Phys. Med. Rehabil.* **93**, 1919-1923 (2012).

199. Isackson, D., McGill, L.D. & Bachus, K.N. Percutaneous implants with porous titanium dermal barriers: An in vivo evaluation of infection risk. *Med. Eng. Phys.* **33**, 418-426 (2011).

200. Pendegrass, C.J., Goodship, A.E. & Blunn, G.W. Development of a soft tissue seal around bone-anchored transcutaneous amputation prostheses. *Biomaterials* **27**, 4183-4191 (2006).

201. Li, Y. & Brånemark, R. Osseointegrated prostheses for rehabilitation following amputation : The pioneering Swedish model. *Unfallchirurg* **120**, 285-292 (2017).

202. von Recum, A.F. Applications and failure modes of percutaneous devices: A review. *J. Biomed. Mater. Res.* **18**, 323-336 (1984).

203. Tillander, J., Hagberg, K., Hagberg, L. & Brånemark, R. Osseointegrated titanium implants for limb prostheses attachments: infectious complications. *Clin. Orthop. Relat. Res.* **468**, 2781-2788 (2010).

204. Pitkin, M. Design features of implants for direct skeletal attachment of limb prostheses. *J. Biomed. Mater. Res. A* **101**, 3339-3348 (2013).

205. Horwitz, A.R. The origins of the molecular era of adhesion research. *Nat. Rev. Mol. Cell Biol.* **13**, 805-811 (2012).

206. Fang, Y. Label-free receptor assays. *Drug Discov. Today Technol.* **7**, e5-e11 (2011).

207. Şeker, Ş. Sensor systems for monitoring mammalian cell behavior. *Glob. J. Contr. Eng. Technol.* **2**, 1-7 (2016).

208. Tan, L. et al. Dynamic measurement of the surface stress induced by the attachment and growth of cells on Au electrode with a quartz crystal microbalance. *Biosens. Bioelectron.* **24**, 1603-1609 (2009).

209. Hong, S., Ergezen, E., Lec, R. & Barbee, K.A. Real-time analysis of cell–surface adhesive interactions using thickness shear mode resonator. *Biomaterials* **27**, 5813-5820 (2006).

210. Fung, C.K. et al. Investigation of human keratinocyte cell adhesion using atomic force microscopy. *Nanomed.* **6**, 191-200 (2010).

211. Patel, H., Marcelo, C., Voorhees, J.J. & Diaz, L.A. In vitro alterations of epidermal cell adhesion induced by temperature, substrate, and cations. *J. Invest. Dermatol.* **76**, 474-479 (1981).

212. Carey, S.P., Charest, J.M. & Reinhart-King, C.A. in Cellular and Biomolecular Mechanics and Mechanobiology. (ed. A. Gefen) 29-69 (Springer Berlin Heidelberg, Berlin, Heidelberg; 2011).

213. Barker, T.H. The role of ECM proteins and protein fragments in guiding cell behavior in regenerative medicine. *Biomaterials* **32**, 4211-4214 (2011).

214. Adams, J.C. & Watt, F.M. Changes in keratinocyte adhesion during terminal differentiation: reduction in fibronectin binding precedes alpha 5 beta 1 integrin loss from the cell surface. *Cell* **63**, 425-435 (1990).

215. Bush, K.A. & Pins, G.D. Carbodiimide conjugation of fibronectin on collagen basal lamina analogs enhances cellular binding domains and epithelialization. *Tissue Eng. Part A* **16**, 829-838 (2010).

216. Maheshwari, G., Wells, A., Griffith, L.G. & Lauffenburger, D.A. Biophysical integration of effects of epidermal growth factor and fibronectin on fibroblast migration. *Biophys. J.* **76**, 2814-2823 (1999).

217. Dudley, D.T., Pang, L., Decker, S.J., Bridges, A.J. & Saltiel, A.R. A synthetic inhibitor of the mitogen-activated protein kinase cascade. *Proc. Natl. Acad. Sci. U. S. A.* **92**, 7686-7689 (1995).

218. Favata, M.F. et al. Identification of a novel inhibitor of mitogen-activated protein kinase kinase. *J.Biol. Chem.* **273**, 18623-18632 (1998).

219. Liu, P., Cheng, H., Roberts, T.M. & Zhao, J.J. Targeting the phosphoinositide 3-kinase (PI3K) pathway in cancer. *Nat. Rev. Drug Discov.* **8**, 627-644 (2009).

220. Kong, D. & Yamori, T. ZSTK474 is an ATP-competitive inhibitor of class I phosphatidylinositol 3 kinase isoforms. *Cancer Sci.* **98**, 1638-1642 (2007).

221. Crooke, C.E., Pozzi, A. & Carpenter, G.F. PLC-γ1 regulates fibronectin assembly and cell aggregation. *Exp. Cell Res.* **315**, 2207-2214 (2009).

222. Vossmeyer, D., Hofmann, W., Löster, K., Reutter, W. & Danker, K. Phospholipase Cγ binds α1β1 integrin and modulates α1β1 integrin-specific adhesion. *J. Biol. Chem.* **277**, 4636-4643 (2002).

223. Klein, R.R. et al. Direct activation of human phospholipase C by its well known inhibitor U73122. *J. Biol. Chem.* **286**, 12407-12416 (2011).

224. Horowitz, L.F. et al. Phospholipase C in living cells: activation, inhibition, Ca2+ requirement, and regulation of M current. *J. Gen. Physiol.* **126**, 243-262 (2005).

225. Pierce, K.L., Premont, R.T. & Lefkowitz, R.J. Seven-transmembrane receptors. *Nat. Rev. Mol. Cell Biol.* **3**, 639-650 (2002).

226. Dorsam, R.T. & Gutkind, J.S. G-protein-coupled receptors and cancer. *Nat. Rev. Cancer* **7**, 79-94 (2007).

227. Fredriksson, R., Lagerström, M.C., Lundin, L.-G. & Schiöth, H.B. The G-protein-coupled receptors in the human genome form five main families. Phylogenetic analysis, paralogon groups, and fingerprints. *Mol. Pharmacol.* **63**, 1256-1272 (2003).

228. McCudden, C.R., Hains, M.D., Kimple, R.J., Siderovski, D.P. & Willard, F.S. G-protein signaling: back to the future. *Cell. Mol. Life Sci.* **62**, 551-577 (2005).

229. Kleuss, C., Raw, A.S., Lee, E., Sprang, S.R. & Gilman, A.G. Mechanism of GTP hydrolysis by G-protein alpha subunits. *Proc. Natl. Acad. Sci. U. S. A.* **91**, 9828-9831 (1994).

230. Julius, D. & Nathans, J. Signaling by sensory receptors. *Cold Spring Harb. Perspect. Biol.* **4**, a005991 (2012).

231. Bockaert, J., Claeysen, S., Becamel, C., Pinloche, S. & Dumuis, A. G protein-coupled receptors: dominant players in cell-cell communication. *Int. Rev. Cytol.* **212**, 63-132 (2002).

232. Billington, C.K. & Penn, R.B. Signaling and regulation of G protein-coupled receptors in airway smooth muscle. *Respir. Res.* **4**, 2-2 (2003).

233. Betke, K.M., Wells, C.A. & Hamm, H.E. GPCR mediated regulation of synaptic transmission. *Prog. Neurobiol.* **96**, 304-321 (2012).

234. Newton, K. & Dixit, V.M. Signaling in innate immunity and inflammation. *Cold Spring Harb. Perspect. Biol.* **4** (2012).

235. Premont, R.T. & Gainetdinov, R.R. Physiological roles of G protein-coupled receptor kinases and arrestins. *Annu. Rev. Physiol.* **69**, 511-534 (2007).

236. Sun, L. & Ye, R.D. Role of G protein-coupled receptors in inflammation. *Acta Pharmacol. Sin.* **33**, 342-350 (2012).

237. Salazar, N.C., Chen, J. & Rockman, H.A. Cardiac GPCRs: GPCR signaling in healthy and failing hearts. *Biochimica et biophysica acta* **1768**, 1006-1018 (2007).

238. Klabunde, T. & Hessler, G. Drug design strategies for targeting G-protein-coupled receptors. *Chembiochem* **3**, 928-944 (2002).

239. Masseck, O.A., Rubelowski, J.M., Spoida, K. & Herlitze, S. Light- and drug-activated G-protein-coupled receptors to control intracellular signalling. *Exp. Physiol.* **96**, 51-56 (2011).

240. Marchese, A., George, S.R., Kolakowski, L.F., Jr., Lynch, K.R. & O'Dowd, B.F. Novel GPCRs and their endogenous ligands: expanding the boundaries of physiology and pharmacology. *Trends Pharmacol. Sci.* **20**, 370-375 (1999).

241. Tang, X.L., Wang, Y., Li, D.L., Luo, J. & Liu, M.Y. Orphan G protein-coupled receptors (GPCRs): biological functions and potential drug targets. *Acta Pharmacol. Sin.* **33**, 363-371 (2012).

242. Tran, T.M. et al. Characterization of agonist stimulation of cAMP-dependent protein kinase and G protein-coupled receptor kinase phosphorylation of the beta2-adrenergic receptor using phosphoserine-specific antibodies. *Mol. Pharmacol.* **65**, 196-206 (2004).

243. Green, S.A., Holt, B.D. & Liggett, S.B. Beta 1- and beta 2-adrenergic receptors display subtype-selective coupling to Gs. *Mol. Pharmacol.* **41**, 889-893 (1992).

244. Schulte, G. & Fredholm, B.B. Human adenosine A1, A2A, A2B, and A3 receptors expressed in chinese hamster ovary cells all mediate the phosphorylation of extracellular-regulated kinase 1/2. *Mol. Pharmacol.* **58**, 477-482 (2000).

245. Mazzoni, M.R. et al. A galpha(s) carboxyl-terminal peptide prevents G(s) activation by the A(2A) adenosine receptor. *Mol. Pharmacol.* **58**, 226-236 (2000).

246. Dror, R.O. et al. Pathway and mechanism of drug binding to G-protein-coupled receptors. *Proc. Natl. Acad. Sci. U. S. A.* **108**, 13118-13123 (2011).

247. Copik, A.J. et al. Isoproterenol acts as a biased agonist of the alpha-1A-adrenoceptor that selectively activates the MAPK/ERK pathway. *PLoS One* **10**, e0115701 (2015).

248. Yanagida, K. et al. Identification and characterization of a novel lysophosphatidic acid receptor, p2y5/LPA6. *J. Biol. Chem.* **284**, 17731-17741 (2009).

249. Zhou, L., Tang, Y., Cryan, E. & Demarest, K. Human epidermoid A431 cells express functional nicotinic Acid receptor HM74a. *Mol. Cell. Biochem.* **294**, 243-248 (2007).

250. Tang, Y. et al. Enhancement of arachidonic acid signaling pathway by nicotinic acid receptor HM74A. *Biochem. Biophys. Res. Commun.* **345**, 29-37 (2006).

251. Huang, N.-N., Wang, D.-J., Gonzalez, F. & Heppel, L.A. Multiple signal transduction pathways lead to extracellular ATP-stimulated mitogenesis in mammalian cells: II. A pathway involving arachidonic acid release, prostaglandin synthesis, and cyclic AMP accumulation. *J. Cell. Physio.* **146**, 483-494 (1991).

252. Waldo, G.L. & Harden, T.K. Agonist binding and Gq-stimulating activities of the purified human P2Y1 receptor. *Mol. Pharmacol.* **65**, 426-436 (2004).

253. Xie, P., Browning, D.D., Hay, N., Mackman, N. & Ye, R.D. Activation of NF-κB by bradykinin through a Gαq- and Gβγ-dependent pathway that involves phosphoinositide 3-kinase and Akt. *J. Biol. Chem.* **275**, 24907-24914 (2000).

254. Liebmann, C. et al. Dual bradykinin B2 receptor signalling in A431 human epidermoid carcinoma cells: activation of protein kinase C is counteracted by a GS-mediated stimulation of the cyclic AMP pathway. *Biochem. J.* **313**, 109-118 (1996).

255. Verrall, S. et al. The thrombin receptor second cytoplasmic loop confers coupling to Gq-like G proteins in chimeric receptors. Additional evidence for a common transmembrane signaling and G protein coupling mechanism in G protein-coupled receptors. *J. Biol. Chem.* **272**, 6898-6902 (1997).

256. Marinissen, M.J., Servitja, J.-M., Offermanns, S., Simon, M.I. & Gutkind, J.S. Thrombin protease-activated receptor-1 signals through Gq- and G13-initiated MAPK cascades regulating c-Jun expression to induce cell transformation. *J. Biol. Chem.* **278**, 46814-46825 (2003).

257. Fang, Y. & Ferrie, A. Optical biosensor differentiates signaling of endogenous PAR1 and PAR2 in A431 cells. *BMC Cell Biol.* **8**, 24 (2007).

258. Aguilar, M.-J., Morales-Olivas, F.J. & Rubio, E. Pharmacological investigation into the effects of histamine and histamine analogues on guinea-pig and rat colon in vitro. *Br. J. Pharmacol.* **88**, 501-506 (1986).

259. Tilly, B.C. et al. Histamine as a growth factor and chemoattractant for human carcinoma and melanoma cells: action through Ca2(+)-mobilizing H1 receptors. *J. Cell Biol.* **110**, 1211-1215 (1990).

260. Cordeaux, Y. & Hill, S.J. Mechanisms of cross-talk between G-protein-coupled receptors. *Neurosignals* **11**, 45-57 (2002).

261. Denis, C., Saulière, A., Galandrin, S., Sénard, J.-M. & Galés, C. Probing heterotrimeric G protein activation: applications to biased ligands. *Curr. Pharm. Des.* **18**, 128-144 (2012).

262. Barnes, P.J. Receptor heterodimerization: a new level of cross-talk. *J. Clin. Invest.* **116**, 1210-1212 (2006).

263. Maudsley, S., Martin, B. & Luttrell, L.M. The origins of diversity and specificity in g protein-coupled receptor signaling. *J. Pharmacol. Exp. Ther.* **314**, 485-494 (2005).

264. Vilardaga, J.-P. et al. Conformational cross-talk between [alpha]2A-adrenergic and [mu]-opioid receptors controls cell signaling. *Nat. Chem. Biol.* **4**, 126-131 (2008).

265. Maguire, J.J., Kuc, R.E. & Davenport, A.P. Radioligand binding assays and their analysis. *Methods Mol. Biol.* **897**, 31-77 (2012).

266. Chen, L., Jin, L. & Zhou, N. An update of novel screening methods for GPCR in drug discovery. *Expert Opin. Drug Discov.* **7**, 791-806 (2012).

267. Thomsen, W., Frazer, J. & Unett, D. Functional assays for screening GPCR targets. *Curr. Opin. Biotechnol.* **16**, 655-665 (2005).

268. Nelson, C.P. & Challiss, R.A. The use of translocating fluorescent biosensors for real-time monitoring of GPCR-mediated signaling events. *Methods Mol. Biol.* **746**, 329-343 (2011).

269. Strange, P.G. Agonist binding, agonist affinity and agonist efficacy at G protein-coupled receptors. *Br. J. Pharmacol.* **153**, 1353-1363 (2008).

270. Wild, D. Assays for drug-screening applications and research, Edn. 3rd. (Amsterdam ; Boston : Elsevier, 2005).

271. Peakman, M.C. & Hill, S.J. Adenosine A2B-receptor-mediated cyclic AMP accumulation in primary rat astrocytes. *Br. J. Pharmacol.* **111**, 191-198 (1994).

272. Hooks, S.B. et al. Characterization of a receptor subtype-selective lysophosphatidic acid mimetic. *Mol. Pharmacol.* **53**, 188-194 (1998).

273. Soga, T. et al. Molecular identification of nicotinic acid receptor. *Biochem. Biophys. Res. Commun.* **303**, 364-369 (2003).

274. Richman, J.G. et al. Nicotinic acid receptor agonists differentially activate downstream effectors. *J. Biol. Chem.* **282**, 18028-18036 (2007).

275. Velázquez, B., Garrad, R., Weisman, G. & González, F. Differential agonist-induced desensitization of P2Y2 nucleotide receptors by ATP and UTP. *Mol. Cell. Biochem.* **206**, 75-89 (2000).

276. Antonaccio, M.J., Normandin, D., Serafino, R. & Moreland, S. Effects of thrombin and thrombin receptor activating peptides on rat aortic vascular smooth muscle. *J. Pharmacol. Exp. Ther.* **266**, 125-132 (1993).

277. Blackhart, B.D. et al. Extracellular mutations of protease-activated receptor-1 result in differential activation by thrombin and thrombin receptor agonist peptide. *Mol. Pharmacol.* **58**, 1178-1187 (2000).

278. Quitterer, U., Zaki, E. & AbdAlla, S. Investigation of the extracellular accessibility of the connecting loop between membrane domains I and II of the bradykinin B2 receptor. *J. Biol. Chem.* **274**, 14773-14778 (1999).

279. Fang, Y., Li, G. & Peng, J. Optical biosensor provides insights for bradykinin B2 receptor signaling in A431 cells. *FEBS Lett.* **579**, 6365-6374 (2005).

280. Mangmool, S. & Kurose, H. G(i/o) protein-dependent and -independent actions of pertussis toxin (PTX). *Toxins* **3**, 884-899 (2011).

281. Taniguchi, M. et al. YM-254890 analogues, novel cyclic depsipeptides with Galpha(q/11) inhibitory activity from Chromobacterium sp. QS3666. *Bioorg. Med. Chem.* **12**, 3125-3133 (2004).

282. Nishimura, A. et al. Structural basis for the specific inhibition of heterotrimeric Gq protein by a small molecule. *Proc. Natl. Acad. Sci. U. S. A.* **107**, 13666-13671 (2010).

283. Kamato, D. et al. Gaq proteins: molecular pharmacology and therapeutic potential. *Cell. Mol. Life Sci.* **74**, 1379-1390 (2017).

284. Lieb, S. et al. Label-free versus conventional cellular assays: Functional investigations on the human histamine H1 receptor. *Pharmacol. Res.* **114**, 13-26 (2016).

285. Schiavo, G. & van der Goot, F.G. The bacterial toxin toolkit. *Nat. Rev. Mol. Cell Biol.* **2**, 530-537 (2001).

286. Baker, J.G. & Hill, S.J. Multiple GPCR conformations and signalling pathways: implications for antagonist affinity estimates. *Trends Pharmacol. Sci.* **28**, 374-381 (2007).

287. Chadet, S. et al. The activation of P2Y2 receptors increases MCF-7 breast cancer cells migration through the MEK-ERK1/2 signalling pathway. *Carcinogenesis* **35**, 1238-1247 (2014).

288. van Baal, J., de Widt, J., Divecha, N. & van Blitterswijk, W.J. Translocation of diacylglycerol kinase theta from cytosol to plasma membrane in response to activation of G protein-coupled receptors and protein kinase C. *J. Biol. Chem.* **280**, 9870-9878 (2005).

289. Schäfer, R., Sedehizade, F., Welte, T. & Reiser, G. ATP- and UTP-activated P2Y receptors differently regulate proliferation of human lung epithelial tumor cells. *Am. J. Physiol. Cell Physiol.* **285**, L376-L385 (2003).

290. Ohana, G., Bar-Yehuda, S., Barer, F. & Fishman, P. Differential effect of adenosine on tumor and normal cell growth: Focus on the A3 adenosine receptor. *J. Cell. Physiol.* **186**, 19-23 (2001).

291. Ponsioen, B. et al. Direct spatial control of epac1 by cyclic AMP. *Mol. Cell. Biol.* **29**, 2521-2531 (2009).

292. Rangarajan, S. et al. Cyclic AMP induces integrin-mediated cell adhesion through Epac and Rap1 upon stimulation of the β2-adrenergic receptor. *J. Cell Biol.* **160**, 487-493 (2003).

293. Bruzzone, A. et al. Dosage-dependent regulation of cell proliferation and adhesion through dual β2-adrenergic receptor/cAMP signals. *FASEB J.* **28**, 1342-1354 (2014).

294. Billups, D., Billups, B., Challiss, R.A.J. & Nahorski, S.R. Modulation of G(q) protein-coupled IP(3) and Ca(2+) signaling by the membrane potential. *J. Neurosci.* **26**, 9983-9995 (2006).

295. Sjaastad, M.D., Angres, B., Lewis, R.S. & Nelson, W.J. Feedback regulation of cell-substratum adhesion by integrin-mediated intracellular Ca2+ signaling. *Proc. Natl. Acad. Sci. U. S. A.* **91**, 8214-8218 (1994).

296. Sjaastad, M.D., Lewis, R.S. & Nelson, W.J. Mechanisms of integrin-mediated calcium signaling in MDCK cells: regulation of adhesion by IP3- and store-independent calcium influx. *Mol. Biol. Cell* **7**, 1025-1041 (1996).

297. Sjaastad, M.D. & Nelson, W.J. Integrin-mediated calcium signaling and regulation of cell adhesion by intracellular calcium *BioEssays* **19**, 47-55 (1997).

298. Jourquin, J., Yang, N., Kam, Y., Guess, C. & Quaranta, V. Dispersal of epithelial cancer cell colonies by lysophosphatidic acid (LPA). *J. Cell. Physio.* **206**, 337-346 (2006).

299. Yamashita, H. et al. Lysophosphatidic acid upregulates laminin-332 expression during A431 cell colony dispersal. *J. Oncol.* **2010**, 107075 (2010).

300. Schlessinger, J. Cell signaling by receptor tyrosine kinases. *Cell* **103**, 211-225 (2000).

301. King, A.C. & Cuatrecasas, P. Resolution of high and low affinity epidermal growth factor receptors. Inhibition of high affinity component by low temperature, cycloheximide, and phorbol esters. *J. Biol. Chem.* **257**, 3053-3060 (1982).

302. Boonstra, J., Mummery, C.L., van der Saag, P.T. & de Laat, S.W. Two receptor classes for epidermal growth factor on pheochromocytoma cells, distinguishable by temperature, lectins, and tumor promoters. *J. Cell. Physio.* **123**, 347-352 (1985).

303. Defize, L.H. et al. Signal transduction by epidermal growth factor occurs through the subclass of high affinity receptors. *J. Cell Biol.* **109**, 2495-2507 (1989).

304. Macdonald, J.L. & Pike, L.J. Heterogeneity in EGF-binding affinities arises from negative cooperativity in an aggregating system. *Proc. Natl. Acad. Sci. U. S. A.* **105**, 112-117 (2008).

305. Alvarado, D., Klein, D.E. & Lemmon, M.A. Structural basis for negative cooperativity in growth factor binding to an EGF receptor. *Cell* **142**, 568-579 (2010).

306. Krall, J.A., Beyer, E.M. & MacBeath, G. High- and low-affinity epidermal growth factor receptor-ligand interactions activate distinct signaling pathways. *PLoS ONE* **6**, e15945 (2011).

307. Zandi, R., Larsen, A.B., Andersen, P., Stockhausen, M.T. & Poulsen, H.S. Mechanisms for oncogenic activation of the epidermal growth factor receptor. *Cell. Signal.* **19**, 2013-2023 (2007).

308. Arteaga, C.L. Epidermal growth factor receptor dependence in human tumors: more than just expression. *Oncologist* **7**, 31-39 (2002).

309. Fang, Y., Ferrie, A.M., Fontaine, N.H. & Yuen, P.K. Characteristics of dynamic mass redistribution of epidermal growth factor receptor signaling in living cells measured with label-free optical biosensors. *Anal. Chem.* **77**, 5720-5725 (2005).

310. Atienza, J.M., Yu, N., Wang, X., Xu, X. & Abassi, Y. Label-free and real-time cell-based kinase assay for screening selective and potent receptor tyrosine kinase inhibitors using microelectronic sensor array. *J. Biomol. Screen.* **11**, 634-643 (2006).

311. Chinkers, M., McKanna, J.A. & Cohen, S. Rapid rounding of human epidermoid carcinoma cells A-431 induced by epidermal growth factor. *J. Cell Biol.* **88**, 422-429 (1981).

312. Coulson, J. & Akhtar, S. An oligonucelotide which blocks EGFR tyrosine phosphorylation modulates the rapid morphological change induced by EGF stimulation of A431 cells. *J. Pharm. Sci.* **2**, 339-343 (1996).

313. Schliwa, M. Action of cytochalasin D on cytoskeletal networks. *J. Cell Biol.* **92**, 79-91 (1982).

314. Moolenaar, W.H., Aerts, R.J., Tertoolen, L.G. & de Laat, S.W. The epidermal growth factor-induced calcium signal in A431 cells. *J. Biol. Chem.* **261**, 279-284 (1986).

315. Bers, D.M., Patton, C.W., Nuccitelli, R. & Michael, W. in Methods Cell Biol., Vol. Volume 99 1-26 (Academic Press, 2010).

316. Tinelli, A. et al. An outlook on ovarian cancer and borderline ovarian tumors: focus on genomic and proteomic findings. *Curr. Genomics* **10**, 240-249 (2009).

317. Gupta, D. & Lis, C.G. Role of CA125 in predicting ovarian cancer survival - a review of the epidemiological literature. *J. Ovarian Res.* **2**, 13-13 (2009).

318. Smolle, E. et al. Targeting signaling pathways in epithelial ovarian cancer. *Int. J. Mol. Sci.* **14**, 9536 (2013).

319. Rauh-Hain, J.A., Krivak, T.C., del Carmen, M.G. & Olawaiye, A.B. Ovarian cancer screening and early detection in the general population. *Rev. Obstet. Gynecol.* **4**, 15-21 (2011).

320. Hudson, L.G., Zeineldin, R., Silberberg, M. & Stack, M.S. Activated epidermal growth factor receptor in ovarian cancer. *Cancer Res. Treat.* **149**, 203-226 (2009).

321. Siwak, D.R. et al. Targeting the epidermal growth factor receptor in epithelial ovarian cancer: current knowledge and future challenges. *J. Oncol. Transl. Res.* **2010** (2010).

322. Yu, X., Zhang, Y. & Chen, H. LPA receptor 1 mediates LPA-induced ovarian cancer metastasis: an in vitro and in vivo study. *BMC Cancer* **16**, 846 (2016).

323. Pua, T.L., Wang, F.Q. & Fishman, D.A. Roles of LPA in ovarian cancer development and progression. *Future Oncol.* **5**, 1659-1673 (2009).

324. Oda, K., Matsuoka, Y., Funahashi, A. & Kitano, H. A comprehensive pathway map of epidermal growth factor receptor signaling. *Mol. Syst. Biol.* **1**, 2005.0010-2005.0010 (2005).

325. Morishige, K.-i. et al. Evidence for the involvement of transforming growth factor α and epidermal growth factor receptor autocrine growth mechanism in primary human ovarian cancers in vitro. *Cancer Res.* **51**, 5322-5328 (1991).

326. Sewell, J.M., Macleod, K.G., Ritchie, A., Smyth, J.F. & Langdon, S.P. Targeting the EGF receptor in ovarian cancer with the tyrosine kinase inhibitor ZD 1839 (‘Iressa’). *Br. J. Cancer* **86**, 456-462 (2002).

327. Bast, R.C., Hennessy, B. & Mills, G.B. The biology of ovarian cancer: new opportunities for translation. *Nat. Rev. Cancer* **9**, 415 (2009).

328. Yung, Y.C., Stoddard, N.C. & Chun, J. LPA receptor signaling: pharmacology, physiology, and pathophysiology. *J. Lipid Res.* **55**, 1192-1214 (2014).

329. Goetzl, E.J., Graeler, M., Huang, M.-C. & Shankar, G. Lysophospholipid growth factors and their G protein-coupled receptors in immunity, coronary artery disease, and cancer. *Sci. World J.* **2** (2002).

330. Bian, D. et al. Lysophosphatidic acid stimulates ovarian cancer cell migration via a Ras-MEK kinase 1 pathway. *Cancer Res.* **64**, 4209-4217 (2004).

331. Zhong, Y.-C., Zhang, T., Di, W. & Li, W.-P. Thrombin promotes epithelial ovarian cancer cell invasion by inducing epithelial-mesenchymal transition. *J. Gynecol. Oncol.* **24**, 265-272 (2013).

332. Krishna, A., Beesley, K. & Terranova, P.F. Histamine, mast cells and ovarian function. *J. Endocrinol.* **120**, 363-371 (1989).

333. Wang, X., Wang, E., Kavanagh, J.J. & Freedman, R.S. Ovarian cancer, the coagulation pathway, and inflammation. *J. Transl. Med.* **3**, 1-20 (2005).

334. Medina, V.A. & Rivera, E.S. Histamine receptors and cancer pharmacology. *Br. J. Pharmacol.* **161**, 755-767 (2010).

335. Medina, V.A. et al. Histamine in cancer. (Walter de Gruyter, 2014).

336. Batra, S. & Fadeel, I. Release of intracellular calcium and stimulation of cell growth by ATP and histamine in human ovarian cancer cells (SKOV-3). *Cancer Lett.* **77**, 57-63 (1994).

337. Nimse, S.B., Sonawane, M.D., Song, K.-S. & Kim, T. Biomarker detection technologies and future directions. *Analyst* **141**, 740-755 (2016).

338. Rusling, J.F., Kumar, C.V., Gutkind, J.S. & Patel, V. Measurement of biomarker proteins for point-of-care early detection and monitoring of cancer. *The Analyst* **135**, 2496-2511 (2010).

339. Zangar, R.C., Daly, D.S. & White, A.M. ELISA microarray technology as a high-throughput system for cancer biomarker validation. *Expert Rev. Proteomics* **3**, 37-44 (2006).

340. Issaq, H.J. & Veenstra, T.D. The role of electrophoresis in disease biomarker discovery. *Electrophoresis* **28**, 1980-1988 (2007).

341. Wang, X., Zhao, M., Nolte, D.D. & Ratliff, T.L. Prostate specific antigen detection in patient sera by fluorescence-free BioCD protein array. *Biosens. Bioelectron.* **26**, 1871-1875 (2011).

342. Wignarajah, S. et al. Colorimetric assay for the detection of typical biomarkers for periodontitis using a magnetic nanoparticle biosensor. *Anal. Chem.* **87**, 12161-12168 (2015).

343. Wei, F. et al. Electrochemical sensor for multiplex biomarkers detection. *Clin. Cancer Res.* **15**, 4446-4452 (2009).

344. Chinen, A.B. et al. Nanoparticle probes for the detection of cancer biomarkers, cells, and tissues by fluorescence. *Chem. Rev.* **115**, 10530-10574 (2015).

345. Otto, K. & Silhavy, T. Surface sensing and adhesion of Escherichia coli controlled by the Cpx-signaling pathway. *Proc. Natl. Acad. Sci. U. S. A.* **99**, 2287-2292 (2002).

346. Otto, K., Elwing, H. & Hermansson, M. Effect of ionic strength on initial interactions of Escherichia coli with surfaces, studied on-line by a novel quartz crystal microbalance technique. *J. Bacteriol.* **181**, 5210-5218 (1999).

347. Reipa, V., Almeida, J. & Cole, K.D. Long-term monitoring of biofilm growth and disinfection using a quartz crystal microbalance and reflectance measurements. *J. Microbiol. Methods* **66**, 449-459 (2006).

348. Cans, A.-S. et al. Measurement of the dynamics of exocytosis and vesicle retrieval at cell populations using a quartz crystal microbalance. *Anal. Chem.* **73**, 5805-5811 (2001).

349. Shankaran, H., Resat, H. & Wiley, H.S. Cell surface receptors for signal transduction and ligand transport: a design principles study. *PLoS Comput. Biol.* **3**, e101 (2007).

350. Becker, K.F. & Hofler, H. Mutant cell surface receptors as targets for individualized cancer diagnosis and therapy. *Curr. Cancer Drug Targets* **1**, 121-128 (2001).

351. Bohunicky, B. & Mousa, S.A. Biosensors: the new wave in cancer diagnosis. *Nanotechnol. Sci. and Appl.* **4**, 1-10 (2011).

352. Umezu-Goto, M. et al. Lysophosphatidic acid production and action: Validated targets in cancer? *J. Cell. Biochem.* **92**, 1115-1140 (2004).

353. Joh, T. et al. Physiological concentrations of human epidermal growth factor in biological fluids: use of a sensitive enzyme immunoassay. *Clin. Chim. Acta* **158**, 81-90 (1986).

354. Sedláková, I., Vávrová, J., Tošner, J. & Hanousek, L. Lysophosphatidic acid (LPA)—a perspective marker in ovarian cancer. *Tumor Biol.* **32**, 311-316 (2011).

355. Zdravkovic, V. et al. Histamine blood concentration in ischemic heart disease patients. *J. Biomed. Biotechnol.* **2011**, 8 (2011).

356. Naldini, A. et al. Thrombin enhances T cell proliferative responses and cytokine production. *Cell. Immunol.* **147**, 367-377 (1993).

357. Kinzer-Ursem, T.L. & Linderman, J.J. Both ligand- and cell-specific parameters control ligand agonism in a kinetic model of g protein-coupled receptor signaling. *PLoS Comput. Biol.* **3**, e6 (2007).

358. Watson, C. et al. The use of stimulus-biased assay systems to detect agonist-specific receptor active states: implications for the trafficking of receptor stimulus by agonists. *Mol. Pharmacol.* **58**, 1230-1238 (2000).

Appendix

AI. Abbreviations

7TM	Seven Transmembrane Domain Receptors
AC	Adenylyl Cyclase
AFM	Atomic Force Microscopy
ATP	Adenosine triphosphate
BFP	Biomembrane Probe
BioCD	Bio-optical Compact Disc
BP	Bullous Pemphigoid
BSA	Bovine Serum Albumin
CAM	cell adhesion molecule
cAMP	3',5'-cyclic adenosine monophosphate
CD	Cytochalasin D
Cr	Chromium
CRP	complement regulatory protein
CTX	Chloera Toxin
CVI	Cell Viscoelastic Index
D	Dissipation
DAG	Diacylglycerol
DMEM	Dulbecco's modified Eagle's medium
DMEM/F12	Dulbecco's modified Eagle's medium: nutrient mix F12
ECIS	Electric Cell-Substrate Impedance Sensing
ECM	Extra Cellular Matrix

EDTA	Ethylenediaminetetraacetic acid
EGF	Epidermal Growth Factor
EGFR	Epidermal Growth Factor Receptor
EGTA	Ethylene Glycol Tetraacetic Acid
ELISA	Enzyme-linked Immunosorbent Assay
Epi	Epinephrine
f	Frequency
FA	Focal Adhesions
FAK	Focal Adhesion kinases
FBS	Fetal Bovine Serum
FN	Fibronectin
GDP	Guanidine Diphosphate
GFP	Green Fluorescent Protein
GTP	Guanidine Triphosphate
GPCR	G protein Coupled Receptor
HBSS	Hanks Balanced Salt Solution
HEPES	4-(2-hydroxyethyl)-1-piperazineethanesulfonic acid
HER	Human Epidermal Growth Factor Receptor
Hist	Histamine
IF	Intermediate Filament
Ig	Immunoglobin
IP3	Inositol-1,4,5-trisphosphate
ISO	Isoproterenol

LPA	Lysophosphatidic Acid
MAPK	Mitogen Activated Protein Kinase
$MgCl_2$	Magnesium Chloride
MLC	Myosin Light Chain
MMP	Matrix Metalloproteinase
NA	Nicotinic Acid
NECA	5'-N-Ethylcarboxamidoadenosine
PA-TFM	Polyacrylamide (PA) Gel-based Traction Force Microscopy
PBS	Phosphate Saline Buffer
PFA	Paraformaldehyde
PI3K	Phosphoinositide 3-Kinase
PIP2	Phosphoinositol 4,5-bisphosphate
PIPES	Piperazine-N,N'-bis(2-ethanesulfonic acid)
PKC	Protein Kinase C
PLCγ	Phospholipase C Gamma
PTX	Pertussis Toxin
QCM	Quartz Crystal Microbalance
QCM-D	Quartz Crystal Microbalance with Dissipation
RBC	Red Blood Cell
RTK	Receptor Tyrosine Kinases
SCFS	Single Cell Force Spectroscopy
SDS	Sodium Dodecyl Sulfate
SPR	Surface Plasmon Resonance

SRE	Serum Response Element
STAT	Signal Transducer and Activator of Transcription
Ta	Tantalum
TGF-α	Transforming Growth Factor-α
TIRF	Total Internal Reflection fluorescence Microscopy
Thr	Thrombin
YM	YM-254890

Vita

Jennifer Ying Chen was born on August 28, 1987 in Philadelphia, Pennsylvania to immigrant parents from Xinhui, China. Jennifer attended Philadelphia High School for Girls, where she had two inspiring teachers, Mona Bradwell and Kilfe Gebremedhin, who encouraged her to pursue a career in science. After high school, she attended Drexel University and she received a Bachelor Degree of Science in Chemistry. While pursuing her undergraduate degree, she had the opportunity to intern at several biotech and pharmaceutical companies. She had the opportunity to intern at Morphotek Inc, Merck Co, and Astra Zeneca. After completion of her undergraduate studies she began her doctoral studies in Biochemistry at Drexel University under the advisement of Professor Jun Xi. In the course of her graduate career, she contributed to multiple peer reviewed journal articles (listed on next page) and presented her work in several oral and poster presentation at many national and local conferences including, ACS, MARM, and BPS. At the 252nd ACS National Meeting in August 2016, she was awarded 3rd place in the division of chemical toxicology poster session. She also volunteered as science presenter at The Franklin Institute. There she presented science demonstrations to the general public and encouraged kids and young adults to be passionate about science. Additionally, during her graduate studies at Drexel University she had the opportunity to teach undergraduate labs and recitations for which she was awarded The Ruth and Eugene Rosenbaum Graduate Teaching Assistant Award in 2014. Lastly, Jennifer obtained her doctorate degree in Chemistry from Drexel University in 2017.

Publications

- **Chen, JY,** Penn, LS, Xi, J. Quartz crystal microbalance: Sensing cell-substrate adhesion and beyond. *Biosens. Bioelectron.* 99 (2018) 593-602.

- **Chen JY**, Garcia MP, Penn LS, Xi J. Use of the quartz crystal microbalance with dissipation monitoring for pharmacological evaluation of cell signaling pathways mediated by epidermal growth factor receptors. *Label-Free Biosensor Methods in Drug Discovery* (2015) 253-268.

- Xi J, **Chen JY**, Garcia MP, Penn LS. Quartz crystal microbalance in cell biology studies. *J Biochip Tissue Chip* S5 (2013)

- Garcia MP, Shahid A, **Chen JY**, Xi J. Effects of the expression level of epidermal growth factor receptor on the ligand-induced restructuring of focal adhesions: a QCM-D study. *Anal. Bioanal. Chem.* 4 (2013) 1153-1158.

- Garcia MP, Shahid A, **Chen JY**, Xi J. Evaluating inhibition of the epidermal growth factor (EGF)-induced response of mutant MCF10A cells with an acoustic sensor. *Biosensors* 2 (2012) 448-464.

- **Chen JY**, Shahid A, Garcia MP, Penn LS, Xi J. Dissipation monitoring for assessing EGF-induced changes of cell adhesion. *Biosens. Bioelectron.* 38 (2012) 375-381.

- Yang R, **Chen JY**, Xi N, Lai KWC, Qu C, Fung CKM, Penn LS, Xi J. Characterization of mechanical behavior of an epithelial monolayer in response to epidermal growth factor stimulation. *Exp. Cell. Res.* 318 (2012) 521-526.

- **Chen JY**, Li M, Penn LS, Xi J. Real-time and label-free detection of cellular response to signaling mediated by distinct subclasses of epidermal growth factor receptors. *Anal. Chem.* 83 (2011) 3141-3146.

(page intentionally left blank)